June 2020

Mechanical properties and cyclic behavior of high strength steel after fire exposure

Fang Wang

Syracuse University

Abstract

Behavior of High Strength Steels (HSS) after exposure to high temperature has become an important research topic in recent years. A number of studies have demonstrated that different grades of HSS can exhibit noticeable differences in their mechanical properties under and after fire exposure, and different cooling methods may have an effect on the post-fire mechanical properties of HSS. In this research, the post-fire mechanical properties of Q690 steel and the post-fire residual stress distributions of Q690 welded I-sections heated to various temperatures using different heating rates and cooled using two cooling methods are determined experimentally and simple empirical equations to represent these measured data are proposed. Furthermore, the cyclic behavior of welded I-shaped columns made from Q690 steel after fire exposure is investigated.

In the first phase of the study, the post-fire mechanical properties of Q690 steel, which is a typical HSS with 690MPa nominal yield strength, are determined experimentally and discussed. The major variables considered are the level of temperature exposure and cooling methods used. The temperature used in the experimental work ranges from room temperature to 900°C, and two cooling methods – natural air and quenching water – are used to study whether they have an effect on the post-fire mechanical properties of HSS. In addition, the effect of the use of different heating methods, consideration of repeated heating and cooling, and various loading conditions are also studied. The test results show that while the post-fire elastic modulus is not too sensitive to the exposed temperature level and the manner of cooling, it decreases about 10% when a higher initial heating rate, repeated heating and cooling, or a load

is applied to the specimen. The post-fire yield strength tends to decrease with the exposed temperature level when the temperature reaches 400°C if the air cooling method is used and 500°C if the water quenching method is used. Further reduction in yield strength occurs when the specimen is subjected to a higher initial heating rate, repeated heating and cooling, or an applied load. The post-fire tensile strength does not show significant variations if air cooling is used but for specimens heated to a temperature above 700°C and rapidly cooled by submersion in water, noticeably higher post-fire tensile strength is observed as a result of the formation of martensite. Martensite formation also reduces the ductility (as measured by the fracture strain) of steel heated above 700°C and cooled suddenly.

In the second phase of the work, the residual stresses of Q690 welded I-sections after fire exposure are determined using the sectioning method. Like phase one, temperature and cooling method are the two main parameters that are studied. Furthermore, the effect of section dimensions will be considered. The results show that when the exposed temperature is below 300°C, the influence is not very important. However, when the exposed temperature exceeds 300°C, the magnitudes of the maximum residual stresses start to decrease. Once the temperature reaches 700°C, the maximum residual stress magnitudes are less than 5% of the nominal steel yield stress. The heating rate does not seem to affect the residual stress results. However, for specimens heated to a temperature at or above 700°C and suddenly cooled by water quenching, noticeable residual stresses are generated on the edges of the flanges and at the web-flange junctions. The residual stress magnitudes on the flange edges are -0.13F_y for 700°C and -0.24F_y for 900°C, while the magnitudes at the web-flange junctions are +0.29F_y for

700°C and +0.21F_y for 900°C (where F_y is the nominal yield stress of Q690 steel and +/- represents tension or compression).

In the last phase of this research, a Finite Element Model (FEM) is developed, calibrated and verified against the test results of cyclic behavior of Q690 welded I-shaped columns reported by other researchers. Using this FEM, the loss in energy dissipation under cyclic loads after fire exposure is investigated. The analysis results show that energy dissipation tends to decrease when the level of temperature exposure increases.

Finally, to facilitate design, empirical equations for the post-fire mechanical properties of Q690 steel, and the post-fire residual stress patterns of Q690 welded I-sections are developed and proposed. An equation to describe the capacity loss of Q690 welded I-shaped columns under cyclic loads after fire exposure is also proposed.

Keywords: High strength steel, Q690 steel, Mechanical properties, Post-fire behavior, Residual stresses, Cyclic performance

MECHANICAL PROPERTIES AND CYCLIC BEHAVIOR OF HIGH STRENGTH STEEL AFTER FIRE EXPOSURE

by

Fang Wang

B.S., Hubei University of Technology, 2011

M.S., Syracuse University, 2013

Dissertation

Submitted in partial fulfillment of the requirements for the degree of

Doctor of Philosophy in Civil Engineering.

Syracuse University

June 2020

Acknowledgments

This dissertation is one of the most demanding and challenging projects of my life. Starting with the literature review, through the experimental work and dissertation write up, and finally to the oral defense, I have received valuable assistance from various individuals. Without their help, it would have been impossible for me to complete this monumental task.

First and foremost, I would like to express my sincere appreciation to my advisor Professor Eric M. Lui. This research work would not have been completed without his guidance, encouragement, patience and support. He provided me with valuable suggestions during each phase of the work and he inspired me to do my best while keeping on the right track throughout the process.

I would also like to express my sincere appreciation to Professor Riyad S. Aboutaha, Professor Shobha Bhatia, Professor Junho Chun, Professor Dawit Negussey, and Professor Zhao Qin for serving on my oral exam committee, and for their valuable comments on this work. I am also thankful to Ms. Elizabeth Buchanan and Mr. Nick Clarke for their continuous help.

In addition, I want to express my gratitude to Professor Guobiao Lou of Tongji University and Professor Feng Yue of Shanghai Jiao Tong University. They provided me with valuable guidance and support when I was performing the experimental tests to obtain data for Chapter 4 and Chapter 5.

I would also like to thank you all my friends for their encouragement and support throughout this work. They have given me a lot of encouragement and valuable memories. Furthermore, I would love to express my sincere appreciation to my parents for their unconditional love, patience and continuous support through these years.

Finally, I am thankful to Syracuse University and the Department of Civil and Environmental Engineering for offering me the Teaching Assistantship. These years were the best years of my life and these good memories will stay with me forever.

Table of Contents

List of Figures

List of Tables

1 INTRODUCTION

From 1960s to 1990s, ASTM A36 steel with a yield strength of 36 ksi (248 MPa) was the predominant structural steel used for building construction while high-strength low-alloy and quenched and tempered alloy steels with yield strength that varies from 50 to 100 ksi (248 to 690 MPa) were used as alternatives for special applications. Nowadays, ASTM A992 steel which was adopted in 1998, is the most commonly used steel for W-shaped sections [1]. High strength steel (HSS), with a nominal yield strength no less than 67 ksi (460 MPa), is permitted for use under special circumstances, such as for high-rise buildings and long-span bridges. When compared with conventional steel, structures built using HSS offer advantages in increased strength and reduced weight, which could lead to economy in construction. As a result, research on the behavior and applications of HSS has become an important topic in civil engineering.

Historical events have clearly demonstrated that fire hazard is a major threat to the integrity of a structure throughout its service life. Although most steel structures can withstand a fire and exhibit no visible structural damage after fire exposure, post-fire elements may experience residual stress change and deformations during cooling. These changes need to be quantified in order to evaluate the post-fire performance of steel structures. Current research on post-fire behavior of HSS is mostly based on the air-cooling method, although water-cooling method is more realistic. One of the main objectives of this research is therefore to investigate the post-fire behavior of HSS components using different cooling methods.

Another objective of the proposed research is to investigate the cyclic behavior of post-fire structural members using finite element analysis. The finite element model used for this analysis will be calibrated using experimental data, and empirical equations for post-fire energy dissipation loss will be developed. The proposed approach can be used to simplify the inspection process for HSS structures after fire exposure and improve confidence in the design of HSS structures considering the fire hazard.

1.1 Standard Test Fire

The standard fire test prescribed by ISO 834 is used by various building and fire codes around the world. The time-temperature relationship used is given in Eq. (1.1) and plotted in Figure 1-1.

$$T = 345\, log_{10}(8t + 1) + 20 \tag{1.1}$$

where T= temperature in °C and t= time in minutes.

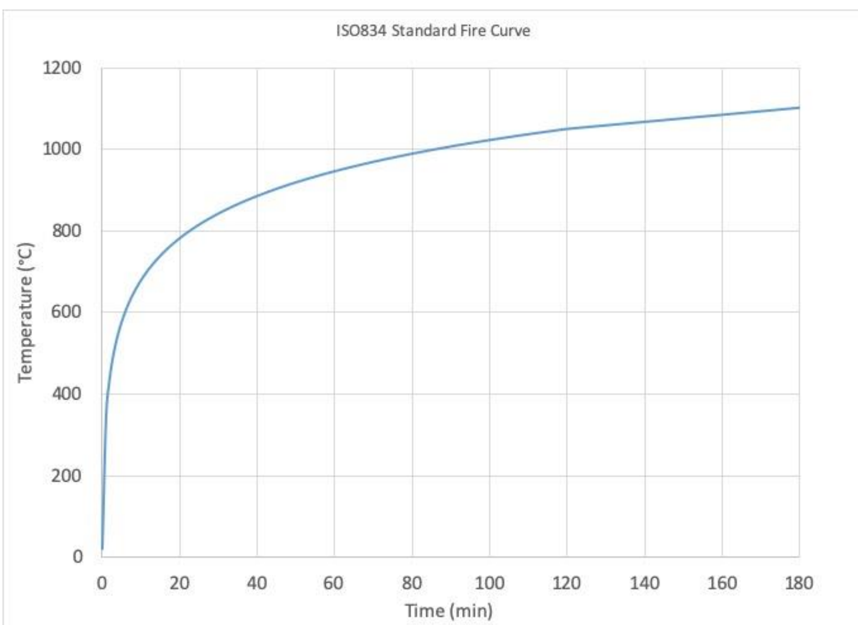

Figure 1-1 ISO 834 Standard Fire Curve [2,3]

1.2 Steel Grade Representation

Generally, different countries have different notations for designating steel grade. Based on Chinese Standard GB/T 1591-2008, 420 MPa steel is designated as Q420, where the letter Q is the Chinese phonetic alphabet of the word “Qu” meaning steel yield strength and 420 is the nominal yield strength in MPa. In Europe, according to EN10025-2004, 420 MPa steel is designated as S420, where S represents structural steel and 420 is the nominal yield strength in MPa.

1.3 Organization of Chapters

This thesis has seven chapters, including background introduction, literature review, research objectives, experimental tests, numerical analysis and conclusions:

- Chapter 1, this chapter, provides background information on this research work.
- Chapter 2 is a literature review on research related to the performance of high strength steel under or after fire exposure.
- Chapter 3 introduces the research objectives of this thesis. In this study, post-fire mechanical properties of Q690 steel are investigated. The post-fire residual stresses of Q690 welded I-shaped sections will also be obtained. Furthermore, finite element analysis is performed to determine the cyclic behavior of Q690 steel columns after fire exposure.
- Chapter 4 summarizes the post-fire mechanical properties of Q690 steel based on experimental tests. Empirical equations are then developed and presented to calculate these mechanical properties.

- Chapter 5 provides post-fire residual stress measurements of Q690 welded I-shaped sections. Simplified residual stress distribution patterns are then proposed for use in analysis and design.
- Chapter 6 is the numerical analysis of the cyclic behavior of post-fire Q690 welded I-shaped columns. The effect of fire exposure on energy dissipation of these columns under cyclic loads is then investigated.
- Chapter 7 presents a summary and conclusions of the present work. In addition, recommendations for further studies are proposed.

2 LITERATURE REVIEW

2.1 Behavior of HSS under Elevated Temperature

After the 9/11 attack on the twin towers in New York City, fire resistance of steel structures has become an important research topic in the structural engineering community. Research on the mechanical properties of mild and HSS steels at elevated temperatures has been carried out by a number of researchers. A summary of tests for different types of HSS under elevated temperature is given in Table 2-1. In the table, the letter M designates thermomechanical rolled steel, N designates normalized rolled steel, Q designates quenching and tempering, L designates low notch toughness testing temperature, and RQT designates reheated, quenched and tempered. BISPLATE 80 is fabricated by an Australian company BISALLOY®, which is somewhat equivalent to ASTM A514 and S690. 20MnTiB is a type of HSS with a yield strength exceeding 940 MPa.

There are two common methods that can be used to test the mechanical properties of steel under elevated temperatures, steady-state and transient-state [13,14]. In a steady-state test, the test specimen is first heated to a predefined temperature. A tensile load is then applied to the specimen while the temperature is held constant. In a transient-state test, the test specimen is first pre-loaded to a predetermined force. It is then heated slowly to the target temperature. Steady-state tests are more often conducted because they can be performed over a shorter period of time. However, transient-state tests tend to produce more realistic results since the effects of creep and relaxation can be accounted for.

Table 2-1 Summary of Tests on HSS at Elevated Temperature

Steel Type	Test Method	Temperature Range (°C)	Heating Rate (°C/min)	Control Parameter
Q420 [4]	Steady	20~600	-	Load: 0.1 kN/s
	Transient	30~550	48~54	-
Q460 [5, 6]	Steady	20~800	-	Load: 0.5 kN/s
S420M [7]	Transient	20~700	10	-
S460 [8]	Transient	20~950	20	-
S460M [9-12]	Steady	200~800	-	Strain: 0.002~0.005/min
S460N [9-12]	Transient		3, 6, 10, 20, 30	-
S460N [13-15]	Steady	20~700	-	Strain: 0.005/min
	Transient		10	-
BISPLATE80 [16]	Steady	22~940	-	Strain: 0.006/min
	Transient	22~660	-	-
S690QL [17]	Steady	20~700	-	Strain: 0.005/min
	Transient		10	-
RQT-S690 [18]	Steady	25~800	-	Strain: 0.003/min
20 Mn-TiB [19]	Steady	20~700	-	Strain: 0.1/min

The mechanical properties (elastic modulus, yield strength, tensile strength) of HSS under elevated temperatures can be determined from the stress-strain curves. Since these properties usually degrade as temperature rises, reduction factors are often introduced to represent the change in mechanical properties with temperature. Table 2-2 and Table 2-3 provide a summary of reduction factors determined for elastic modulus for different types of HSS.

Table 2-2 Summary of Reduction Factor for Elastic Modulus

T (°C)	Q460 [5]	S460N [11]	S460M [11]	S460N [13-15]		S690QL [17]		RQT- S690 [18]
				Steady	Transient	Steady	Transient	
20	1	-	-	1	1	1	1	1 (25°C)
100	0.983	1	1	0.985	0.989	1	0.982	1.01
200	0.960	0.885	0.976	0.881	0.870	0.875	0.869	1.02
250	0.945	0.838	0.964	0.840	0.831	0.857	0.857	0.99
300	0.928	0.791	0.952	0.799	0.792	0.839	0.841	0.96
350	0.911	0.730	0.920	0.712	0.702	0.807	0.781	0.99
400	0.885	0.668	0.887	0.669	0.666	0.775	0.736	1.01
450	0.862	0.575	0.796	0.578	0.585	0.730	0.692	0.91
500	0.836	0.481	0.704	0.509	0.482	0.685	0.647	0.77
550	0.809	0.392	0.555	0.374	0.359	0.546	0.537	0.72
600	0.764	0.302	0.406	0.291	0.272	0.372	0.370	0.66
650	0.636	0.219	0.305	0.248	0.222	0.257	0.204	0.38
700	0.480	0.135	0.204	0.153	0.132	0.141	0.099	0.34
800	-	0.049	0.105	-	-	-	-	0.29
900	-	0.017	0.038	-	-	-	-	-

Table 2-3 Summary of Reduction Factor for Elastic Modulus (Cont'd)

T (°C)	BISPLATE80 [16]	
	Steady	Transient
22	1	1
60	1.04	0.92
120	1.01	0.89
150	1.04	0.86
180	1.02	0.82
240	0.98	0.77
300	1.00	0.74
360	0.95	0.68
410	0.92	0.64
460	0.94	0.61
540	0.87	0.6
600	0.73	0.44
660	0.73	0.32
720	0.51	-
770	0.49	-
830	0.33	-
940	0.12	-

According to Table 2-2 and Table 2-3, the reduction in elastic modulus varies depending on the type of HSS and tests used. Also, different fabrication methods and alloy compositions will lead to different results. For design purposes, Wang et al. [5] and Qiang et al. [15] performed regression analysis on the test results for Q460 and S460N steels and developed equations that can be used to determine E_T, the elastic modulus at temperature T (°C), given E_{20}, the elastic modulus at 20°C (room temperature), and T. The equations are given in Table 2-4.

Table 2-4 Empirical Equations for Elastic Modulus of HSS at Elevated Temperatures

Steel Type	Empirical Equation	T Range (°C)
Q460 [5]	$E_T/E_{20} = 1.02 - 0.035e^{T/280}$	20≤T≤800
S460N [15]	$E_T/E_{20} = 2.961 \times 10^{-9}T^3 - 4.317 \times 10^{-6}T^2 + 3.867 \times 10^{-4}T + 0.986$	20≤T≤900

For purpose of comparison, the elastic modulus reduction factors for four HSS (Q460, S460N, S690QL based on steady-state test and BISPLATE80) [16] and those recommended by the American Institute of Steel Construction (AISC) developed based on tests of mild steel are plotted in Figure 2-1. As can be seen, they do differ over the range of temperature shown, although the reduction factors for S460N and mild steel are somewhat comparable.

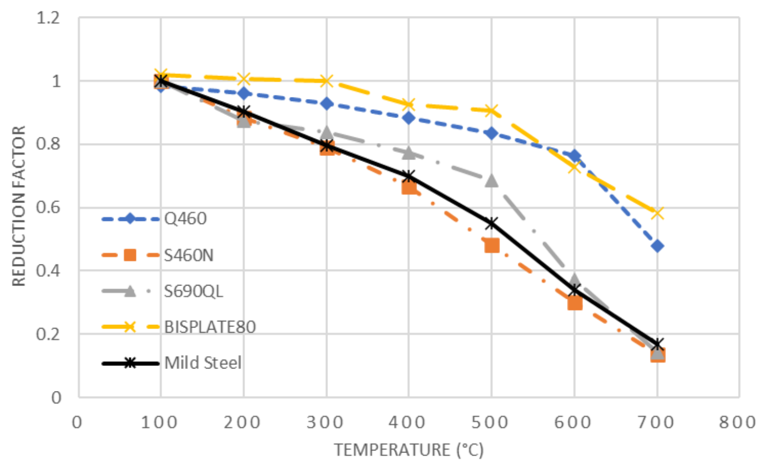

Figure 2-1 Comparison of Reduction Factor for Elastic Modulus

Study on the yield strength of HSS at elevated temperatures has also been conducted. Since most HSS show no obvious yield plateau, the yield strength is determined at an offset of 0.2% strain as per ASTM E21-09 [20].

In current design standards, the reduction factors for yield strength recommended by European Steel Design Code (EC3) are based on a strain level of 2.0%, and in the British Standard for Steel Work Design (BS5950) different reduction factors are given based on three strain levels 0.5%, 1.5% and 2.0%. In AISC and the Australian Standard for Steel Structures Design (AS 4100), no specific strain level is mentioned, but a 0.2% yield strength is assumed. The 0.2% yield strength is the intersection point of the stress-strain curve and a line drawn parallel to the proportional line at a strain value of 0.2%. On the other hand, the yield strength at 0.5%, 1.5% and 2.0% strain levels are determined as the intersection point of the stress-strain curve and a vertical line drawn at the specified strain [20].

Table 2-5 and Table 2-6 summarize the reduction factors for yield strength obtained for different types of HSS.

Table 2-5 Summary of Reduction Factor for Yield Strength

T (°C)	Q460 [5]	S460N [11]	S460M [11]	S460N [13-15]					RQT- S690 [18]			
				Steady	Transient				Steady			
				2%	0.2%	0.5%	1.5%	2%	0.2%	0.5%	1.5%	2%
20	1	1	1	1	1	1	1	1	1	1	1	1
100	0.88	0.878	0.947	0.987	0.9	0.903	0.952	0.989	0.947	0.874	0.958	0.968
150	0.98	0.901	0.948	0.991	0.902	0.9	0.944	0.975	0.916	0.866	0.957	0.975
200	1.07	0.924	0.949	0.994	0.809	0.821	0.923	0.97	0.884	0.854	0.956	0.982
250	1.11	0.913	0.952	0.998	0.802	0.796	0.909	0.966	0.882	0.803	0.954	0.979
300	1.14	0.901	0.954	1.001	0.78	0.773	0.903	0.962	0.879	0.751	0.952	0.975
350	1.09	0.884	0.956	0.984	0.756	0.741	0.895	0.958	0.837	0.773	0.908	0.913
400	1.03	0.867	0.958	0.949	0.716	0.718	0.883	0.942	0.794	0.794	0.864	0.85
450	1.06	0.769	0.916	0.877	0.665	0.69	0.848	0.899	0.711	0.7	0.76	0.737
500	0.85	0.67	0.874	0.739	0.532	0.635	0.777	0.771	0.628	0.605	0.655	0.624
550	0.74	0.551	0.722	0.559	0.446	0.534	0.644	0.639	0.554	0.438	0.557	0.533
600	0.73	0.432	0.57	0.415	0.364	0.457	0.499	0.495	0.38	0.345	0.382	0.371
650	0.55	0.316	0.445	0.313	0.276	0.318	0.384	0.381	0.24	0.23	0.258	0.252
700	0.36	0.2	0.32	0.187	0.22	0.246	0.287	0.247	0.1	0.114	0.133	0.133
800	0.18	0.071	0.12	-	-	-	-	-	-	-	-	-
900	-	0.034	0.048	-	-	-	-	-	-	-	-	-

Table 2-6 Summary of Reduction Factor for Yield Strength (Cont'd)

T (°C)	S690QL [17]								T (°C)	BISPLATE80 [16]			
	Steady				Transient					Steady			
	0.2%	0.5%	1.5%	2%	0.2%	0.5%	1.5%	2%		0.2%	0.5%	1.5%	2%
20	1	1	1	1	1	1	1	1	22	1	1	1	1
100	0.947	0.874	0.958	0.968	0.985	0.989	0.91	0.923	60	0.95	0.96	0.96	0.96
150	0.916	0.864	0.957	0.975	0.924	0.934	0.873	0.896	120	0.94	0.94	0.96	0.96
200	0.884	0.854	0.956	0.982	0.863	0.878	0.836	0.868	150	0.96	0.95	0.98	0.99
250	0.882	0.803	0.954	0.979	0.858	0.875	0.831	0.861	180	0.92	0.92	0.97	0.97
300	0.879	0.751	0.952	0.975	0.837	0.872	0.826	0.855	240	0.89	0.89	0.99	1
350	0.837	0.773	0.908	0.913	0.803	0.839	0.813	0..839	300	0.89	0.9	0.98	0.99
400	0.794	0.794	0.864	0.85	0.797	0.812	0.786	0.798	410	0.87	0.87	0.94	0.94
450	0.711	0.7	0.76	0.717	0.758	0.763	0.73	0.738	460	0.8	0.81	0.85	0.84
500	0.628	0.605	0.655	0.624	0.627	0.631	0.716	0.716	540	0.75	0.75	0.76	0.74
550	0.554	0.438	0.557	0.533	0.54	0.542	0.554	0.554	600	0.6	0.61	0.56	0.59
600	0.38	0.345	0.382	0.371	0.396	0.397	0.445	0.445	660	0.43	0.44	0.43	0.42
650	0.24	0.23	0.258	0.252	0.295	0.213	0.278	0.278	720	0.21	0.21	0.22	0.22
700	0.1	0.114	0.133	0.133	0.163	0.228	0.203	0.203	770	0.14	0.14	0.15	0.14
800	-	-	-	-	-	-	-	-	830	0.08	0.08	0.08	0.09
900	-	-	-	-	-	-	-	-	940	0.05	0.05	0.05	0.05

Because of the blue brittleness effect in the steady-state test of Q460 steel, a small increase in strength and a decrease in ductility were observed. This phenomenon occurred in 200~450°C and resulted in a "reduction factor" larger than 1 at 300°C [5].

Using regression analysis, empirical equations that relate f_{yT}, the yield strength of HSS at temperature T (°C) and f_y, the yield strength at 20°C (room temperature) before the HSS is exposed to high temperature, were developed [5,15] and shown in Table 2-7.

Table 2-7 Empirical Equations for Yield Strength of HSS at Elevated Temperatures

Steel Type	Empirical Equation	T Range (°C)
Q460 [5]	$f_{yT}/f_y = 1$	20≤T≤450
	$f_{yT}/f_y = 4.32e^{-T/880} - 1.6$	450<T≤800
S460N [15]	$f_{yT}/f_y = 1.001 - 1 \times 10^{-4}T$	20≤T≤350
	$f_{yT}/f_y = -1.672 \times 10^{-11}T^4 + 5.135 \times 10^{-8}T^3 - 5.41 \times 10^{-5}T^2 + 2.138 \times 10^{-2}T - 1.835$	350<T≤900

The yield strength reduction factors for four HSS (Q460, S460N, S690QL 0.2% yield strength based on steady-state test, and BISPLATE80) are compared in Figure 2-2 to those recommended by the AISC developed based on tests of mild steel. As can be seen, noticeable differences are observed for the different types of steel.

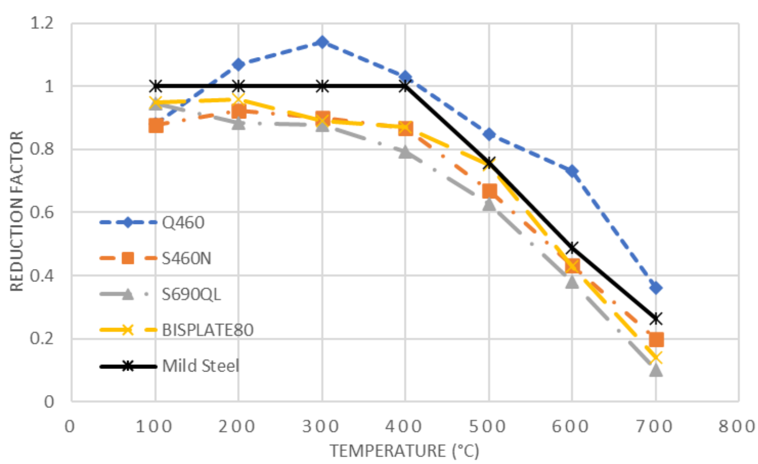

Figure 2-2 Comparison of Reduction Factor for Yield Strength

When temperature rises, the ultimate or tensile strength of HSS decreases. However, the effect of tensile strength loss is negligible until the temperature rises above 350°C. Reduction factors for tensile strength are summarized in Table 2-8 and empirical equations that can be used for design are given in Table 2-9.

Table 2-8 Summary of Reduction Factor for Tensile Strength

T (°C)	Q420 [4]	Q460 [5]	S460N [13-15]		S690QL [17]		RQT- S690 [18]	T (°C)	BISPLATE80 [16]
	Steady	Steady	Steady	Transient	Steady	Transient	Steady		Steady
20	1	1	1	1	1	1	1(25°C)	22	1
100	0.974	0.93	0.945	0.998	0.968	0.923	0.96	60	0.959
150	0.958	0.96	0.957	0.969	0.975	0.896	0.96	120	0.97
200	0.925	0.98	0.969	0.968	0.982	0.868	0.95	150	0.992
250	1.012	1	0.996	0.968	0.979	0.861	0.96	180	0.983
300	1.082	1.02	1.023	0.968	0.975	0.855	0.97	240	0.999
350	1.156	1.03	1.024	0.968	0.913	0.839	0.91	300	0.994
400	1.107	1.03	0.88	0.968	0.85	0.798	0.84	410	0.929
450	0.994	1	0.75	0.897	0.737	0.738	0.64	460	0.819
500	0.828	0.82	0.601	0.693	0.624	0.716	0.5	540	0.732
550	0.668	0.63	0.443	0.556	0.533	0.554	0.35	600	0.588
600	0.431	0.6	0.328	0.421	0.371	0.445	0.19	660	0.421
650	-	0.45	0.249	0.278	0.252	0.278	0.15	720	0.21
700	-	0.29	0.157	0.206	0.133	0.203	0.1	770	0.14
800	-	0.15	-	-	-	-	0.07	830	0.089
900	-	-	-	-	-	-		940	0.051

Table 2-9 Empirical Equations for Tensile Strength of HSS at Elevated Temperatures

Steel Type	Empirical Equation	T Range (°C)
S460N [15]	$f_{yT}/f_y = 1 - 1.855 \times 10^{-5} T$	20≤T≤350
	$f_{yT}/f_y = -7.079 \times 10^{-11} T^4 + 1.73 \times 10^{-7} T^3 - 1.526 \times 10^{-4} T^2 + 5.52 \times 10^{-2} T - 5.985$	350<T≤900

In the above table, f_{uT} is the tensile strength at temperature T (°C) and f_u is the tensile strength at 20°C before the HSS is exposed to high temperature.

In Figure 2-3, the tensile strength reduction factors for four HSS (Q460, S460N, S690QL based on steady-state test, BISPLATE80) are compared to those recommended by the AISC based on tests of mild steel. As can be seen, except for Q460, the reduction factors for other HSS are generally lower than those for mild steel when the temperature exceeds 300°C.

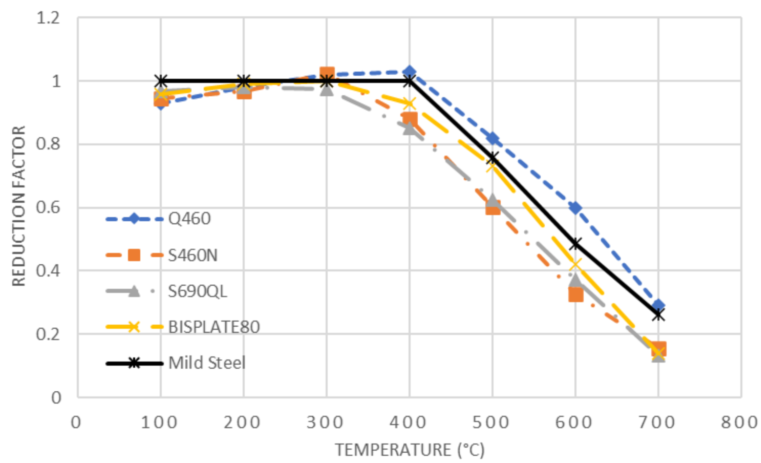

Figure 2-3 Comparison of Reduction Factor for Tensile Strength

2.2 Post-fire Behavior of HSS

Generally, two methods can be used to conduct cooling tests on steel after exposure to elevated temperature. They are the air-cooling and water-cooling methods. Of the two, the water-cooling method is more realistic. Wang et al. [21] showed that the use of water cooling had a dramatic influence on the post-fire tensile strength and elongation of the test specimens. Table 2-10 summarizes the post-fire tests on some HSS.

Table 2-10 Summary of Post-fire Tests on HSS

Steel Type	Temp. Range (°C)	Test Method	Heating Rate (°C/min)	Constant T. Duration (min)	Cooling Method	Control Parameter
Q460 [21]	20~900	Steady	15	20	Air/ Water	Elastic Stage: 10MPa/s
						Yield Stage: 0.001/s
						Hardening Stage: 10mm/min
S460 [22]	20~1000	Steady	10	10	Air	0.005/min
S690 [22]	20~1000	Steady	10	10	Air	0.005/min
S960 [23]	20~1000	Steady	10	10	Air	0.005/min
RQT-S690 [18]	25~800	Steady	-	10	Air	0.003/min

Using regression analysis, Wang et al. [21] proposed empirical equations for determining post-fire mechanical properties of Q460 steel. Depending on the type of cooling used, two sets of equations are proposed. They are shown in Table 2-11.

Table 2-11 Empirical Equations for Post-fire Mechanical Properties of Q460 Steel

Temperature Range 20°C~900°C	
Air Cooling	**Water Cooling**
$\frac{E_T}{E} = -4 \times 10^{-10}T^3 + 3.93 \times 10^{-7}T^2 - 7.79 \times 10^{-5}T + 1$	$\frac{E_T}{E} = -7.15 \times 10^{-10}T^3 + 6.86 \times 10^{-7}T^2 - 9.27 \times 10^{-5}T + 1$
$\frac{f_{yT}}{f_y} = -1.17 \times 10^{-9}T^3 + 5.54 \times 10^{-7}T^2 + 1.33 \times 10^{-4}T + 1$	$\frac{f_{yT}}{f_y} = -1.73 \times 10^{-9}T^3 + 1.25 \times 10^{-6}T^2 - 8.05 \times 10^{-5}T + 1$
$\frac{f_{uT}}{f_u} = -3.81 \times 10^{-10}T^3 - 6.36 \times 10^{-8}T^2 + 1.79 \times 10^{-4}T + 1$	$\frac{f_{uT}}{f_u} = 8.11 \times 10^{-10}T^3 - 7.03 \times 10^{-7}T^2 + 1.93 \times 10^{-4}T + 1$
$\frac{\varepsilon_T}{\varepsilon} = 1.68 \times 10^{-9}T^3 - 9.55 \times 10^{-7}T^2 - 1.62 \times 10^{-4}T + 1$	$\frac{\varepsilon_T}{\varepsilon} = -1.37 \times 10^{-9}T^3 + 1.78 \times 10^{-6}T^2 - 7.62 \times 10^{-4}T + 1$

Qiang et al. [22, 23] pointed out that when the temperature was below 600°C the post-fire mechanical properties loss of S460, S690 and S960 were negligible. Furthermore, all test specimens showed ductile failure with necking and no brittle failure was observed. Empirical equations for post-fire mechanical properties of these HSS were developed and they are summarized in Table 2-12 to Table 2-14.

Table 2-12 Empirical and Simplified Equations for Post-fire Mechanical Properties of S460 Steel

Empirical Equations		**Simplified Equations**	
$\frac{E_T}{E} = -2.69 \times 10^{-7}T^2 + 6.55 \times 10^{-5}T + 0.999$	20≤T≤600°C	$\frac{E_T}{E} = -3.84 \times 10^{-10}T^3 + 1.43 \times 10^{-7}T^2 - 4.18 \times 10^{-5}T + 1$	20≤T≤1000°C
$\frac{E_T}{E} = 0.947 - \frac{(T-600)^{1.618}}{68.84T}$	600<T≤800°C		
$\frac{E_T}{E} = -2.545 \times 10^{-6}T^2 + 3.856 \times 10^{-3}T + 0.598$	800<T≤1000°C		
$\frac{f_{yT}}{f_y} = -1.19 \times 10^{-9}T^3 + 1.03 \times 10^{-6}T^2 + 2.25 \times 10^{-4}T + 1.004$	20≤T≤800°C	$\frac{f_{yT}}{f_y} = -3.24 \times 10^{-10}T^3 + 4.98 \times 10^{-8}T^2 + 4.52 \times 10^{-5}T + 0.998$	20≤T≤1000°C
$\frac{f_{yT}}{f_y} = 0.876 - \frac{(T-800)^{3.634}}{2.048 \times 10^6 T}$	800<T≤1000°C		
$\frac{f_{uT}}{f_u} = -1.24 \times 10^{-9}T^3 + 1.07 \times 10^{-6}T^2 - 2.54 \times 10^{-4}T + 1.005$	20≤T≤750°C	$\frac{f_{uT}}{f_u} = -2.79 \times 10^{-7}T^2 + 1.08 \times 10^{-4}T + 0.996$	20≤T≤1000°C
$\frac{f_{uT}}{f_u} = 0.876 - \frac{(T-800)^{3.634}}{2.048 \times 10^6 T}$	750<T≤1000°C		

Table 2-13 Empirical Equations for Post-fire Mechanical Properties of S690 Steel

Empirical Equations	Temperature Range (°C)
$\frac{E_T}{E} = -1.52 \times 10^{-10}T^3 + 2.7 \times 10^{-8}T^2 - 3.35 \times 10^{-5}T + 1$	20≤*T*≤600
$\frac{E_T}{E} = 6.27 \times 10^{-9}T^3 - 1.38 \times 10^{-5}T^2 + 8.95 \times 10^{-3}T - 0.806$	600<*T*≤1000
$\frac{f_{yT}}{f_y} = 1 - \frac{(T-20)^{1.584}}{9957T}$	20≤*T*≤650
$\frac{f_{yT}}{f_y} = 1.8 \times 10^{-8}T^3 - 4.03 \times 10^{-5}T^2 + 2.74 \times 10^{-2}T - 4.711$	650<*T*≤1000
$\frac{f_{uT}}{f_u} = 1$	20≤*T*≤600
$\frac{f_{uT}}{f_u} = -1.24 \times 10^{-10}T^4 + 4.13 \times 10^{-7}T^3 - 5.077 \times 10^{-4}T^2 + 0.271T - 52.21$	600<*T*≤1000

Table 2-14 Empirical and Simplified Equations for Post-fire Mechanical Properties of S960 Steel

Empirical Equations	Simplified Equations	Temperature Range (°C)
$\frac{E_T}{E} = -1.52 \times 10^{-10}T^3 + 2.7 \times 10^{-8}T^2 - 3.35 \times 10^{-5}T + 1$		20≤*T*≤600
$\frac{E_T}{E} = 6.27 \times 10^{-9}T^3 - 1.38 \times 10^{-5}T^2 + 8.95 \times 10^{-3}T - 0.806$		600<*T*≤1000
$\frac{f_{yT}}{f_y} = 1$	$\frac{f_{yT}}{f_y} = 1$	20≤*T*≤600
$\frac{f_{yT}}{f_y} = 8.157 \times 10^{-9}T^3 - 1.685 \times 10^{-5}T^2 + 9.388 \times 10^{-3}T - 0.333$	$\frac{f_{yT}}{f_y} = 4.4 \times 10^{-6}T^2 - 8.637 \times 10^{-3}T + 4.596$	600<*T*≤1000
$\frac{f_{uT}}{f_u} = 1$		20≤*T*≤600
$\frac{f_{uT}}{f_u} = 1.006 - \frac{(T-600)^{1.158}}{9.567 \times 10^5 T}$		600<*T*<800
$\frac{f_{uT}}{f_u} = 7.762 \times 10^{-6}T^2 - 1.568 \times 10^{-2}T + 8.564$		800≤*T*≤1000

2.3 Residual Stresses of HSS

Residual stresses are developed as a result of uneven cooling of the different parts of the cross-section during the fabrication process. The presence of residual stresses could result in early yielding and reduction in stiffness. While residual stresses of normal strength hot-rolled and welded steel sections have been widely studied, the same cannot be said for HSS.

Wang et al. [24] studied three welded flame-cut Q460 HSS H-section members with three different width-to-thickness ratios, 3.4, 5 and 7.1. Ban et al. [25] and Yang et al. [26] conducted a similar study with a larger range of width-to-thickness ratios on 460MPa HSS welded I-shaped members and Q460GJ HSS welded I-shaped members, respectively. The residual stress distributions they obtained were found to be similar to that of mild steel with lower magnitudes and were related to section dimensions. Furthermore, Kim et al. [27] tested 800MPa HSS welded box-, cruciform- and H-sections, and Li et al. [28] provided information on the magnitude and distribution of residual stresses for box- and H-sections made of Q690 steels.

However, it should be noted that the investigation on the magnitude and distribution of residual stresses for post-fire HSS welded section members is rather limited. Wang et al. [29,30] performed residual stress tests on welded Q460 H-sections after fire exposure, shown in Table 2-15, and found that the magnitude of post-fire residual stresses decreased significantly with an increase in temperature.

Table 2-15 Residual Stress Tests on Post-fire HSS Welded H-sections (Wang et al. [29,30])

Steel Properties	Welding Details	Section Dimension (mm)	Heated Temperatures (°C)
E= 208.5GPa f_y= 538.1MPa f_u= 611.1MPa	Fillet welds with 8mm leg size CO_2 shielded arc welding Voltage= 25V and Amps= 230A Welding speed= 35cm/min Filler wire type is JM-60, with f_y= 545MPa and 25% elongation after fracture	Flame-cut 200x200x8x8	200/400/600/800 air cooling

2.4 Behavior of HSS Columns under Elevated Temperature

Valente and Neves [31], Rodrigues et al. [32] and Tan et al. [33] studied the fire resistance of mild steel columns and found that the presence of axial restraint would decrease the critical temperature, which is the temperature at which failure of the member occurs. Wang and Ge [34] conducted a similar research on four Q460 H-shaped columns using two levels of axial constrained stiffness and two levels of axial load ratio. The test results, given in Table 2-16, show that for a given constrained stiffness, the critical temperature decreases when the axial load ratio increases; or for a given axial load ratio, the constrained stiffness needs to be increased to maintain the critical temperature. Using finite element analysis, Ge and Wang [35] compared the inelastic strength of Q460 with Q235 steels shown in Table 2-17, and demonstrated the beneficial effect of using higher strength steel to counteract the loss of inelastic stability caused by the larger slenderness ratio of HSS.

Table 2-16 Tests on Q460 H-shaped Axially Restrained Columns for Critical Temperature (Wang and Ge [34])

Specimen Labels	Method	Mechanical Properties	Length	Section Type	Section Size (mm)	Axial Load Ratio	Axial Restrained Ratio (%)	Critical Temp. (°C)
S1	ISO-834 Increasing temperature under constant load	8mm Steel Plate E= 212GPa F_y= 585MPa F_u= 660MPa	4.3m	Welded H-shaped	H300x150x6.5x9	0.25	9.4	620
S2						0.41	9.4	510
S3					H200x150x6x9	0.26	3.8	625
S4						0.41	3.8	564

Table 2-17 Finite Element Analysis on Critical Temperature of Axially Restrained Columns (Ge and Wang [35])

Specimen Labels	Steel Type	Element Type	Dimension (mm)	Load Ratio	Slenderness Ratio	Restrained Ratio (%)	Critical Temp. (°C)
1	Q460	PLANE82 BEAM188 COMBINE14	Length: 3000 Section: H200x150x6x9	0.3	60	2.5	714
2				0.3	60	1.5	732
3				0.3	100	2.5	662
4				0.3	100	1.5	703
5				0.5	60	2.5	626
6				0.5	60	1.5	641
7				0.5	100	2.5	525
8				0.5	100	1.5	555
9	Q235			0.3	60	2.5	601
10				0.3	60	1.5	624
11				0.3	100	2.5	588
12				0.3	100	1.5	615
13				0.5	60	2.5	534
14				0.5	60	1.5	556
15				0.5	100	2.5	486
16				0.5	100	1.5	531

Wang et al. [36] tested twelve welded H-shaped Q460/Q235 steel stub columns given in Table 2-18 under axial compression with the objective of studying the local instability behavior at different elevated temperatures. The failure modes of all the specimens were local buckling, which are similar to those under room temperature.

Table 2-18 Stability Analysis of Welded H-shaped Columns under Axial Compression at Elevated Temperatures (Wang et al. [36])

Specimen Labels	Temp. (°C)	Section Dimension (mm)	Study Objective	Test Yield Strength (MPa)	Test Buckling Stress (MPa)
Q235A-1	25	H250x250x6x8	Flange Local Buckling	306.3	240.6
Q235A-2	450			251.6	148
Q235A-3	650			101.4	44.4
Q460A-1	25	H250x220x8x8		538.1	391.9
Q460A-2	450			532	278.2
Q460A-3	650			275	74.2
Q235B-1	25	H316x200x6x8	Web Local Buckling	321.9	192.6
Q235B-2	450			264.5	150
Q235B-3	650			106.6	53
Q460B-1	25	H336x160x8x8		538.1	356.4
Q460B-2	450			532	273.4
Q460B-3	650			275	70.3

From Table 2-18, it can be seen that the decrease of buckling strength is occurring at a higher rate than yield strength. This is because inelastic buckling is a function of both yield strength and stiffness. Since both are decreasing with an increasing temperature, their combined effect is manifested in the noticeable reduction in inelastic buckling strength.

Using the finite element software ABAQUS, Chen and Young [37] analyzed several HSS box and I-section columns (Table 2-19) at elevated temperatures, and concluded that while the current AISC Specification conservatively predicted the behavior of HSS columns at elevated temperatures, it gave unreliable results when the temperature was raised beyond 700°C.

Table 2-19 Numerical Analysis of HSS Box and I-section Columns at Elevated Temperatures (Chen and Young [37])

Element Type	Mesh Size	Boundary Conditions	Column Size	Analysis Method
S4R5	10mmx10mm	Fixed-end Pinned-end	Stub Slender	Step 1: Eigenvalue Analysis (linear and elastic) Step 2: Load-displacement nonlinear Analysis

Cyclic Loading Behavior of HSS

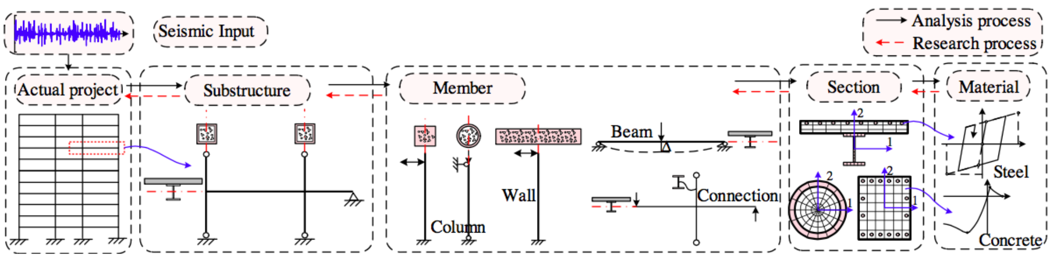

Figure 2-4 Analysis and Research Process for Multi-floor Structure Systems (Shi et al. [39])

Earthquake is one of the most harmful natural hazards in the world. When compared with normal strength steel, HSS has a higher mechanical strength, but a lower ductility and its yield to tensile stress ratio f_y/f_u is closer to 1 as well (See Table 2-20). This may result in deterioration of its seismic resistance. Studies conducted by Wang et al. [38] and Shi et al. [39] have found that both Q460C and Q460D HSS exhibited similar cyclic characteristics, such as plasticity, cyclic hardening and softening, average stress relaxation and Bauschinger effect, as mild steel. Lamarche and Tremblay [40] investigated the cyclic behavior of A992 steel W-section columns subjected to different axial compressive loads. The effects of width-to-thickness ratio, height-to-thickness ratio and axial load ratio were evaluated. Newell and Uang [41] tested nine full-scale wide-flange A992 steel columns under high axial force ratios of 35%, 55%, and 75% combined with story drift ratio up to 10%. They showed that the columns under high axial load could undergo large inelastic rotation. Nakashima et al. [42] and Kurata et al. [43] carried out experimental studies on box columns and arrived at the same conclusion.

Table 2-20 Experimental Tests on Cyclic Behavior of HSS (Wang et al. [38])

<table>
<tr><th colspan="6">Average Mechanical Properties of Monotonic Loading Tests</th></tr>
<tr><th colspan="2">Specifications</th><th>E (GPa)</th><th>F_y (MPa)</th><th>F_u (MPa)</th><th>F_y/F_u</th><th>Elongation after Fracture (%)</th></tr>
<tr><td colspan="2">11mm Q460C Plate Steel</td><td>207.8</td><td>505.8</td><td>597.5</td><td>0.85</td><td>23.7</td></tr>
<tr><td colspan="2">21mm Q460C Plate Steel</td><td>217.6</td><td>464</td><td>585.9</td><td>0.79</td><td>30.4</td></tr>
<tr><td colspan="2">14mm Q460C H-shaped Steel</td><td>220.2</td><td>565</td><td>671.3</td><td>0.84</td><td>23.9</td></tr>
<tr><td colspan="2">Q345B I-shaped Steel</td><td>-</td><td>385</td><td>535</td><td>0.72</td><td>27.5</td></tr>
<tr><th colspan="7">Cyclic Loading Tests</th></tr>
<tr><th>Specimen Label</th><th colspan="2">Steel Type</th><th colspan="4">Loading Protocol</th></tr>
<tr><td>P11-1</td><td colspan="2" rowspan="2">11mm Q460C Plate Steel</td><td colspan="4" rowspan="4">Seven cyclic strain amplitudes from 0.5% to 3.5% with two cycles repeated at each strain amplitude.
Loading Rate: 1mm/min</td></tr>
<tr><td>P11-2</td></tr>
<tr><td>P21-1</td><td colspan="2" rowspan="2">21mm Q460C Plate Steel</td></tr>
<tr><td>P21-2</td></tr>
<tr><td>H14-1</td><td colspan="2" rowspan="2">14mm Q460C H-shaped Steel</td><td colspan="4" rowspan="4">Three cycles repeated at first five strain amplitudes (1/300, 1/200, 1/150, 1/100 and 1/80) and ten cycles repeated at the last strain amplitude of 2%
Loading rate: 1Hz</td></tr>
<tr><td>H14-2</td></tr>
<tr><td>O14-1</td><td colspan="2" rowspan="2">Q345B I-shaped Steel</td></tr>
<tr><td>O14-2</td></tr>
</table>

**In the above table, the letters C and B designate the level of quality classification.*

For columns made from HSS, Wang et al. [44] tested six Q460 steel I-section columns as shown in Table 2-21 under lateral cyclic load with constant axial load, with width-to-thickness and axial load ratios as the main parameters. Chen et al. [45] performed experimental and numerical study on welded Q690D H-section. In both of these studies, the HSS columns have shown good hysteretic behavior.

Table 2-21 Lateral Cyclic Load Behavior Tests on Q460 I-section Columns under Axial Load (Wang et al. [44])

Specimen Label	Mechanical Properties	Section Size (mm)	b/t_f	h_w/t_w	Load Ratio	Yielding Load P_y	Yield Dist. δ_y
HH-1	Q460 welded I-section L=1790mm 10mm plate: E=2.1GPa f_y= 531.9MPa f_u= 657MPa 12mm plate: E=2.12GPa f_y= 492.3MPa f_u= 643.5MPa	200x150x12x10	6.3	17.6	0.2	87kN	18mm
HH-2		300x180x12x10	7.5	27.6	0.2	170kN	12mm
HH-3		300x220x12x10	9.2	27.6	0.2	202kN	12mm
HH-4		300x280x12x10	11.7	27.6	0.2	249kN	12mm
HH-5		360x280x12x10	11.7	33.6	0.2	311kN	10mm
HH-6		300x220x12x10	9.2	27.6	0.3	179kN	10mm

Furthermore, Wang et al. [44] proposed limiting values for 460 MPa HSS I-section columns for two levels of deformation requirements. Since the number of cyclic tests performed on HSS columns is quite few, our knowledge of their hysteretic behavior is still rather limited.

3 RESEARCH OBJECTIVES

Although study on the behavior of HSS at elevated temperatures has been carried out by a number of researchers at both the material and structural levels, research on post-fire behavior of HSS is quite limited and current standards do not contain sufficient information on how to evaluate the residual capacity of HSS after fire exposure. In addition, since the manner of how the test specimen is cooled could influence its post-fire mechanical properties, study on different cooling methods on the post-fire behavior of HSS needs to be performed.

For steel structures, the presence of residual stresses in welded built-up members is an important design parameter to consider as it affects the inelastic behavior of the members. Due to the difference in strength between mild steel and HSS, the residual stresses in HSS sections tend to be less detrimental to member strength [24]. However, because both the magnitudes and distributions of residual stresses could undergo noticeable changes after fire, additional study beyond those reported by Wang et al. [29, 30] on post-fire effect of residual stresses on HSS sections needs to be carried out.

To fill this knowledge gap, the present research aims to investigate the post-fire behavior of Q690 steel, which has a nominal yield strength of 100 ksi (690 MPa). At the material level, the post-fire mechanical properties of Q690 steel subjected to different cooling methods, namely natural air cooling and quenching water cooling, will be determined. The distribution of residual stresses in post-fire welded I-shaped sections will be examined as well. Finally, considering the potential effect of bi-hazard due to earthquake and fire, numerical analysis on the post-fire cyclic response of Q690 welded I-shaped columns will be performed. The proposed research will be carried out in three phases as follows.

3.1 Post-fire Mechanical Properties of Q690 Steel

The main variables considered in this phase of the study are temperature and cooling methods. The test temperature used will range from room temperature to 900°C, and two different cooling methods – natural air and quenching water – will be used to study the effect of different cooling methods on the post-fire mechanical properties of Q690 steel.

3.2 Post-fire Residual Stresses of Q690 Welded I-shaped Sections

In the second phase of the study, residual stresses of Q690 welded I-shaped sections after fire exposure will be determined experimentally using the sectioning method. Similar to the study on mechanical properties carried out in phase one, temperature and cooling method will be the two main parameters used in this phase of the study. Furthermore, the effect of section dimensions will be considered. In particular, a comparison of how the width-to-thickness ratios of the component elements could affect the magnitude and distribution of residual stress will be studied.

3.3 Cyclic Behavior of Post-fire Q690 Welded I-shaped Columns

In the last phase of this research, the energy dissipation capacity loss of Q690 welded I-shaped columns under cyclic load after fire exposure will be determined. Based on another researcher's experimental results of cyclic test on I-shaped columns, a Finite Element Model (FEM) is developed, validated and calibrated for use in a parametric study. The main variables used here are mechanical properties determined in the first phase of this research. The FEM is used to estimate the energy dissipation capacity loss of Q690 welded I-shaped columns after fire exposure.

Details of the experimental and numerical work carried out in this research will be discussed in subsequent chapters.

4 POST-FIRE MECHANICAL PROPERTIES OF Q690 STEEL

In this chapter, the post-fire mechanical properties of Q690 high strength steel will be obtained experimentally. Empirical equations that can be used to determine the mechanical properties of Q690 steel will also be proposed.

4.1 Introduction

Historical events have demonstrated that fire hazard is a major threat to the integrity of a civil structure throughout its service life. Although most steel frame structures can withstand fire and exhibit no visible structural damage after fire exposure, post-fire structural elements may experience mechanical changes as well as permanent deformations. These changes need to be quantified in order to evaluate the post-fire performance of steel structures. With the rapid development and an increased use of high strength and ultra-high strength steels in high-rise buildings, long-span bridges, and other special structural elements such as hollow corrugated columns [57], concrete-filled double skin columns [58] and hybrid compression members [59], researchers have turned their attention to investigating the post-fire behavior of these steels. In this phase, simple tension tests are used to determine the post-fire mechanical properties of a specific type of high strength steel (Q690) under different temperature exposure, heating, cooling and loading conditions. The post-fire mechanical properties commonly used in the design of civil structures to be determined in the present test series include stress-strain curves, elastic moduli (a measure of stiffness), yield and tensile stresses (a measure of strength). Fracture strain, which is a measure of ductility, will also be determined and reported. The main variables considered here are the level of temperature and cooling methods used. The temperature to which the test specimens will be exposed ranges from 300°C to 900°C, and two cooling methods – natural air and submersion in water – will be used to study if different manners of cooling will have an effect on the post-fire mechanical properties of Q690 steel. In addition, two different heating rates will be used to determine if the rate of heating will have an effect on the mechanical properties. To investigate the effect of repeated heating and cooling, specimens that have undergone two cycles of heating and cooling will be tested. Moreover, since the mechanical properties will likely be affected by the initial loading condition [60], specimens subjected to different load magnitudes during the heating and cooling cycle will be tested.

Using these test data, empirical equations will be proposed to estimate the post-fire mechanical properties of Q690 steel. Furthermore, comparison of test results obtained in the present study with those reported by other researchers for steels with a nominal yield stress of 690 MPa and other lower grade steels commonly used in structural applications will be made to highlight the effects of steel grades and chemical compositions on the post-fire mechanical properties of steel.

4.2 Test Method

Tensile tests are most commonly used to determine the mechanical properties of materials. In order to study the post-fire mechanical properties of Q690 steel, the specimens were heated to a pre-determined temperature from 300°C to 900°C in 100°C increment. They were then cooled to room temperature (20°C) using air or water. In the air cooling method, the specimens were allowed to cool slowly in air. In the water quenching method, the specimens were quickly dipped in water maintained at room temperature. Air cooling is a general cooling method used by a number of researchers. It is relatively easy to perform. However, water cooling is more realistic as it can simulate the condition when water is being splashed on structural members in the process of putting out a fire. After the specimens were cooled, a strain-controlled tensile load was applied to the specimens until failure. To cover as many different scenarios as possible and to avoid cost overrun, only one test was performed for each combination of test parameters. A test was repeated only if it failed or if the test result was deemed unacceptable.

4.3 Test Material and Specimens

All test specimens were cut from a quenched and tempered Q690 steel sheet with a nominal thickness of 12 mm. The letter Q is the Chinese phonetic alphabet of the word “Qu” which means the yield strength of steel, and 690 is the nominal steel yield strength in MPa. Table 4-1 shows the alloying elements of the Q690 steel used for the tests. The steel was produced by Nanjing Iron & Steel Co. Ltd.

Table 4-1 Alloying Elements of Q690 Steel (wt%)

Chemical Element	C	Si	Mn	P	S	Ti	Cr	Mo	CEV*	Ni	Cu	B
Q690	0.14	0.23	1.38	0.011	0.001	0.012	0.27	0.15	0.46	0.01	0.01	0.0016

*CEV denotes Carbon Equivalent Value.

The dimensions of the specimens are in accordance with ASTM standard E8/E8M-16a [46] and are shown in Figure 4-1 and Table 4-2. The gauge length of the specimens is denoted as G. All strains are calculated based on this gauge length.

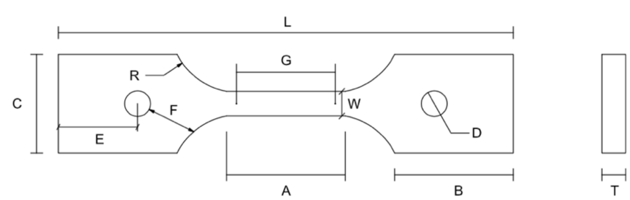

Figure 4-1 Dimensions of the Test Specimens

Figure 4-2 Photo of the Test Specimens

Table 4-2 Dimensions of the Test Specimens in Comparison with ASTM E8/E8M

	G (mm)	W (mm)	T (mm)	R (mm)	L (mm)	A (mm)	B (mm)	C (mm)	D (mm)	E (mm)	F (mm)
ASTM E8/E8M	50	12.5	≤16	≥13	≥200	≥57	≥50	50	≥13	40	≥13
Specimen	50	12.5	12	35	230	60	60	50	13	40	25

4.4 Test Procedure

The test specimens were heated in a temperature-controlled electrical furnace (Model AI-518P manufactured by YUDIAN Automation Technology) shown in Figure 4-3 at pre-determined heating rates to the target temperature. Seven elevated temperatures – 300°C, 400°C, 500°C, 600°C, 700°C, 800°C and 900°C – were used. Temperature below 300°C was not used because it had been shown to have negligible effect on post-fire performance [22]. Once the pre-determined elevated temperature was reached, a 10-minute holding time was maintained to achieve uniform temperature throughout the specimens. This uniform temperature condition is said to have been reached when the thermocouples mounted on the top and bottom of a temperature specimen (as shown in Figure 4-4) both show target temperatures that are within a few degrees of each other. This temperature specimen was placed side-by-side with each test specimen during the heating and cooling process. Because the surrounding and heating conditions were the same for this temperature and the adjacent test specimen, the temperature of the test specimen was taken as the temperature recorded for the temperature specimen. By using this temperature specimen, the test procedure can be simplified and the testing time reduced since it is not necessary to mount and calibrate the thermocouples for each of the test specimen.

Also shown in Figure 4-4 is the temperature data acquisition system (model MIK-RX9600 manufactured by Hangzhou Meacon Automation Technology) used in this research.

Figure 4-3 Temperature-controlled Electrical Furnace

To achieve test condition comparable to that of other researchers, the test specimens were then cooled down to ambient temperature (20°C) and sat for at least 48 hours before tensile tests were performed. All specimens were tested to failure under tension. For purpose of comparison, tensile test was also performed on a specimen that had not been exposed to elevated temperature. All tensile tests were carried out using an electric universal testing machine (Model SANS CMT5605 manufactured by MTS Systems) shown in Figure 4-5. The tests were performed at a fixed strain rate of 0.005/min per ASTM E21-09 [20]. The data were collected using a data acquisition system and the load-displacement diagram were generated automatically by the built-in software of the electric universal testing machine. For strains less than or equal to 1.5%, the displacement from which strain is calculated was measured by an extensometer. When the strains exceeded 1.5%, the displacement was obtained from the movement of the actuator.

(a)

(b)

Figure 4-4 (a) Temperature Specimen and (b) Temperature Data Acquisition

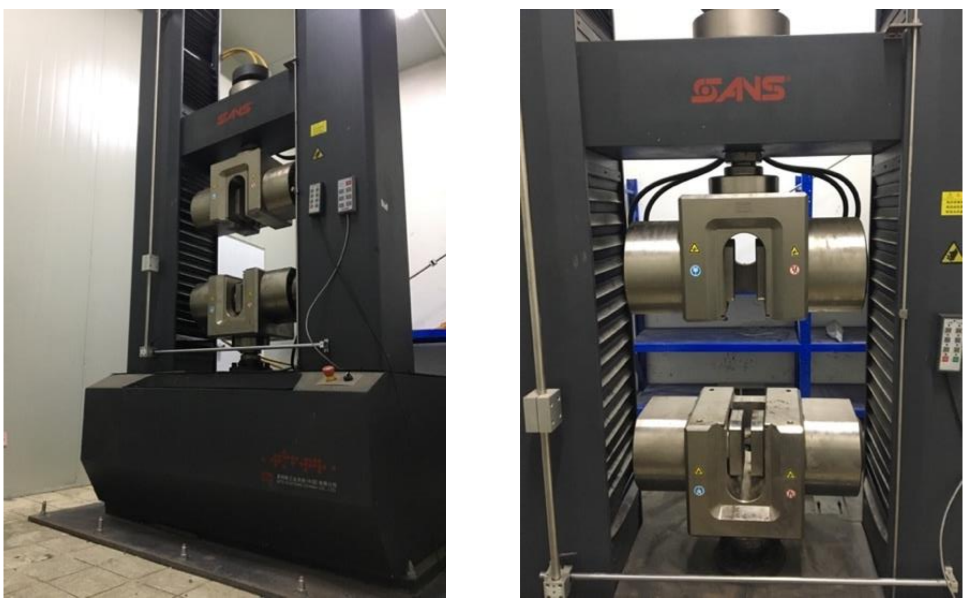

Figure 4-5 Electric Universal Testing Machine

The first set of tests aims to investigate how temperature and cooling methods will affect the post-fire mechanical properties of Q690 high strength steel. A total of 15 tests (14 as summarized in Table 4-3 plus one reference specimen that had not been exposed to any elevated temperature) were performed. In general, the specimens are labeled as: the letter H means the specimen is heated only once; the number that follows the letter H denotes the heating rate used (1 means the heating rate used is 10°C/min, 2 means the heating rate used is 20°C/min, and 3 means the ISO heating protocol is used); the letter T means test; the number after the letter T denotes the temperature to which the specimen is heated (e.g., 3 means the specimen is heated to 300°C); and the letter A or W denotes air or water cooling, respectively.

Table 4-3 Tensile Test Specimens Used for Different Cooling Methods

Specimen	Heating Rate	Heated Temperature (°C)	Cooling Method
H1T3A	10°C/min	300	Air
H1T4A		400	Air
H1T5A		500	Air
H1T6A		600	Air
H1T7A		700	Air
H1T8A		800	Air
H1T9A		900	Air
H1T3W		300	Water
H1T4W		400	Water
H1T5W		500	Water
H1T6W		600	Water
H1T7W		700	Water
H1T8W		800	Water
H1T9W		900	Water

The second set of tests involves using two different heating rates: 20°C/min and ISO 834 (as shown in Figure 4-6). Table 4-4 shows the air cooling tests for both the 20°C/min and ISO 834 heating rates, and Table 4-5 shows the water quenching tests for the two heating rates.

The heating rate can be obtained by taking derivative of Eq. (1.1) as

$$\frac{dT}{dt} = \frac{1200}{8t+1} \tag{4.1}$$

From Eq. (4.1), it can be seen that heating rate of the ISO 834 fire curve is higher than 20°C/min and 10°C/min for target temperatures below 633°C and 737°C, respectively.

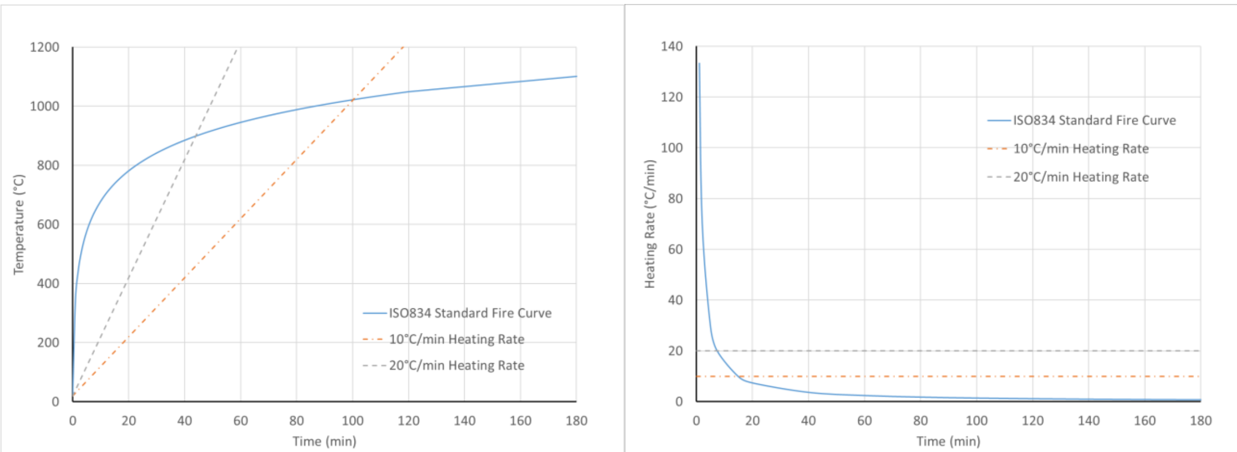

(a) Temperature vs. Time **(b) Heating Rate vs. Time**

Figure 4-6 ISO-834 Time-temperature Curve [2,3]

Table 4-4 Tensile Test Specimens Used for Different Heating Rates and Air Cooling Method

Specimen	Heating Rate	Heated Temperature (°C)	Cooling Method
H2T3A	20°C/min	300	Air
H2T5A		500	Air
H2T7A		700	Air
H2T9A		900	Air
H3T3A	ISO834	300	Air
H3T5A		500	Air
H3T7A		700	Air
H3T9A		900	Air

Table 4-5 Tensile Test Specimens Used for Different Heating Rates and Water Quenching Method

Specimen	Heating Rate	Heated Temperature (°C)	Cooling Method
H2T3W	20°C/min	300	Water
H2T5W		500	Water
H2T7W		700	Water
H2T9W		900	Water
H3T3W	ISO834	300	Water
H3T5W		500	Water
H3T7W		700	Water
H3T9W		900	Water

In actual situations, a structure may undergo non-destructive fire hazards more than once. This means the steel members could experience more than one cycle of heating and cooling. To investigate the effect of repeated heating and cooling on mechanical properties, specimens subjected to two cycles of heating and cooling were tested. Thus, the third set of tests involves the use of six specimens subjected to repeated heating and cooling. They are summarized in Table 4-6.

Table 4-6 Tensile Test Specimens Used for Repeated Heating with Different Cooling Methods

Specimen*	Heating Rate	Heated Temperature (°C)	Cooling Method
R1T5A	10°C/min	500	Air
R1T7A		700	Air
R1T9A		900	Air
R1T5W	10°C/min	500	Water
R1T7W		700	Water
R1T9W		900	Water

*The letter R denotes repeated heating and cooling.

Because the loading condition of the specimens could affect their post-fire mechanical properties, the fourth set of tests involves subjecting the test specimens to four different axial tensile load ratios from $0.2P_y$ to $0.5P_y$ (where $P_y = F_yA$, in which F_y=690 MPa is the nominal yield stress of Q690 steel and A= 150 mm^2 is the area of cross-section) during the heating and cooling cycle. The heating rate used ranged from 10 to 20°C/min and air cooling was used. The force was removed from the specimens after the heating/cooling cycle, and the specimens were allowed to rest for at least 48 hours before the test began. Seven specimens as shown in Table 4-7 were tested in this test series. For this test set, a high-temperature testing machine, Model CM-RDC Series as shown in Figure 4-7 manufactured by China Mechanical Testing Equipment was used, and thermocouples were placed on each specimen to record the temperature directly.

Table 4-7 Tensile Test Specimens under Different Axial Tensile Loads

Specimen*	Heated Temperature (°C)	Axial Tensile Load (L_t)	Cooling Method
L2T3A	300	$0.2P_y$	Air
L2T4A	400		
L2T5A	500		
L2T6A	600		
L3T3A	300	$0.3P_y$	
L4T3A	300	$0.4P_y$	
L5T3A	300	$0.5P_y$	

*The letter L means the specimens are being loaded during the heating and cooling cycle; the number that follows the letter L denotes the magnitude of the applied load (e.g., 2 means a load of $0.2P_y$ is applied).

Figure 4-7 Heating with Axial Tensile Load

4.5 Experimental Results

4.5.1 Test Set 1 – Effect of the Two Cooling Methods

For the first test set, the post-fire mechanical properties of Q690 steel under air cooling and water quenching were determined. As shown in Table 4-3, two series of test specimens with seven specimens per series were used. They were heated to an elevated temperature that varied from 300°C to 900°C in 100°C increment.

4.5.1.1 Visual Observations

Figure 4-8 shows the post-fire surface conditions of the air versus water cooled specimens heated to different pre-determined temperatures with a heating rate of 10°C/min. It can be seen that the color on the surface of the specimens is changed after fire exposure. For specimens heated to 300°C, the color of the air-cooled specimen is dark brown with a bit of red while the color of the water-cooled specimen is brown with some yellow. For specimens exposed to 400 and 500°C heat, the color of the air-cooled specimens is silver with some metallic luster while the color of the water-cooled specimens is darker with rust. For specimens exposed to over 600°C temperature, the color of all specimens is dark blue with no metallic luster, and gets darker with increasing temperature exposure. In addition, when the exposed temperature is over 700°C, a thin layer of loose iron hydroxide deposits which flakes off easily is seen on the surface of the water-cooled specimens.

10°C/min AIR COOLING

10°C/min WATER COOLING

Figure 4-8 Post-fire Surface Conditions of the Specimens Using Different Cooling Methods

4.5.1.2 Temperature-time Curves

Figure 4-9 shows the temperature-time curves for the furnace, the measured temperature of the top and bottom thermocouples for the specimens being heated and cooled using the air cooling and water quenching methods, and the reference 10°C/min reference heating curve. It can be seen that while the heating rate is almost constant at 10°C/min, the air-cooled specimens experience a gradual decrease in temperature (the rate of decrease is higher in the beginning but slower towards the end with an average value of about 23°C/min) while the water-cooled specimens undergo a dramatic drop in temperature (approximately 3400°C/min) when they are quenched in water.

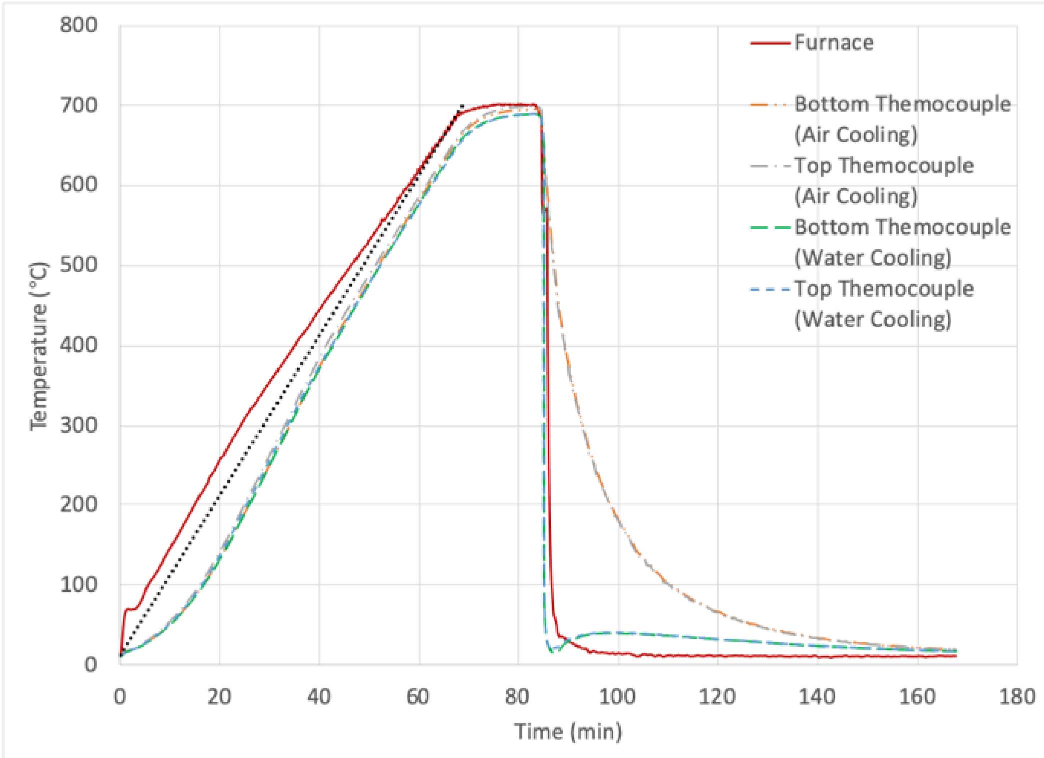

Figure 4-9 Typical Temperature-time Curve for Air Cooling and Water Cooling

4.5.1.3 Stress-strain Relationships

After the specimens are exposed to elevated temperature and cooled using either the air cooling or water quenching method, they were tested to failure under tension. The engineering stress-strain curves for these specimens obtained from the measured load-displacement data, recorded automatically by the built-in software from the extensometer (for strains ≤1.5%) and movement of the actuator (for strains >1.5%), are plotted in Figures 4-10 and 4-11 for the air cooling and water quenching methods, respectively. For both the air-cooled and water-cooled specimens, when compared with the reference specimen that has not been exposed to elevated temperature, the deviation from linearity is delayed for specimens that have been exposed to an elevated temperature at or below 700°C, but accelerated at temperature above 700°C. In addition, when the exposed temperature is in the range 250-400°C, tempered martensite embrittlement [61,62] or "blue brittleness" occurs, which slightly increases the post-fire yield strength of steel regardless of the cooling method used. Otherwise, for the air-cooled specimens, the yield strength and to a certain extent the tensile strength both decrease with increasing exposed temperature. For the water-cooled specimens, while the yield strength decreases with increasing exposed temperature, the tensile strength for the specimen heated to 900°C is much higher. This is because when steel is heated above its austenitic temperature (about 723°C) and cooled rapidly (i.e., quenched), martensite will form which makes steel much harder and stronger but becomes less ductile.

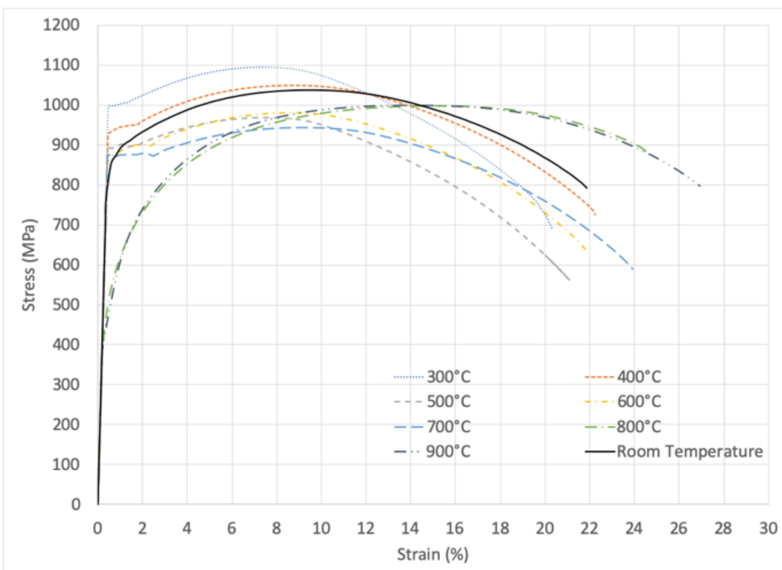

Figure 4-10 Stress-strain Curves for Post-fire Q690 Steel (Air Cooling)

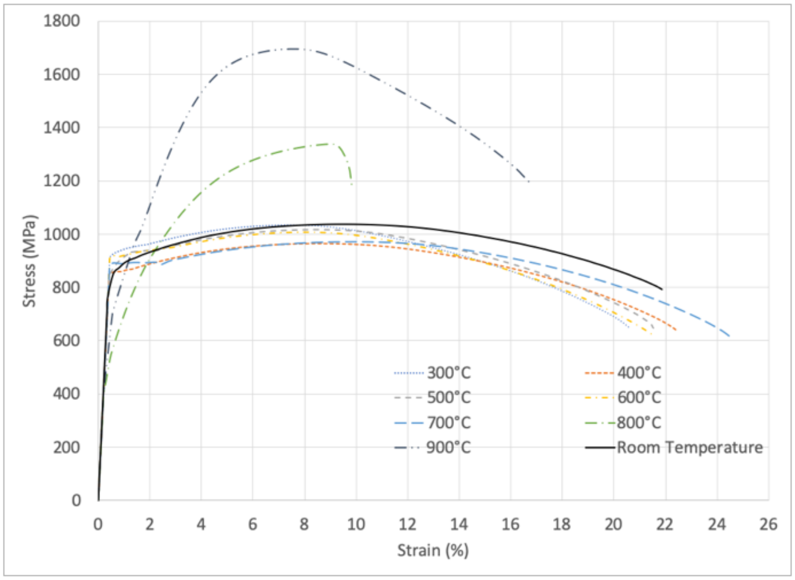

Figure 4-11 Stress-strain Curves for Post-fire Q690 Steel (Water Cooling)

4.5.1.4 Mechanical Properties

The post-fire mechanical properties of Q690 steel are obtained from the engineering stress-strain curves. With reference to Figure 4-12, the elastic modulus is calculated based on the initial slope of the stress-strain curve. However, because the yield plateau is not always apparent, the 0.2% offset method is used to obtain the yield strength. The 0.2% yield strength is obtained as the stress where a line parallel to the initial slope of the stress-strain curve drawn from a strain of 0.2% intersects with the stress-strain curve. The tensile strength is obtained as the peak point of the stress-strain curve, and the fracture strain is obtained as the strain when the specimen fractures under tension. The mechanical properties of Q690 steel so obtained are summarized in Tables 4-8 and 4-9 for both cooling methods.

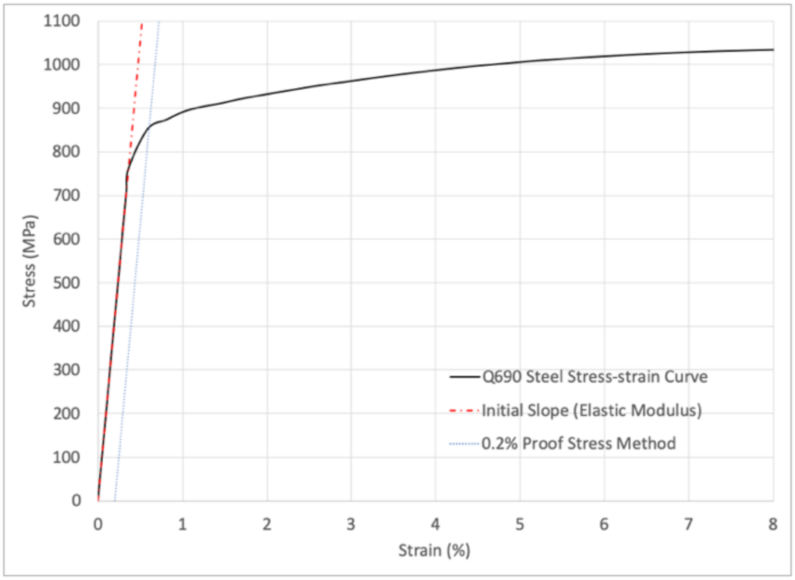

Figure 4-12 Determination of Elastic Modulus and 0.2% Offset Yield Strength

Table 4-8 Post-fire Mechanical Properties of Q690 Steel (Air Cooling)

Temperature (°C)	Elastic Modulus E_T (GPa)	Yielding Strength $F_{y,T}$ (MPa)	Tensile Strength $F_{u,T}$ (MPa)	Fracture Strain ε_T (%)
20	210.5	866	1037	21.86
300	217.4	915	1094.4	20.33
400	203.9	910	1049	20.44
500	199.6	815	968	20.68
600	199.5	685	980.4	20.64
700	205.4	635	943	20.63
800	196.8	505	997.6	24.55
900	193.7	461	999.2	26.64

Table 4-9 Post-fire Mechanical Properties of Q690 Steel (Water Quenching)

Temperature (°C)	Elastic Modulus E_T (GPa)	Yielding Strength $F_{y,T}$ (MPa)	Tensile Strength $F_{u,T}$ (MPa)	Fracture Strain ε_T (%)
300	205.0	880	1034.2	20.63
400	201.9	852	964.7	22.45
500	196.7	865	1017.1	21.53
600	206.0	738	1007.5	21.5
700	201.9	562	971.4	24.6
800	196.4	540	1337.9	9.84
900	201.4	705	1694.8	16.77

4.5.2 Test Set 2 – Effect of Different Heating Rates

Although it has been demonstrated that the cooling rate affects the post-fire mechanical properties of Q690 steel, the effect of heating rate has not been carefully studied. This test set was therefore designed to study the effect of the heating rate. For this test set, four series of four specimens per series were tested. The first series of tests used 20°C/min heating rate with air cooling. The second series used 20°C/min heating rate with water quenching. The third series used ISO 834 heating rate (see Figure 4-6) with air cooling, and the last series uses ISO 834 heating rate with water quenching. The exposed temperature was from 300°C to 900°C in 200°C increment.

4.5.2.1 Visual Observations

From Figures 4-13 and 4-14, it can be seen that the different heating rates do not appear to have a significant effect on the surface condition of the specimens. However, for those specimens exposed to 300°C using 20°C/min heating rate, the color is metallic blue for both the air cooling and water cooling methods.

20°C/min AIR COOLING

20°C/min WATER COOLING

Figure 4-13 Post-fire Surface Conditions of the Specimens (20°C/min Heating Rate)

Figure 4-14 Post-fire Surface Conditions of the Specimens (ISO 834 Heating Rate)

4.5.2.2 Stress-strain Relationships

The engineering stress-strain curves obtained for Q690 steel heated using the two heating protocols and cooled using air and water are shown in Figures 4-15 to 5-18. For specimens subjected to the 20°C/min heating rate, regardless of whether they are air or water cooled, the deviation from linearity occurs earlier and the yield strength is lower as the exposed temperature is increased. However, the tensile strength for the water cooled specimen heated to 900°C is much higher than the other specimens due to martensite formation as a result of rapid cooling after the austenitic temperature has been reached.

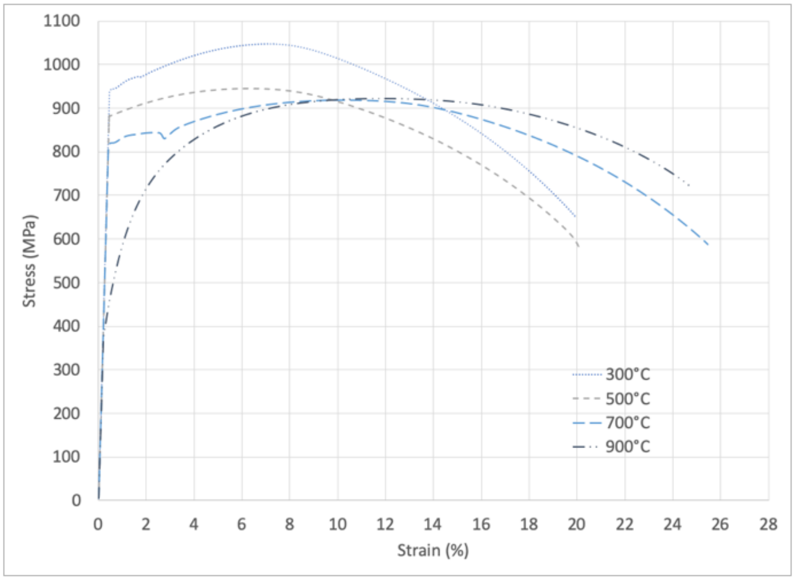

Figure 4-15 Stress-strain Curves for Post-fire Q690 Steel (20°C/min Heating and Air Cooled)

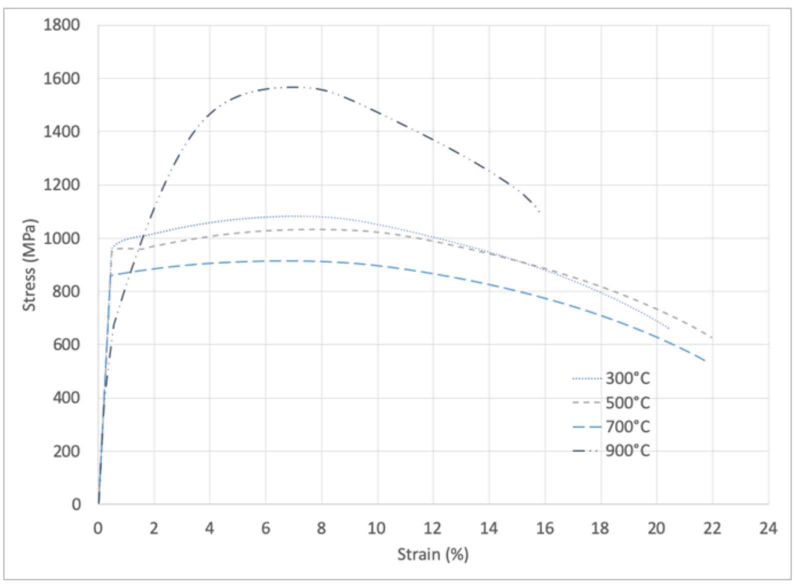

Figure 4-16 Stress-strain Curves for Post-fire Q690 Steel (20°C/min Heating and Water Cooled)

For specimens subjected to the ISO 834 heating protocol using a heating rate as expressed in Eq. (4.1), the stress-strain behavior is similar to the specimens subjected to the 20°C heating rate, except that the yield strength appears to be slightly lower.

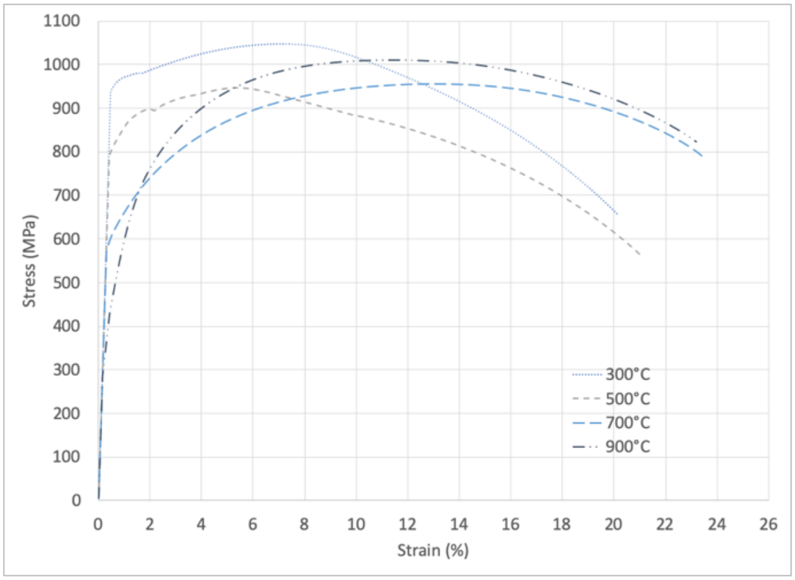

Figure 4-17 Stress-strain Curves for Post-fire Q690 Steel (ISO 834 Heating and Air Cooled)

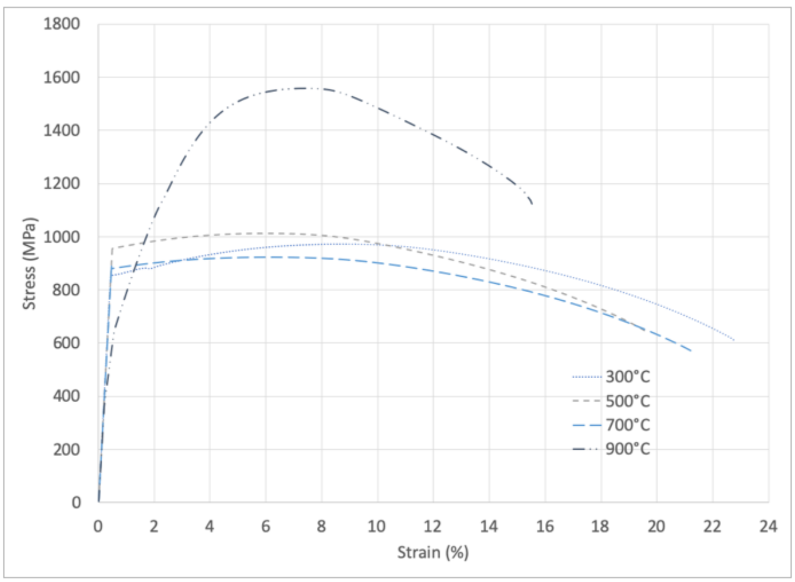

Figure 4-18 Stress-strain Curves for Post-fire Q690 Steel (ISO 834 Heating and Water Cooled)

4.5.2.3 Mechanical Properties

Tables 4-10 to 4-13 show the post-fire mechanical properties of Q690 Steel for the four different test conditions. A slight decrease in yield strength and elastic modulus is observed when the ISO 834 heating protocol is used.

Table 4-10 Post-fire Mechanical Properties of Q690 Steel (20°C/min Heating and Air Cooled)

Temperature (°C)	Elastic Modulus E_T (GPa)	Yielding Strength $F_{y,T}$ (MPa)	Tensile Strength $F_{u,T}$ (MPa)	Fracture Strain ε_T (%)
300	207.7	858	1047	19.94
500	200.3	785	944.4	20.08
700	200.5	643	918.8	25.48
900	186.8	457	922	24.43

Table 4-11 Post-fire Mechanical Properties of Q690 Steel (20°C/min Heating and Water Cooled)

Temperature (°C)	Elastic Modulus E_T (GPa)	Yielding Strength $F_{y,T}$ (MPa)	Tensile Strength $F_{u,T}$ (MPa)	Fracture Strain ε_T (%)
300	206.1	831	1081.7	20.43
500	201.2	841	1034.3	21.96
700	202.9	596	915.6	21.72
900	196.3	674	1567.2	15.86

Table 4-12 Post-fire Mechanical Properties of Q690 Steel (ISO 834 Heating and Air Cooled)

Temperature (°C)	Elastic Modulus E_T (GPa)	Yielding Strength $F_{y,T}$ (MPa)	Tensile Strength $F_{u,T}$ (MPa)	Fracture Strain ε_T (%)
300	203.0	799	1046.6	20.14
500	192.9	691	947	21.06
700	189.8	571	956.2	23.4
900	189.8	429	1010.4	23.2

Table 4-13 Post-fire Mechanical Properties of Q690 Steel (ISO 834 Heating and Water Cooled)

Temperature (°C)	Elastic Modulus E_T (GPa)	Yielding Strength $F_{y,T}$ (MPa)	Tensile Strength $F_{u,T}$ (MPa)	Fracture Strain ε_T (%)
300	200.9	739	971.9	22.75
500	195.2	696	1011.4	19.61
700	192.5	602	923.7	21.36
900	180.6	646	1558.5	15.52

4.5.3 Test Set 3 – Effect of Repeated Heating and Cooling

Given its long design life, a structure may undergo non-destructive fire hazards more than once. This means steel members could undergo more than one heating and cooling cycle during their life time. For this test set, specimens were subjected to two cycles of heating and cooling at certain pre-determined temperatures to determine if repeated heating and cooling would have an effect on mechanical properties. The tests consist of two series of three specimens each. While the same heating rate of 10°C/min was used for both series, air cooling was used for one series and water quenching was used for the other. The exposed temperature ranges from 500°C to 900°C in 200°C increment. 300°C was not used in this test set because its effect on post-fire mechanical properties is not as significant.

4.5.3.1 Visual Observations

Regardless of whether the specimens are air or water cooled, their post-fire surface conditions after two cycles of heating and cooling are consistent with those subjected to only one cycle of heating and cooling. The only difference is that more rust is observed.

TWICE AIR COOLING　　TWICE WATER COOLING

Figure 4-19 Post-fire Surface Conditions of Specimens after Repeated Heating/Cooling

4.5.3.2 Stress-strain Relationships

The stress-strain curves for this test set are shown in Figures 4-20 and 4-21. Compared to the specimens subjected to just one cycle of heating and cooling, some decrease in mechanical properties are observed. The local peak stress observed for specimens subjected to a temperature of 500°C and 700°C is a manifestation of the Portevin-Le Chatelier (PLC) effect due to dynamic strain aging [63,64]. This phenomenon has been observed for materials like steel that have a mix of fcc and bcc crystal structures within a certain temperature range. The PLC effect occurs when dislocation movement is temporarily arrested when obstacles such as interstitial particles are present in the dislocation paths. However, with sufficient stress these dislocations will overcome the obstacles. Also, for the water-cooled specimens heated to 900°C, the martensite strengthening effect is once again observed.

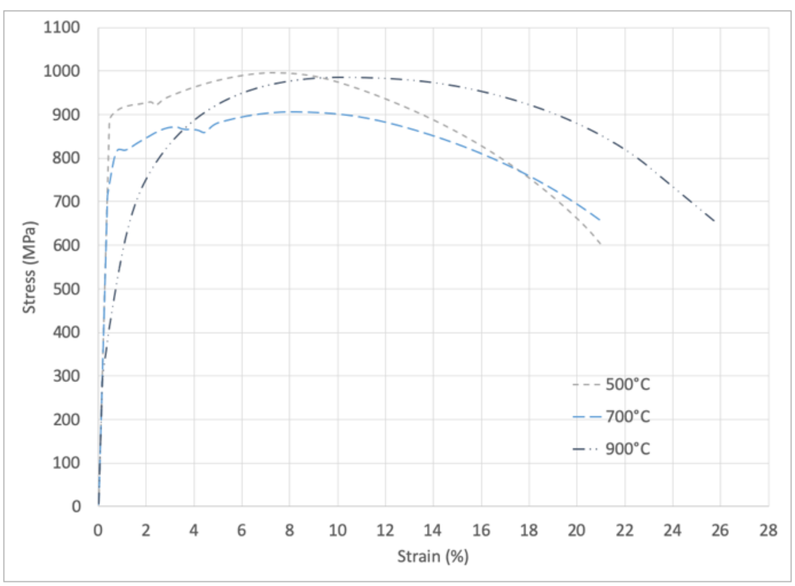

Figure 4-20 Stress-strain Curves for Post-fire Q690 Steel with Repeated Heating and Air Cooling

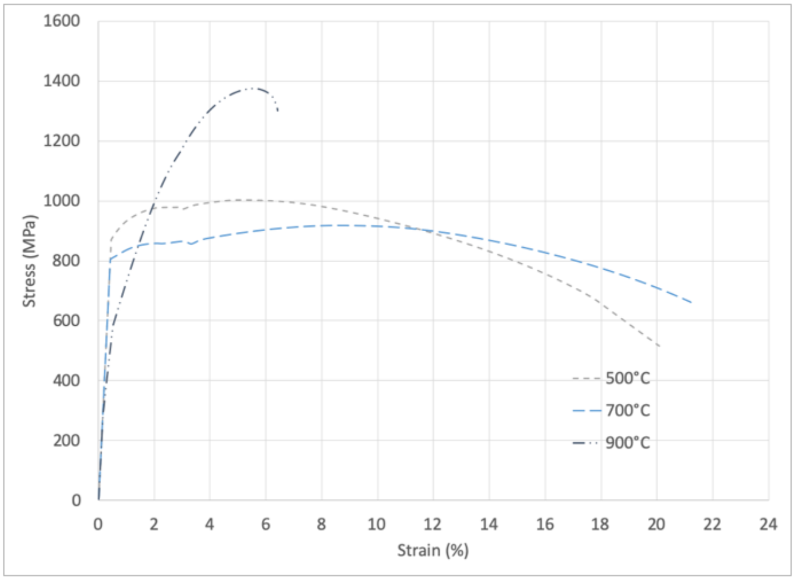

Figure 4-21 Stress-strain Curves for Post-fire Q690 Steel with Repeated Heating and Water Cooling

4.5.3.3 Mechanical Properties

Tables 4-14 and 4-15 show the post-fire mechanical properties of Q690 steel after two cycles of heating and cooling under air cooled and water cooled conditions, respectively. When compared to the mechanical properties given in Tables 4-8 and 4-9, it can be seen that almost all the measured mechanical properties show lower values. However, the effect on elastic modulus and yield strength is more noticeable. The deterioration of mechanical properties after repeated heating and cooling is the result of the formation of microcracks in steel [65,66].

Table 4-14 Post-fire Mechanical Properties of Q690 Steel with Repeated Heating and Air Cooling

Temperature (°C)	Elastic Modulus E_T (GPa)	Yielding Strength $F_{y,T}$ (MPa)	Tensile Strength $F_{u,T}$ (MPa)	Fracture Strain ε_T (%)
500	197.9	726	996.6	20.95
700	193.5	564	906.3	20.93
900	189.1	398	985.7	26.04

Table 4-15 Post-fire Mechanical Properties of Q690 Steel with Repeated Heating and Water Cooling

Temperature (°C)	Elastic Modulus E_T (GPa)	Yielding Strength $F_{y,T}$ (MPa)	Tensile Strength $F_{u,T}$ (MPa)	Fracture Strain ε_T (%)
500	193.2	718	1003.9	20.08
700	191.6	508	919.2	21.20
900	185.7	583	1374.9	6.42

4.5.4 Test Set 4 – Effect of Load Condition

For this test set, a total of seven specimens as shown in Table 4-7 were tested. For the first test series, an axial tensile load equal to 20% of the nominal yield strength of Q690 steel (i.e., $0.2F_y$) was applied to all the specimens while they were being heated to temperature that ranges from 300°C to 600°C in 100°C increment. According to Qiang's research on S690 (yield strength is 690 MPa) steel at elevated temperatures and after fire exposure [17,22], the steel will lose about 63% of its mechanical properties at 600°C and regain some of its properties upon cooling. The tests were conducted only for temperatures in the 300°C to 600°C to avoid pre-mature failure during the heating and cooling cycle. For the second test series, the exposed temperature was set at 300°C while an axial tensile load that ranges from $0.2P_y$ to $0.5P_y$ was applied to the specimens. A heating rate of 10-20°C/min and air cooling were used for all specimens.

The displacement-time-axial load and displacement-time-temperature curves plotted for the heating and cooling phases of a specimen subjected to a constant axial load of $0.2P_y$ heated to a target temperature of 400°C are shown in Figure 4-22. Since the mechanical properties of Q690 steel decrease under heat and recover slowly when cooled, the displacement of the actuators first increases with time during the heating phase, then decreases with time during the cooling phase. It can be seen that the displacement-time curve shown in the right matches rather closely with the temperature-time curve. In addition, it should be noted that throughout the entire heating and cooling process, the specimen remains elastic.

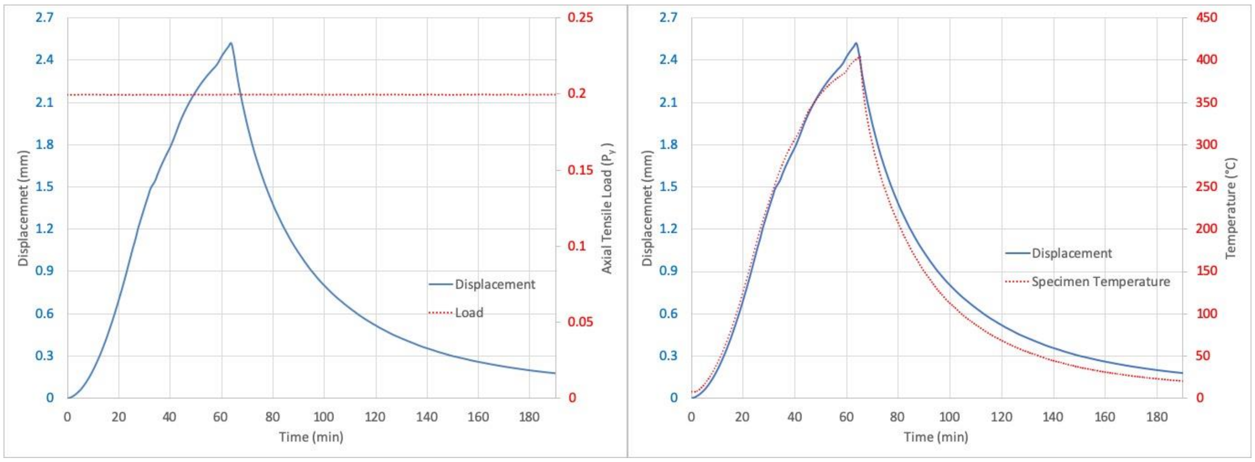

(a) **(b)**

Figure 4-22 (a) Typical Displacement-Time-Axial load Curve and (b) Typical Displacement-Time-Temperature Curve

4.5.4.1 Visual Observations

The post-fire surface conditions of the tested specimens are shown in Figure 4-23. It can be seen that they are not particularly affected by the applied axial tensile load magnitudes.

L_t=0.2P_y
AIR COOLING

300°C
AIR COOLING

Figure 4-23 Post-fire Surface Conditions of Specimens Subjected to Different Axial Tensile Loads

4.5.4.2 Stress-strain Relationships

The stress-strain curves for these two test series are shown in Figure 4-24 and Figure 4-25 respectively. Upon comparison with Figure 4-10, it can be observed that the elastic modulus, yield strength, tensile strength and ductility (fracture strain of the specimen at failure) of the specimens are all smaller when an applied load is present during the heating and cooling process. The combined action of heat and stress enhances dislocation movement, which leads to these reductions.

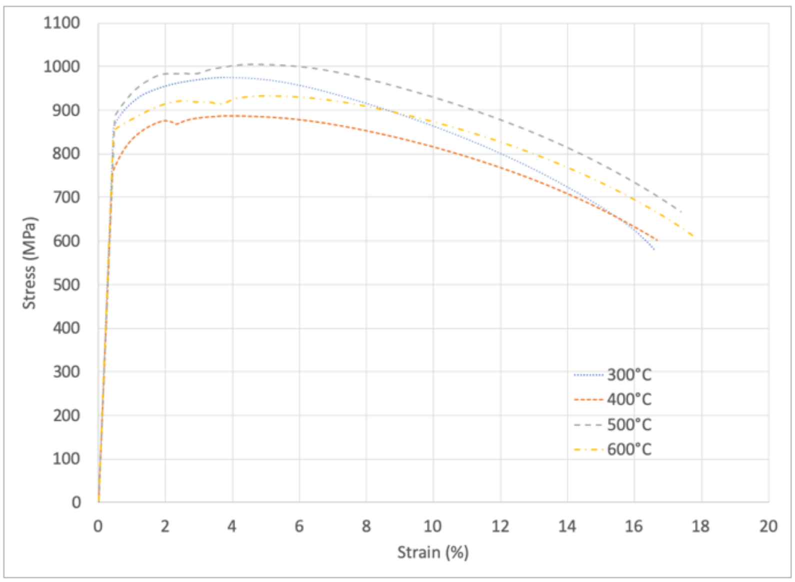

Figure 4-24 Stress-strain Curves for Post-fire Q690 Steel (0.2P_y)

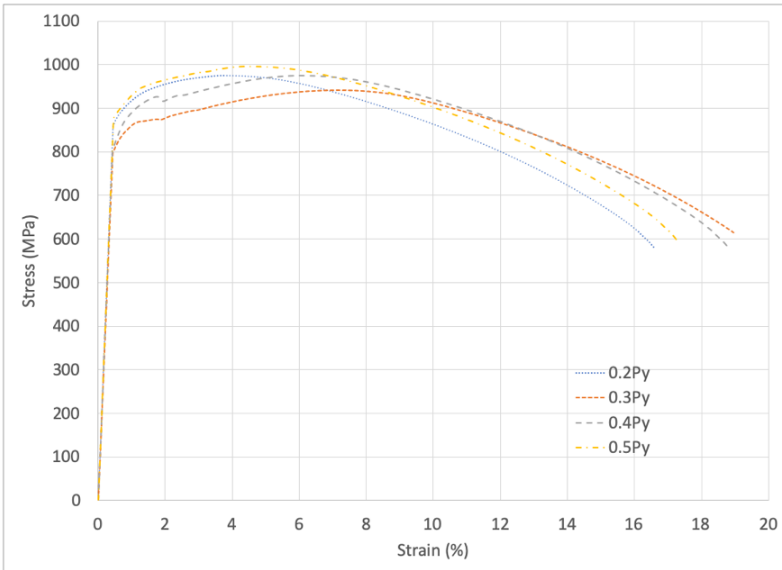

Figure 4-25 Stress-strain Curves for Post-fire Q690 Steel (300°C)

4.5.4.3 Mechanical Properties

Table 4-16 shows the post-fire mechanical properties of Q690 steel for different temperature exposures under an applied axial tensile load of $0.2P_y$ and Table 4-17 shows the post-fire mechanical properties of Q690 steel for different applied axial tensile load magnitudes when the exposed temperature is 300°C. Note that all these values are smaller than the corresponding values given in Table 4-8.

Table 4-16 Post-fire Mechanical Properties of Q690 Steel ($0.2P_y$ Axial Tensile Load)

Temperature (°C)	Elastic Modulus E_T (GPa)	Yielding Strength $F_{y,T}$ (MPa)	Tensile Strength $F_{u,T}$ (MPa)	Fracture Strain ε_T (%)
300	195.0	746	975.1	16.59
400	183.8	709	887.2	16.67
500	184.1	691	1004.5	17.38
600	191.3	574	932.3	17.86

Table 4-17 Post-fire Mechanical Properties of Q690 Steel (300°C Temperature Exposure)

Axial Tensile Load (P_y)	Elastic Modulus E_T (GPa)	Yielding Strength $F_{y,T}$ (MPa)	Tensile Strength $F_{u,T}$ (MPa)	Fracture Strain ε_T (%)
0.2	191.0	746	975.1	16.59
0.3	185.3	715	942.4	18.97
0.4	191.1	723	974.3	18.82
0.5	193.1	764	995.8	17.25

4.6 Results Comparison

In this section, the experimental results obtained from the four test sets described in the preceding sections are compared. Based on this comparison, modification factors (summarized in Tables 4-18 and 4-19) will be developed and empirical equations will be proposed to account for the effects of the various parameters being studied here will have on the mechanical properties of Q690 high strength steel.

Table 4-18 Modification Factors for the Post-fire Mechanical Properties of Q690 Steel under Various Test Conditions

Test Conditions		Elastic Modulus E_T/E_0	Yielding Strength $F_{y,T}/F_{y,0}$	Tensile Strength $F_{u,T}/F_{u,0}$	Fracture Strain $\varepsilon_T/\varepsilon_0$
Temperatures (°C)	Heating and Cooling Methods				
300	10°C/min Heating Rate with Air Cooling	1.033	1.057	1.055	0.930
400		0.969	1.051	1.012	0.935
500		0.948	0.941	0.933	0.946
600		0.948	0.791	0.945	0.944
700		0.976	0.733	0.909	0.944
800		0.935	0.583	0.962	1.123
900		0.920	0.532	0.964	1.219
300	10°C/min Heating Rate with Water Cooling	0.974	1.016	0.997	0.944
400		0.959	0.984	0.930	1.027
500		0.934	0.999	0.981	0.985
600		0.979	0.852	0.972	0.984
700		0.959	0.649	0.937	1.125
800		0.933	0.624	1.290	0.450
900		0.957	0.814	1.634	0.767

Table 4-19 Modification Factors for Post-fire Mechanical Properties of Q690 Steel under Various Test Conditions (Cont'd)

Test Conditions		Elastic Modulus E_T/E_0	Yielding Strength $F_{y,T}/F_{y,0}$	Tensile Strength $F_{u,T}/F_{u,0}$	Fracture Strain $\varepsilon_T/\varepsilon_0$
Temperatures (°C)	Heating and Cooling Methods				
300	20°C/min Heating Rate with Air Cooling	0.987	0.991	1.010	0.912
500		0.952	0.906	0.911	0.919
700		0.953	0.742	0.886	1.166
900		0.888	0.528	0.889	1.118
300	20°C/min Heating Rate with Water Cooling	0.979	0.960	1.043	0.935
500		0.956	0.971	0.997	1.005
700		0.964	0.688	0.883	0.994
900		0.933	0.778	1.511	0.726
300	ISO 834 Heating Rate with Air Cooling	0.964	0.923	1.009	0.921
500		0.916	0.798	0.913	0.963
700		0.902	0.659	0.922	1.070
900		0.902	0.495	0.974	1.061
300	ISO 834 Heating Rate with Water Cooling	0.955	0.853	0.937	1.041
500		0.928	0.804	0.975	0.897
700		0.915	0.695	0.891	0.977
900		0.858	0.746	1.503	0.710
500	10°C/min Repeated Heating with Air Cooling	0.940	0.838	0.961	0.959
700		0.919	0.651	0.874	0.957
900		0.898	0.460	0.951	1.191
500	10°C/min Repeated Heating with Water Cooling	0.918	0.829	0.968	0.919
700		0.911	0.587	0.886	0.97
900		0.882	0.673	1.326	0.294
300 (0.2P_y)	10-20°C/min Heating Rate with Air Cooling	0.926	0.861	0.940	0.759
400 (0.2P_y)		0.873	0.819	0.856	0.763
500 (0.2P_y)		0.875	0.798	0.969	0.795
600 (0.2P_y)		0.909	0.663	0.899	0.817
300 (0.2P_y)	10-20°C/min Heating Rate with Air Cooling	0.926	0.861	0.940	0.759
300 (0.3P_y)		0.880	0.826	0.909	0.868
300 (0.4P_y)		0.908	0.835	0.940	0.861
300 (0.5P_y)		0.917	0.882	0.960	0.789

In Tables 4-18 and 4-19, modification factors expressed as ratios of elastic moduli (a measure of stiffness), yield strengths (a measure of strength), tensile strengths (a measure of strength), and fracture strains (a measure of ductility) obtained experimentally for specimens that have been exposed to high temperature to the corresponding values of the reference specimen (i.e., the specimen that has not been exposed to high temperature) are summarized. These modification factors are also plotted in Figures 4-26 to 4-29. Discussion of the four post-fire mechanical properties of Q690 steel tested under various conditions is given in the following sections.

4.6.1 Post-fire Elastic Modulus

For the post-fire elastic modulus, it can be seen from Figure 4-26 that the effects of the type of cooling methods used and the level of exposed temperature are not very significant. The results for specimens with 10°C/min and 20°C/min heating rates are also quite consistent and close to 1. Additionally, when the heating rate follows the ISO 834 standard fire curve, which is much higher than 20°C/min, or when the specimens have undergone repeated heating and cooling, the modification factor decreased gradually to about 0.9.

From Table 4-19, it can be seen that for specimens that are subjected to an axial tensile load, their post-fire elastic modulus is about 90% of that without the applied load when the exposed temperature is above 300°C. The variation is relatively small for different applied load magnitudes, and if the exposed temperature is below 300°C, the effect of axial tensile load on the elastic modulus can probably be neglected.

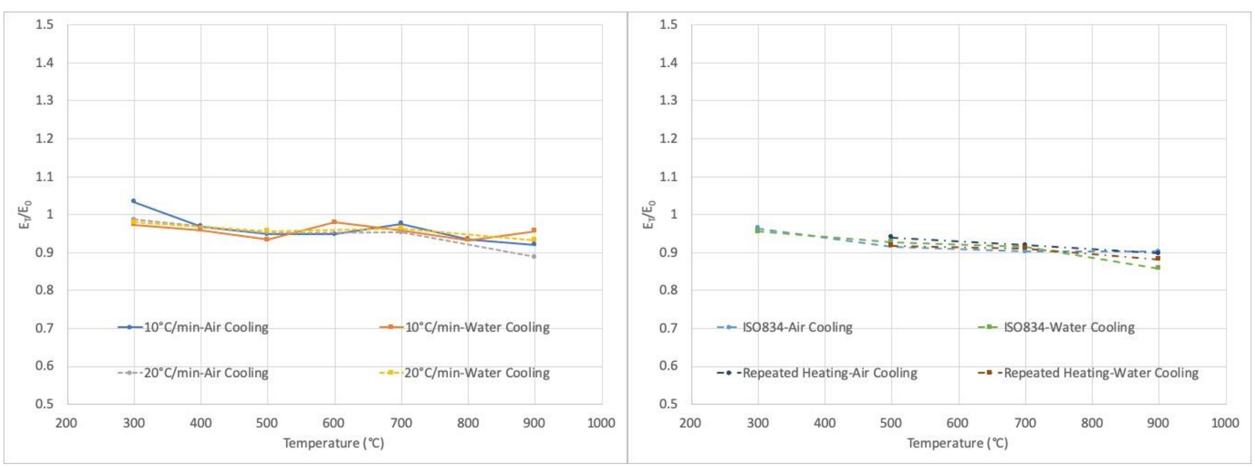

Figure 4-26 Modification Factors for Post-fire Elastic Modulus of Q690 Steel under Various Test Conditions

4.6.2 Post-fire Yield Strength

For the post-fire yield strength, it can be seen from Figure 4-27 that it is affected by both the type of cooling methods used and the level of exposed temperature. When the exposed temperature is below 400°C, the effect of the cooling method used on post-fire yield strength is not particularly significant. However, when the exposed temperature is between 400°C to 700°C, the post-fire yield strength decreased with increasing exposed temperature for both cooling methods. When the exposed temperature is above 700°C, the post-fire yield strength continued to decrease when air cooling is used but increases slightly when water cooling is used. This increase for water cooling is the result of martensite formation when steel heated beyond its austenitic temperature (about 723°C) is rapidly cooled.

As for the effect of heating rate, the post-fire yield strength of specimens heated at 20°C/min heating rate is rather comparable to those heated with 10°C/min heating rate, while the results for specimens heated using the ISO 834 heating protocol and those which are subjected to repeated cycles of heating and cooling are about 10% lower.

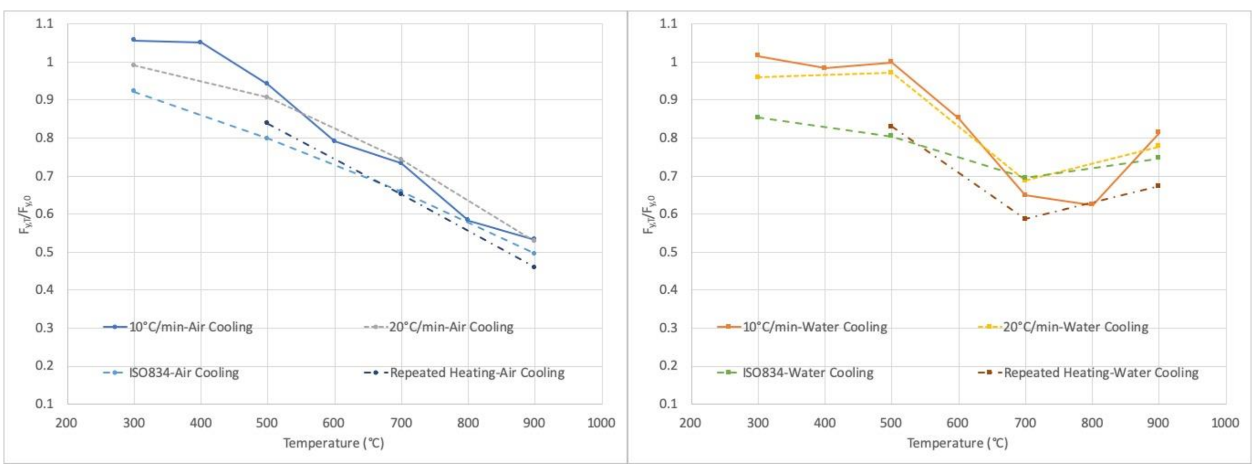

Figure 4-27 Modification Factors for Post-fire Yield Strength of Q690 Steel under Various Test Conditions

The effect of an axial tensile load on the post-fire yield strength of Q690 steel in shown in Table 4-19. It can be seen that when the applied load ratio is 0.2P_y, the post-fire yield strength tends to decrease with increasing exposed temperature. However, for an exposed temperature of 300°C, the yield strength ratio does not seem to change much (from 0.826 to 0.882) with the magnitude of the applied axial tensile load.

4.6.3 Post-fire Tensile Strength

For the post-fire tensile strength, it can be seen from Figure 4-28 that the effects of the used heating protocols and repeated cycles of heating and cooling are not very significant. In addition, when the exposed temperature is below 700°C the results are not particularly affected by the type of cooling methods used. However, the effect of the cooling method used becomes important when the exposed temperature exceeds 700°C. The post-fire tensile strength of Q690 steel increases drastically when water cooling is used. This increase is the result of martensite formation as well.

From Table 4-19, it can be seen that the presence of an axial tensile load does not seem to have a significant effect on the post-fire tensile strength of Q690 steel.

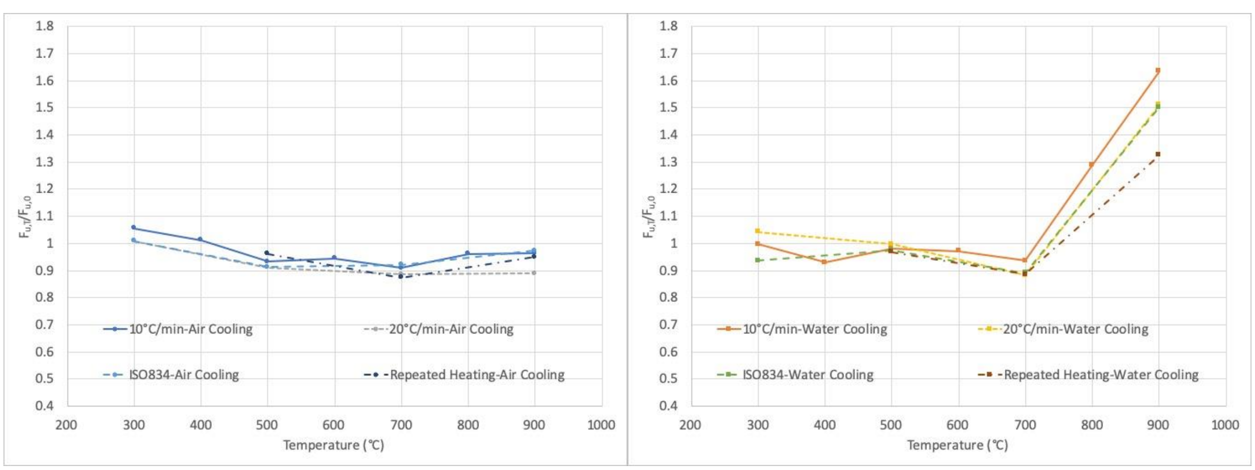

Figure 4-28 Modification Factors for Post-fire Tensile Strength of Q690 Steel under Various Test Conditions

4.6.4 Post-fire Fracture Strain

For the post-fire fracture strain, it can be seen from Figure 4-29 that when the exposed temperature is below 600°C, the temperature effect on post-fire fracture strain is not very important regardless of the cooling method used. However, when the temperature is above 600°C, the fracture strain increased slightly for air cooling, but decreased significantly for water cooling. Furthermore, when the exposed temperature is over 700°C, brittle fracture failure as shown in Figure 4-30 may occur when water cooling is used. This brittleness is the result of martensite formation as alluded to earlier.

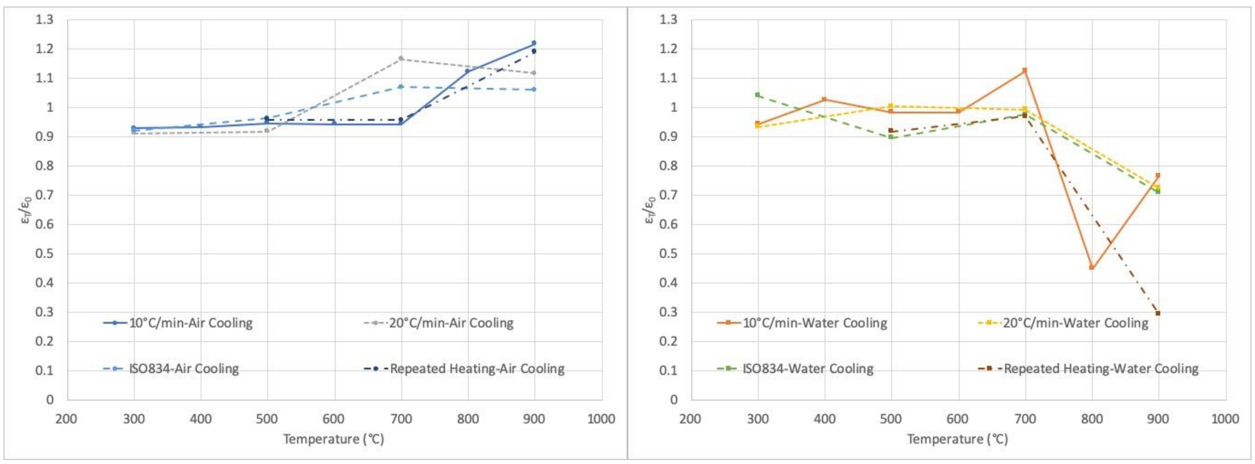

Figure 4-29 Modification Factors for Post-fire Fracture Strain of Q690 Steel under Various Test Conditions

From Table 4-19, it can be seen that the presence of an axial tensile load during the heating/cooling cycle tends to reduce the ductility of the specimens. The reduction is more pronounced when the exposed temperature is low and when the applied tensile load is high.

Figure 4-30 Non-ductile Fracture Failure without Necking

4.7 Empirical Equations

Based on test data obtained in this study and reported and discussed in the preceding sections, empirical equations for the post-fire mechanical properties of Q690 steel were developed using regression analysis. Because these mechanical properties are not only functions of the exposed temperature, but also the cooling method used, two sets of empirical equations – one for air cooling and the other for water cooling are presented. Finally, to account for the effects of heating method used, repeated heating and cooling, and the presence of an applied load during the heating and cooling process, a modification coefficient is proposed at the end of this section.

4.7.1 Post-fire Elastic Modulus

The modification factor proposed for the post-fire elastic modulus of Q690 steel is 1 regardless of whether air cooling and water quenching is used. The use of a modification factor of 1 means the change in elastic modulus is negligible after fire exposure. Figure 4-31 shows a comparison of the proposed value of 1 for the post-fire elastic modulus with test data.

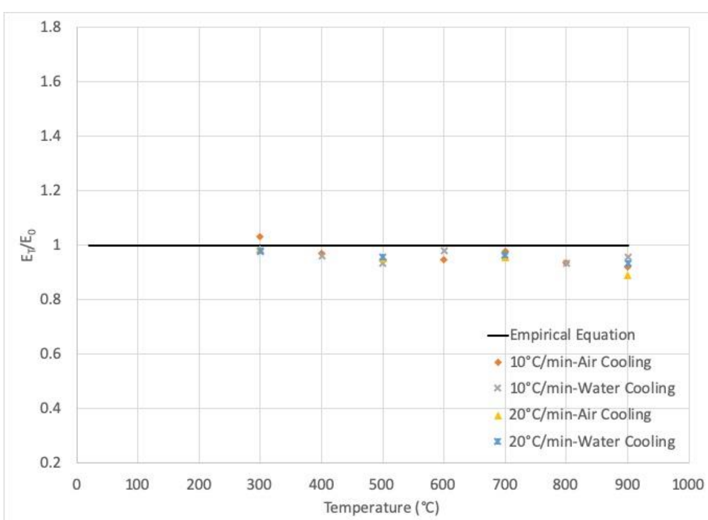

Figure 4-31 Comparison of Empirical Equation with Test Data (Post-fire Elastic Modulus)

4.7.2 Post-fire Yield Strength

The empirical equations for the post-fire yield strength of Q690 steel is proposed as follows:

Air cooling Method:

$$F_{y,T}/F_{y,0} = \begin{cases} 1 & 20℃ \le T < 400℃ \\ -9.786 \times 10^{-4}T + 1.391 & 400℃ \le T \le 900℃ \end{cases} \tag{4.2}$$

Water cooling Method:

$$F_{y,T}/F_{y,0} = \begin{cases} 1 & 20℃ \le T < 500℃ \\ 2.112 \times 10^{-8}T^3 - 3.879 \times 10^{-5}T^2 + 2.19 \times 10^{-2}T + 2.8933 & 500℃ \le T \le 900℃ \end{cases} \tag{4.3}$$

A comparison of the above equations with test data is shown in Figure 4-32.

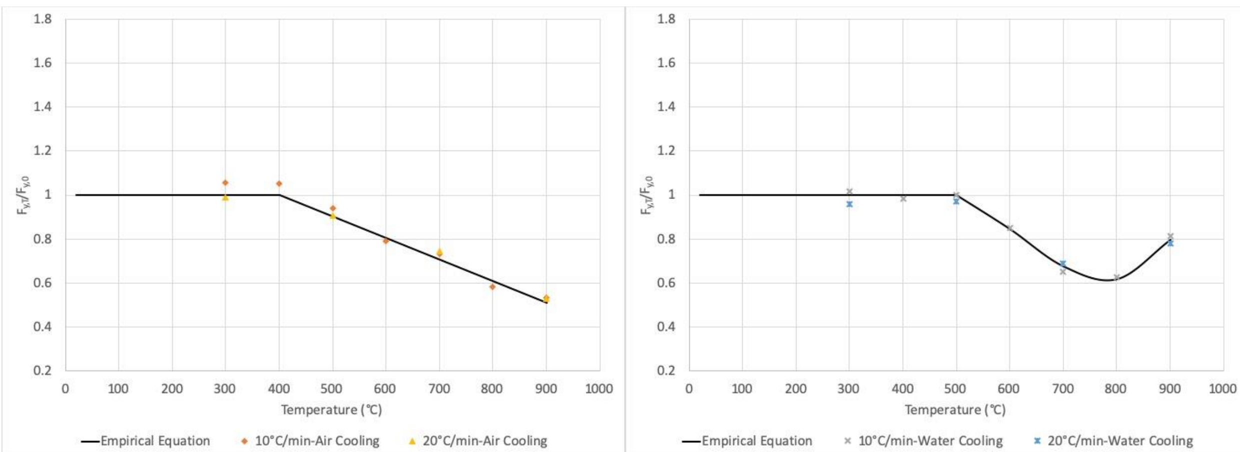

Figure 4-32 Comparison of Empirical Equations with Test Data (Post-fire Yield Strength)

4.7.3 Post-fire Tensile Strength

The empirical equations for the post-fire tensile strength of the Q690 steel is proposed as follows:

Air cooling Method:

$$F_{u,T}/F_{u,0} = 1 \qquad 20℃ \le T \le 900℃ \tag{4.4}$$

Water cooling Method:

$$F_{u,T}/F_{u,0} = \begin{cases} 1 & 20℃ \le T < 700℃ \\ 2.864 \times 10^{-3}T - 1.005 & 700℃ \le T \le 900℃ \end{cases} \tag{4.5}$$

A comparison of the above equations with test data is shown in Figure 4-33.

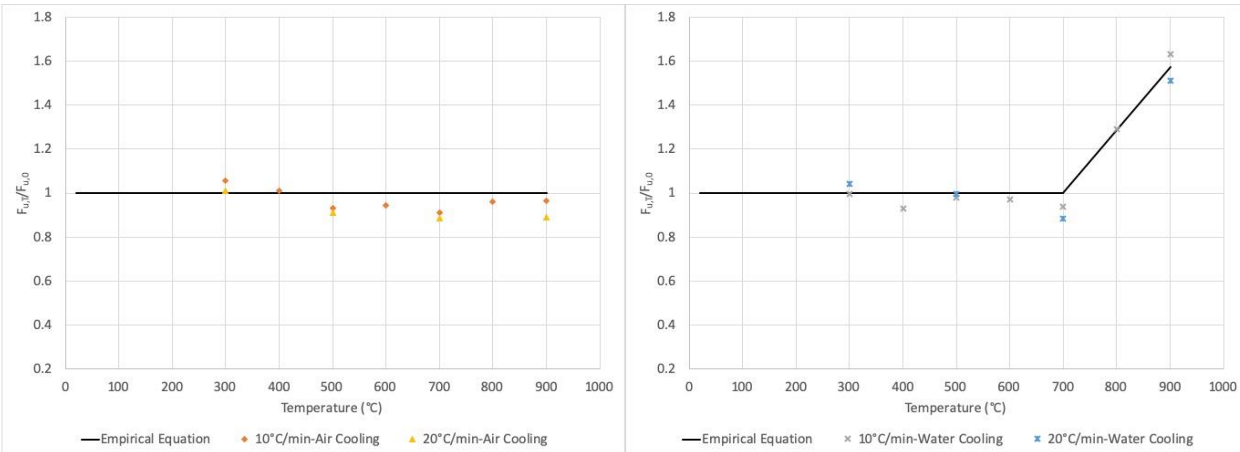

Figure 4-33 Comparison of Empirical Equations with Test Data (Post-fire Tensile Strength)

4.7.4 Post-fire Fracture Strain

The empirical equations for the post-fire fracture strain of Q690 steel is proposed as follows:

Air cooling Method:

$$\varepsilon_T/\varepsilon_0 = \begin{cases} 1 & 20℃ \le T < 600℃ \\ 5.727 \times 10^{-4}T + 0.656 & 600℃ \le T \le 900℃ \end{cases} \quad (4.6)$$

Water cooling Method:

$$\varepsilon_T/\varepsilon_0 = \begin{cases} 1 & 20℃ \le T < 700℃ \\ -1.268 \times 10^{-3}T + 1.888 & 700℃ \le T \le 900℃ \end{cases} \quad (4.7)$$

A comparison of the above equations with test data is shown in Figure 4-34.

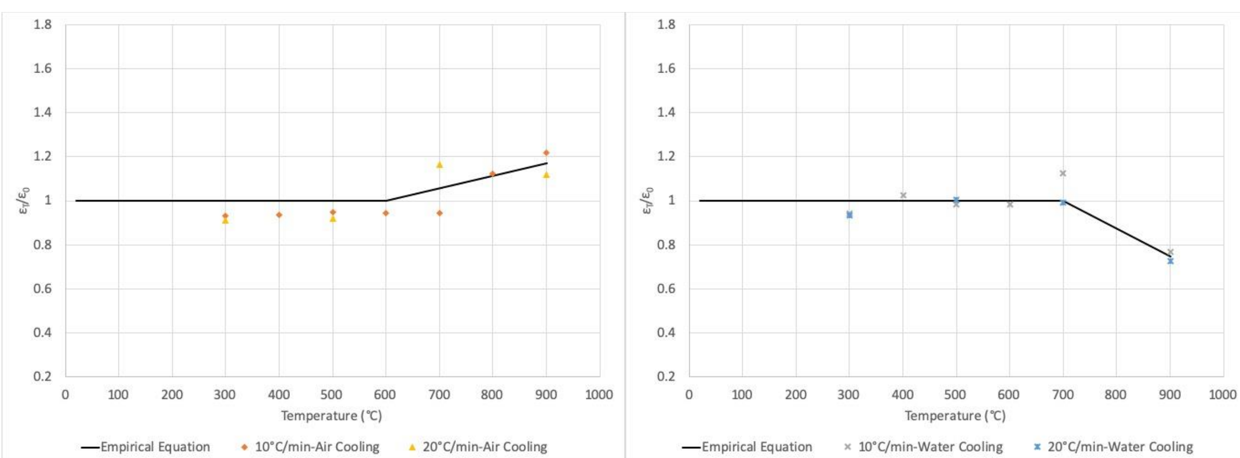

Figure 4-34 Comparison of Empirical Equation with Test Results (Post-fire Fracture Strain)

4.7.5 Modification Coefficients

Finally, to account for the effects of ISO834 heating protocol, repeated heating/cooling, and the presence of an applied load, modification coefficients to be applied to each of the mechanical properties calculated using the above empirical equations are proposed in Table 4-20.

Table 4-20 Modification Coefficients for Post-fire Mechanical Properties of Q690 Steel under Various Conditions

	Elastic Modulus	Yield Strength	Tensile Strength	Fracture Strain
ISO834 Standard Fire Curve	0.9	0.9	1	1
Repeated Heating/Cooling	0.9	0.9	1	1
$0.2F_y$ Axial Tensile Load	0.9	0.8	0.9	0.9

4.8 Comparison with Results from Other Researchers

In this section, the post-fire mechanical properties of Q690 high strength steel obtained in the present research is compared with those of other 690 MPa grade and lower grade steels reported by other researchers.

4.8.1 Comparison with Steel having 690MPa Nominal Yield Strength

The post-fire mechanical properties of steel with 690 MPa nominal yield strength obtained by different researchers as summarized in Table 4-21 are compared in this section.

Table 4-21 Summary of Steel with 690MPa Nominal Yield Strength for Comparison

Steel Type	Standard	Nominal Yield Strength (MPa)	Researcher	Cooling Method
Q690	Chinese	690	Li et al. [48]	Air
Q690			Kang et al. [50]	
Q690			Zhou et al. [49]	
S690QL	European		Qiang et al. [22]	
RQT-S690			Chiew et al. [18]	

For S690QL and RQT-S690 steels, the letter S before the number 690 represents European standard. QL is an abbreviation for quenched and tempered with low notch toughness, and RQT is an acronym for rolling quenched and tempered. Although they all have a nominal yield strength of 690 MPa, the chemical compositions (i.e., types and amount of alloying elements present) of the steels are not the same. Table 4-22 gives a comparison of the chemical compositions and alloying elements present in the reported test samples. In the table, “-” means the data are not reported by the researcher.

Table 4-22 Comparison of Composition of Alloying Elements (wt%)

Chemical Element	C	Si	Mn	P	S	Ti	Cr	Mo	B	Ni	Cu	N	Nb	V	Al
Q690 [Present]	0.14	0.23	1.38	0.011	0.001	0.012	0.27	0.15	0.0016	0.01	0.01	-	-	-	-
Q690 [Li]	0.17	0.19	1.41	0.009	0.003	0.017	0.03	0.01	-	0.02	0.02	-	0.02	0.002	0.036
Q690 [Kang]	0.13	0.25	1.35	0.012	0.002	0.012	0.21	0.111	-	0.03	0.02	-	0.023	0.07	0.025
Q690 [Zhou]	-	-	-	-	-	-	-	-	-	-	-	-	-	-	-
S690QL [Qiang]	0.16	0.21	0.85	0.012	0.001	0.006	0.35	0.2	-	0.05	0.03	0.0026	0.025	0	0.093
RQT-S690 [Chiew]	0.14	0.4	1.35	0.012	0.003	0.025	0.01	0.12	0.002	0.01	0.01	-	0.035	0.05	0.035

The post-fire elastic modulus, yield strength, tensile strength, and fracture strain, normalized by their respective pre-fire values, are compared in Figures 4-35 to 4-38 for different steels with 690 MPa nominal yield strength.

For the post-fire elastic modulus (Figure 4-35), the fluctuation is relatively small regardless of the type of high strength steel tested when the exposed temperature is below 600°C. However, when the exposed temperature exceeds 600°C a noticeable drop in the ratio E_T/E_0 is observed for S690QL steel which has much lower manganese content than the other steels.

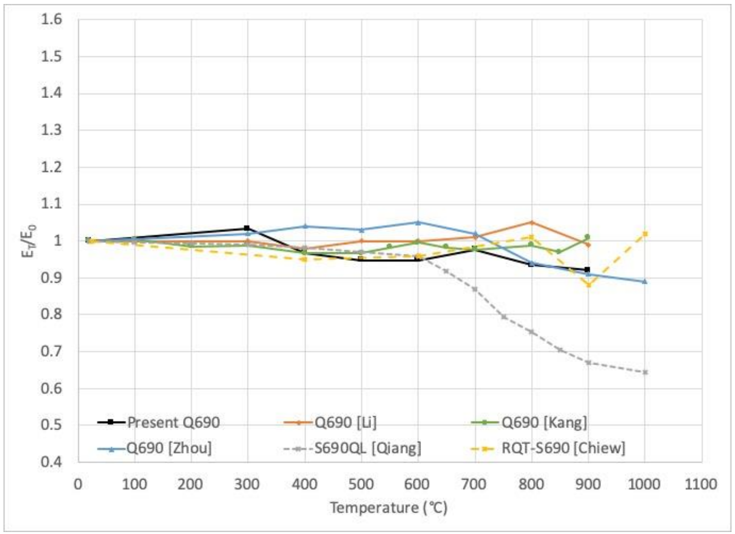

Figure 4-35 Comparison of Post-fire Elastic Modulus for Different 690 MPa Steels

For the post-fire yield strength (Figure 4-36), the trends are similar for all six types of high strength steel. The yield strength starts to decrease from the exposed temperature is in the 450°C to 600°C range, and when the exposed temperature reaches 900°C, the residual yield strength of all the steels tested is equal to or less than half the nominal yield strength before fire exposure.

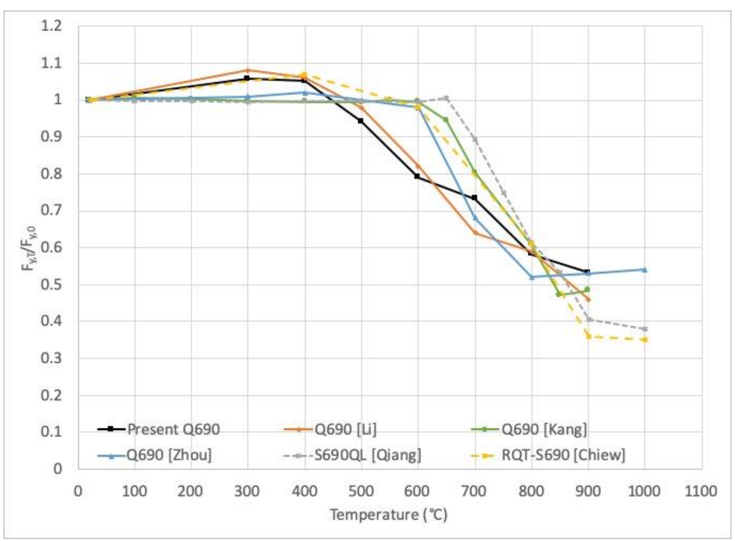

Figure 4-36 Comparison of Post-fire Yield Strength for Different 690 MPa Steels

For the post-fire tensile strength (Figure 4-37), the change does not appear to be important for all six types of steel when the exposed temperature is below 500°C. However, when the exposed temperature is above 600°C, all but the one used in the present research show a noticeable decrease. The steel used in the present research does not contain aluminum as an alloying element. Aluminum is added to steel as a deoxidizing and grain refining agent, but has been shown to cause a decrease in the tensile strength of steel [67].

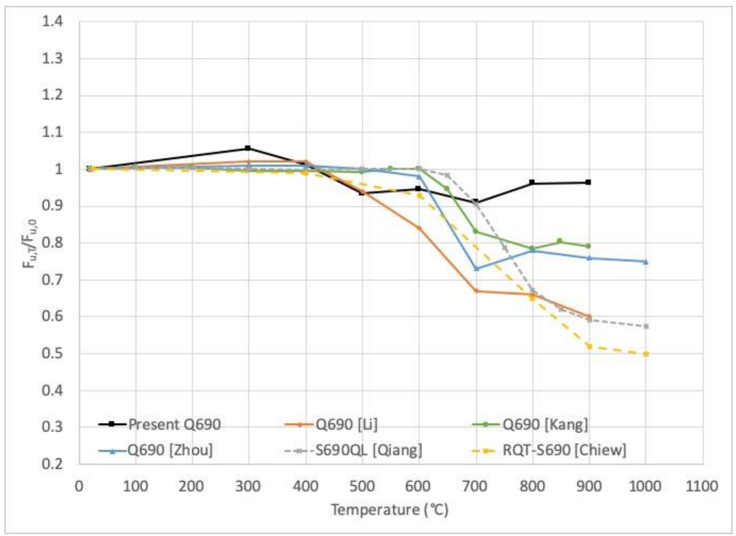

Figure 4-37 Comparison of Post-fire Tensile Strength for Different 690 MPa Steels

For the post-fire fracture strain (Figure 4-38), only four of the six researchers have reported data and so the comparison is only made for four high strength steels. When the exposed temperature is below 500°C, its influence on fracture strain appears negligible. As the exposed temperature increases, the post-fire fracture strain trends up for the Q690 steel used in the present research and that used by Li et al. [48] with the latter showing a rather noticeable increase. The steel studied by Li et al. has a much lower chromium content. Chromium is added to increase the hardenability and corrosion resistance of steel. However, it could cause excessive hardness and a reduction in ductility.

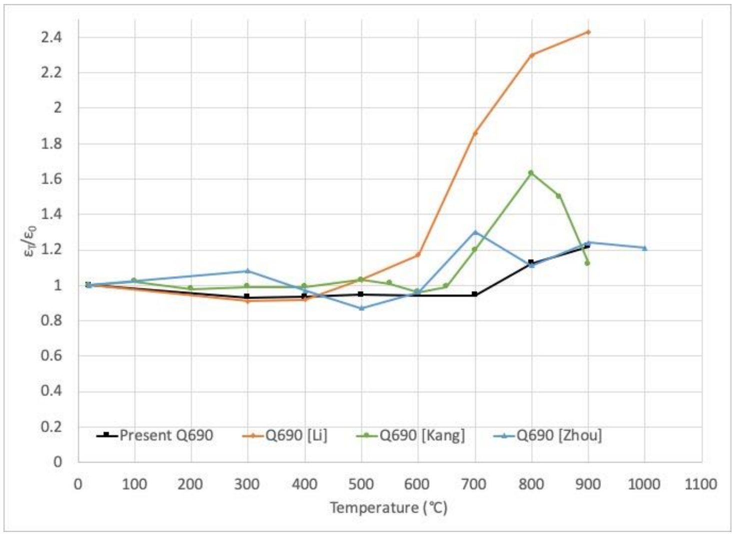

Figure 4-38 Comparison of Post-fire Fracture Strains for Different 690 MPa Steels

4.8.2 Comparison with Steel having Different Steel Grades

A comparison of the post-fire mechanical properties of different types of steel cooled using either air or water cooling as summarized in Table 4-23 is given in this section. Three steel grades (high strength, medium strength and low strength), each with four representative samples, are used in the comparison.

Table 4-23 Summary of Different Grade Steel for Comparison

Steel Type	Steel Grade	Nominal Yield Strength (MPa)	Researcher	Cooling Method
High Strength Steel	Q690	690	Li et al. [48]	Air or Water
	Q690	690	Zhou et al. [49]	
	Q460	460	Wang et al. [21]	
Medium Strength Steel	Q420	420	Lu et al. [51]	
	A992	345	Lee et al. [56]	
	A572 G50	345	Aziz and Kodur [55]	
	Q345	345	Lu et al. [51]	
Low Strength Steel	A36	250	Sajid and Kiran [54]	
	Q235	235	Zhang et al. [53]	
	Q235	235	Chen and Cao [52]	
	Q235	235	Lu et al. [51]	

The post-fire elastic modulus, yield strength, tensile strength, and fracture strain, normalized by their respective pre-fire values, are compared in Figures 4-39 to 4-42 for different types of steel and cooled using either the air cooling or water cooling method. In each figure, the top set represents high strength steel (Q690 and Q460), the second set represents medium strength steel (Q420, A992, A572 G50 and Q345), and the bottom set represents low strength steel (A36 and Q235).

For the post-fire elastic modulus (Figure 4-39), except for A572 G50 [Aziz] steel, neither the cooling method nor the exposed temperature seems to have much influence on this mechanical property.

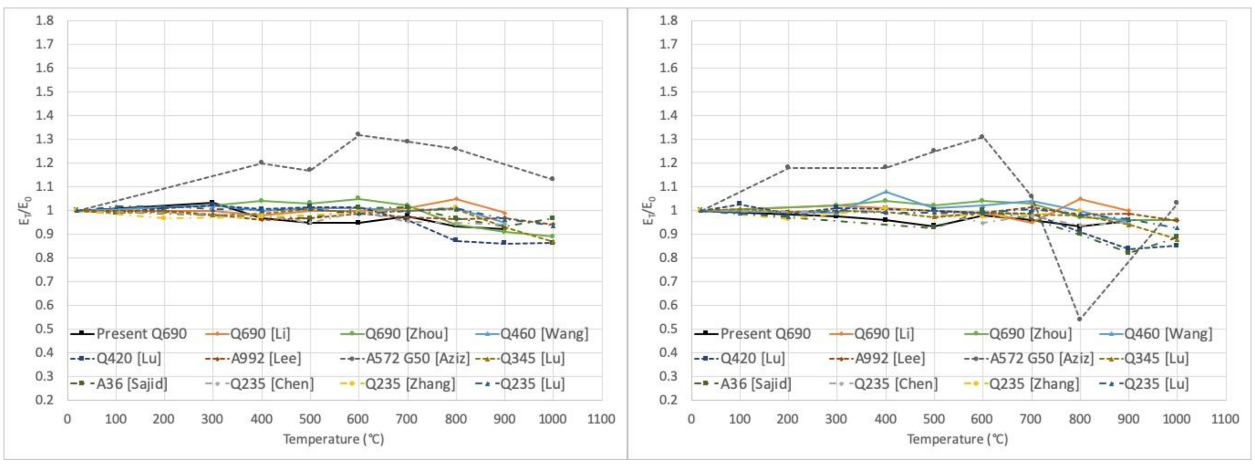

(a) (b)

Figure 4-39 Comparison of Post-fire Elastic Modulus for Different Steel Grades under (a) Air Cooling and (b) Water Cooling

For the post-fire yield strength (Figure 4-40), regardless of the steel grades or whether the specimens are air or water cooled, the effect is not significant as long as the exposed temperature is at or below 500°C. As the exposed temperature gets higher, the general trend is a reduction in post-fire yield strength, with high strength steels exhibiting a higher rate of reduction than low and medium strength steels. When the exposed temperature is around

800°C, the post-fire yield strength begins to restore for most of the water-cooled samples. In particular, the post-fire yield strength of the water-cooled A36 and Q235 [Zhang] steels shows quite a noticeable increase.

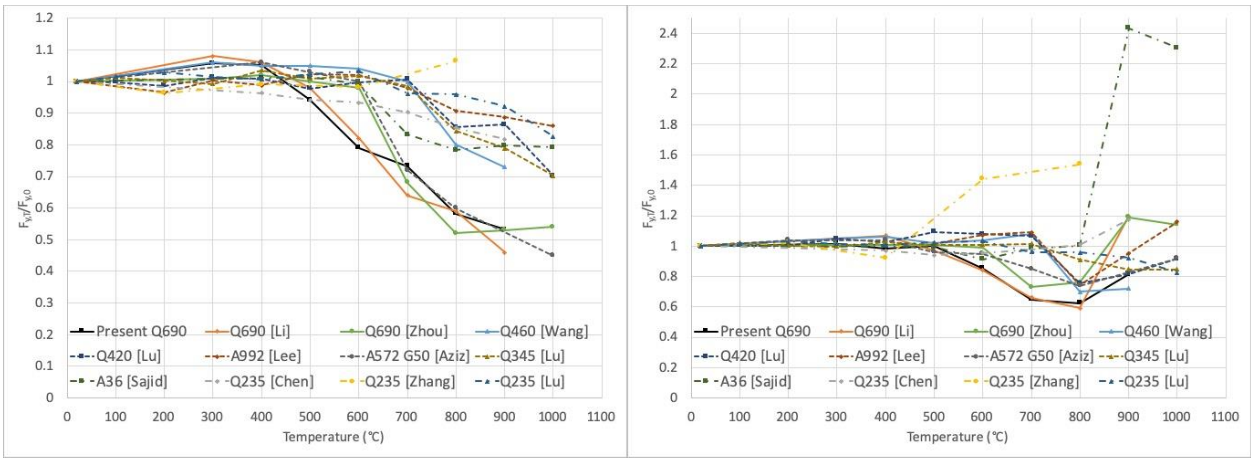

(a) (b)

Figure 4-40 Comparison of Post-fire Yield Strength for Different Steel Grades under (a) Air Cooling and (b) Water Cooling

For the post-fire tensile strength (Figure 4-41), like the post-fire yield strength, as long as the exposed temperature is at or below 500°C, the effect is not significant regardless of the steel grades or manner of cooling. When the exposed temperature gets higher, a slight decrease in tensile strength is observed for the air-cooled samples. The decrease is more noticeable for high and medium grade steels. As for the water-cooled samples, an increase in post-fire tensile strength was observed when the exposed temperature was at or above 800°C. The increase is particularly noticeable for high and medium grade steels.

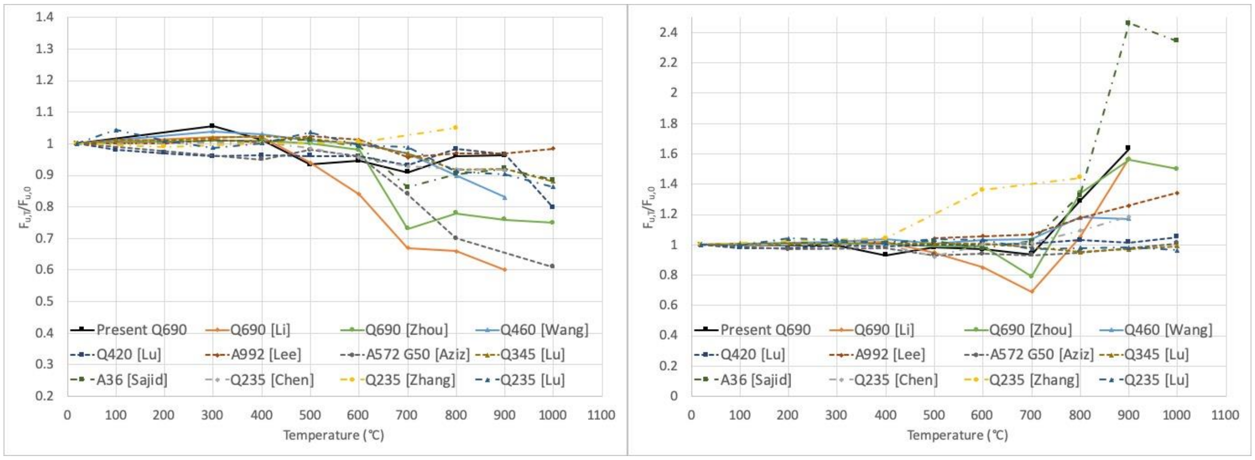

(a) (b)

Figure 4-41 Comparison of Post-fire Tensile Strength for Different Steel Grades under (a) Air Cooling and (b) Water Cooling

For the post-fire fracture strain (Figure 4-42), as long as the exposed temperature is at or below 500°C, the effect does not appear to be important regardless of the steel grades or the manner of cooling. As the exposed temperature increases, the trend is an increase in post-fire fracture strain for the air-cooled samples, and a decrease in post-fire fracture strain for the water-cooled samples. The level of increment or decrement varies according to the steel grades.

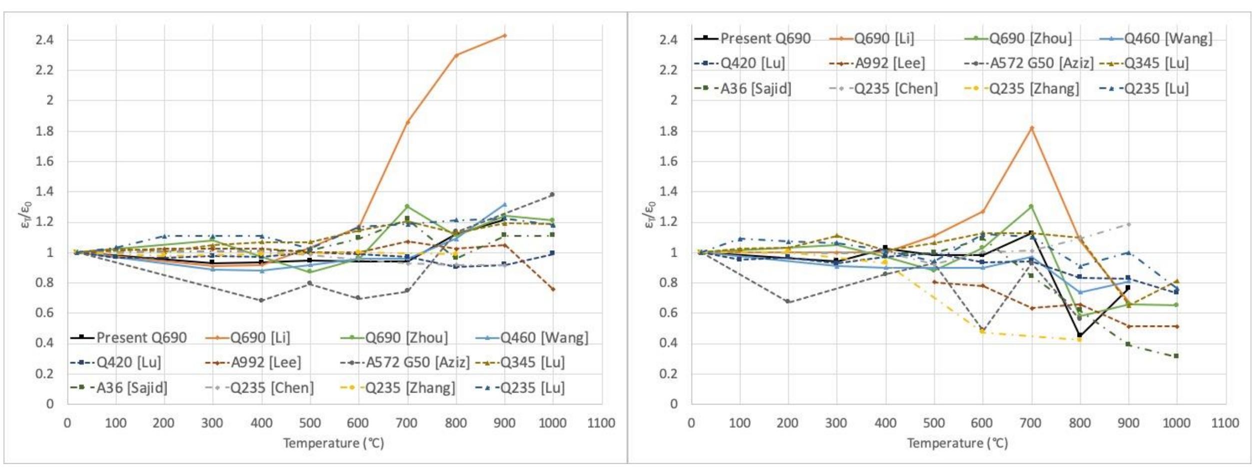

(a) (b)

Figure 4-42 Comparison of Post-fire Fracture Strains for Different Steel Grades under (a) Air Cooling and (b) Water Cooling

4.9 Conclusions

Simple tension tests were performed on 44 specimens fabricated from Q690 high strength steel to evaluate the effect of fire exposure on their mechanical properties. Three heating methods and two cooling methods were used. In addition, the effects of repeated heating and cooling as well as heating under the application of an axial load were considered. Using these test results, empirical equations were developed and reduction coefficients were proposed to account for the influence of heating method used, repeated heating/cooling and the presence of an axial load in calculating the post-fire mechanical properties of Q690 steel. Moreover, comparison with test results on the mechanical properties of different types and grades of steel reported by other researchers were made. Based on these results, the following observations can be made.

1. For post-fire elastic modulus, it is observed that the type of cooling method used and the level of exposed temperature will not have a significant effect and can therefore be ignored.
2. For post-fire yield strength, it is observed that when the exposed temperature is 300°C and 400°C, a light increase in yield strength occurs as a result of the blue brittleness effect. However, when the temperature is between 400°C to 700°C, the yield strength decreases with increasing exposed temperature for both cooling methods. Once the exposed temperature is above 700°C, while the post-fire yield strength continues to decrease when air cooling is used, it increases slightly when water cooling is used.
3. For post-fire tensile strength, it is observed that the change is not very significant when air cooling is used. However, when the exposed temperature is above 700°C, the post-fire tensile strength increases drastically when water cooling is used. This is because

when steel is heated above its austenitic temperature (about 723°C) and rapidly cooled, martensite will form which makes steel stronger and harder but less ductile.

4. For post-fire fracture strain, it is observed that when the temperature is below 600°C, the change is not significant regardless of the type of cooling methods used. However, when the exposed temperature is higher than 600°C, the post-fire Q690 steel becomes more ductile when the air cooling method is used but less ductile when the water cooling method is used. In addition, when the temperature is above 800°C, non-ductile fracture without necking may occur for specimens that are water-cooled.
5. Both the heating rate and repeated heating/cooling can affect the post-fire mechanical properties of Q690 steel. On average, the post-fire elastic modulus and yield strength drop about 10%, but their effect on tensile strength and fracture strain is not significant and can be neglected.
6. When an axial load is applied to the specimens during the heating and cooling process, their post-fire mechanical properties are reduced by 10% to 20%. However, when the exposed temperature is 300°C, the magnitude of the axial load does not seem to have a significant effect on the mechanical properties.
7. By comparing steels with different steel grades and several Q690 steels with different chemical compositions, it is observed that their post-fire mechanical properties do not show large variation when the exposed temperature is below 500°C, but noticeable differences are observed for temperature higher than 500°C. The current standards, which were primarily developed based on the behavior of normal strength steels, need to be updated for the design of high strength steels.

5 POST-FIRE RESIDUAL STRESSES OF Q690 WELDED I-SHAPED SECTIONS

In this chapter, the post-fire residual stresses of several welded I-shaped sections fabricated with Q690 high strength steel will be obtained experimentally. A residual stress model will be developed to determine the distribution and magnitude before and after fire exposure.

5.1 Introduction

Residual stresses are often developed in steel members during the fabrication process as a result of differential cooling when some regions of the member cross-section that have been cooled are constrained by adjacent regions from expanding, contracting, or releasing elastic strains. Residual stresses can be tensile or compressive, and their magnitudes can change as a result of forging, casting, cutting and heat treatment. To maintain equilibrium in the absence of an external applied force, tensile and compressive residual stresses must co-exist within the cross-section and they must be self-equilibrating. In most cases, compressive residual stress is desirable in that it contributes to an improvement in fatigue strength and resistance to stress corrosion cracking [68]. On the other hand, large tensile residual stress could cause component distortion or cracking.

Nowadays, HSS is being widely used in the construction industry for high-rise buildings and long-span bridges. Using HSS as a replacement for mild steel has spawned research interest into the behavior of structural members made from HSS. For steel structures, the presence of residual stresses in welded built-up members is an important design parameter to consider as it affects the inelastic behavior of the members. Due to the difference in heat treatment between fabricating mild steel and HSS, the study of residual stresses in HSS welded sections is the focus of this chapter. In particular, since the magnitudes and distributions of residual stresses could undergo noticeable changes after a fire, study on the post-fire effect of residual stresses on HSS sections is to be conducted. In the present research, twenty-three Q690 welded I-shaped sections are fabricated and the magnitudes and distributions of their post-fire residual stresses are determined experimentally. The parameters included in the study are levels of exposed temperatures, types of cooling methods used, heating rates, and cross-section width-to-thickness ratios.

5.2 Methods for Measuring Residual Stresses

Various non-destructive, semi-destructive and destructive methods are available for residual stresses measurements [70]. However, the two most commonly used approaches to measure residual stresses are hole-drilling and sectioning methods. The advantages of these two methods are that they are very well developed, and are easy and relatively inexpensive to perform. Unfortunately, post-fire Q690 steel is too strong for drilling and saw cutting and a modified sectioning method is used in the present study. Instead of using gauge holes, strain gauges were used; and instead of saw cutting, electric wire cutting was used. Details of this method will be discussed in a later section.

5.3 Test Material and Specimens

The plates used for fabricating the built-up I-shaped sections shown in Figure 5-1 were flame cut from the same Q690 stocks used earlier for the tensile tests. The plates were welded together using gas metal arc welding (GMAW) with two passes. The filler wire was ER120S-G with the same nominal yield strength as the base material. In order to minimize deformations due to shrinkage, a specific welding protocol as shown in Table 5-1 was used.

Figure 5-1 Photo of Specimens

Table 5-1 Welding Parameters

Diameter (mm)	Type	Current Type	Gas Composition	Flow Rate (L/min)	Electric Current (A)	Volts (V)	Travel Speed (cm/min)
ϕ1.2	Semi-auto	DCEP	80%Ar+20%CO_2	15~20	260~290	28~30	25~35

To eliminate end effects, the specimens were made sufficiently long as shown in Figure 5-2 so a distance of 1.5 to 2 times the lateral dimension (B) of the cross-section was maintained from each specimen end to the test region [47].

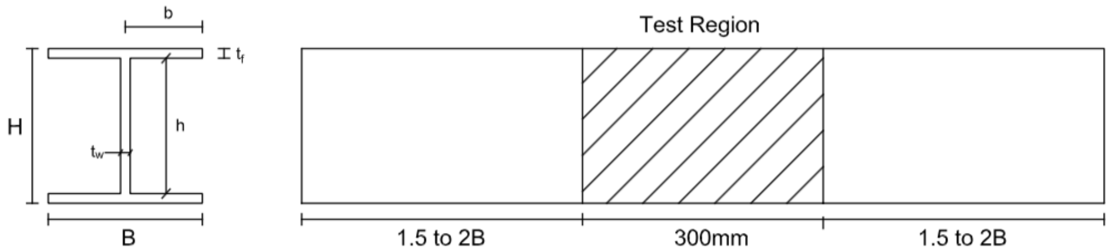

Figure 5-2 Dimensions of Specimen Used for the Residual Stress Tests

In a real fire, the time-temperature curve of steel members can be highly variable in both the heating and cooling phases. In this study, most of the tests are performed using the ISO 834 standard fire curve for heating and natural air for cooling. However, to investigate how the results would change when different heating and cooling rates were used, a heating rate of 10°C/min and a rapid cooling rate obtained by quenching the specimens in water were also used. Details of the specimens used for residual stress measurements are given in Table 5-2.

Table 5-2 Specimens Used for Residual Stress Measurements

Specimen Label	B (mm)	H (mm)	t_w&t_f (mm)	L (mm)	b/t_f	h/t_w	Heating Method	Heated Temperature (°C)	Cooling Method
6S0	144	192	12	800	6	14	ISO 834	-	-
6S3	144	192			6	14		300	Air
6S5	144	192			6	14		500	
6S7	144	192			6	14		700	
6S9	144	192			6	14		900	
7S0	168	192			7	14		-	-
7S3	168	192			7	14		300	Air
7S5	168	192			7	14		500	
7S7	168	192			7	14		700	
7S9	168	192			7	14		900	
8S0	192	192			8	14		-	-
8S3	192	192			8	14		300	Air
8S5	192	192			8	14		500	
8S7	192	192			8	14		700	
8S9	192	192			8	14		900	
7S3W	168	192			7	14		300	Water
7S5W	168	192			7	14		500	
7S7W	168	192			7	14		700	
7S9W	168	192			7	14		900	
7S3L	168	192			7	14	10°C/min	300	Air
7S5L	168	192			7	14		500	
7S7L	168	192			7	14		700	
7S9L	168	192			7	14		900	

*The letter S means the specimen; the number before the letter S denotes the cross-section width-to-thickness ratios; the number after the letter S denotes the temperature to which the specimen is heated (e.g., 3 means the specimen is heated to 300°C); the letter W denotes water cooling; and the letter L denotes a heating rate of 10°C/min.

5.4 Test Procedure

Before any tests were performed, all specimens were stored for one month to allow the residual stresses induced by the fabrication process to stabilize. The specimens were then heated in a programmable gas furnace using either the ISO 834 or 10°C/min heating rate to four elevated temperatures that varied from 300°C to 900°C in 200°C increment (i.e., 300°C, 500°C, 700°C and 900°C). Once heated to the pre-determined temperature, the test specimens were either air or water cooled as reported in Table 5-2.

(a)

(b)

Figure 5-3 (a) Gas Furnace and (b) Electric Furnace

After the specimens were cooled to ambient temperature and sat for at least 48 hours, polishing was performed on the test region to remove any rust that had formed on the surface before measurements were made to determine the residual stresses.

As mentioned earlier, a modified sectioning method which is based on the conventional sectioning method shown in Figures 5-4 and 5-5, was used to determine the residual stresses. The procedure and sectioning details of this modified sectioning method are shown in Figures 5-6 and 5-7. In this method, instead of drilling gauge holes, two 2 mm x 1 mm strain gauges were placed in the middle of each strip – one on top and the other on the bottom of the strip.

The three component elements (the two flanges and the web) of the welded I-shaped member were cut into strips as shown in Figure 5-7. Note that in using this measurement method, waterproofing is needed since the wire-cut electrical discharge machine (Figure 5-8) uses water while cutting. For waterproofing, the strain gauges were entirely covered by two layers of epoxy resin applied 24-hour apart to allow sufficient time for the epoxy to dry.

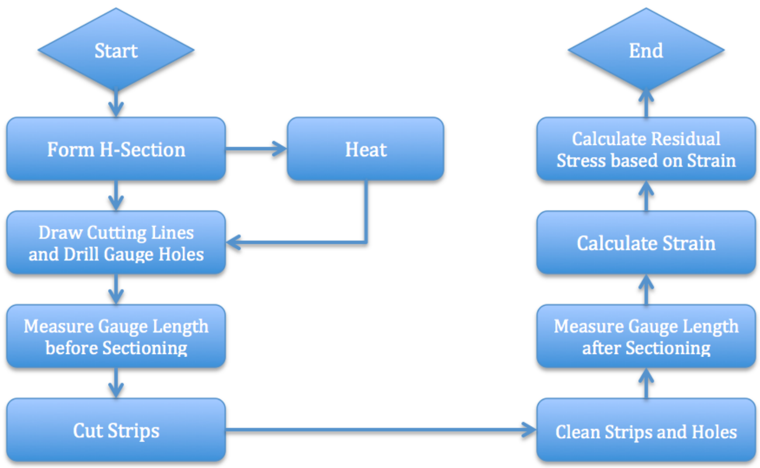

Figure 5-4 Flowchart of the Sectioning Method

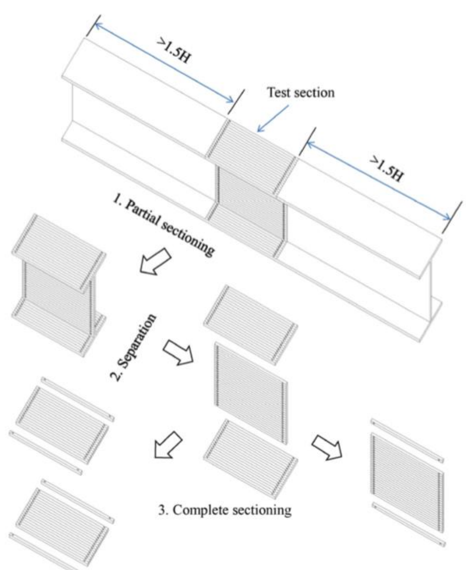

Figure 5-5 Sectioning Details [26]

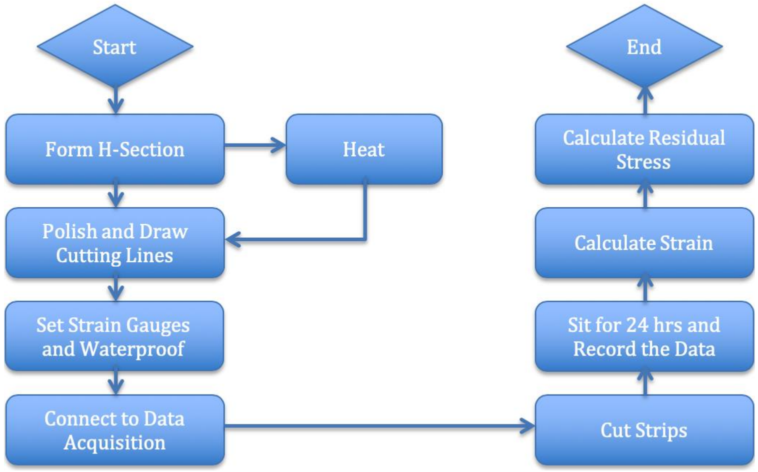

Figure 5-6 Flowchart of the Modified Sectioning Method

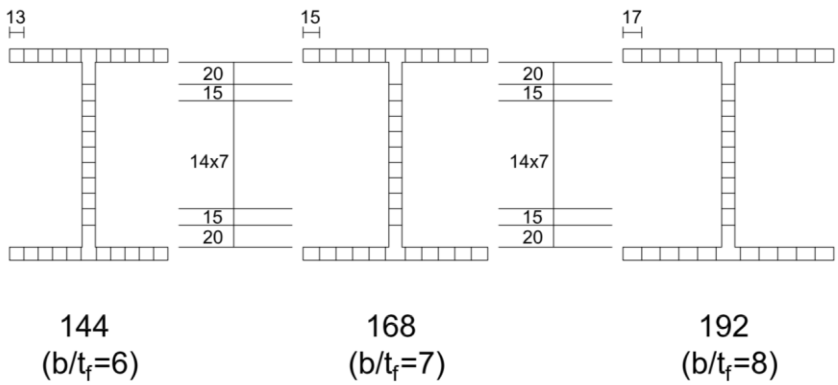

Figure 5-7 Dimensions of Strips used in the Modified Sectioning Method (all dimensions are in mm)

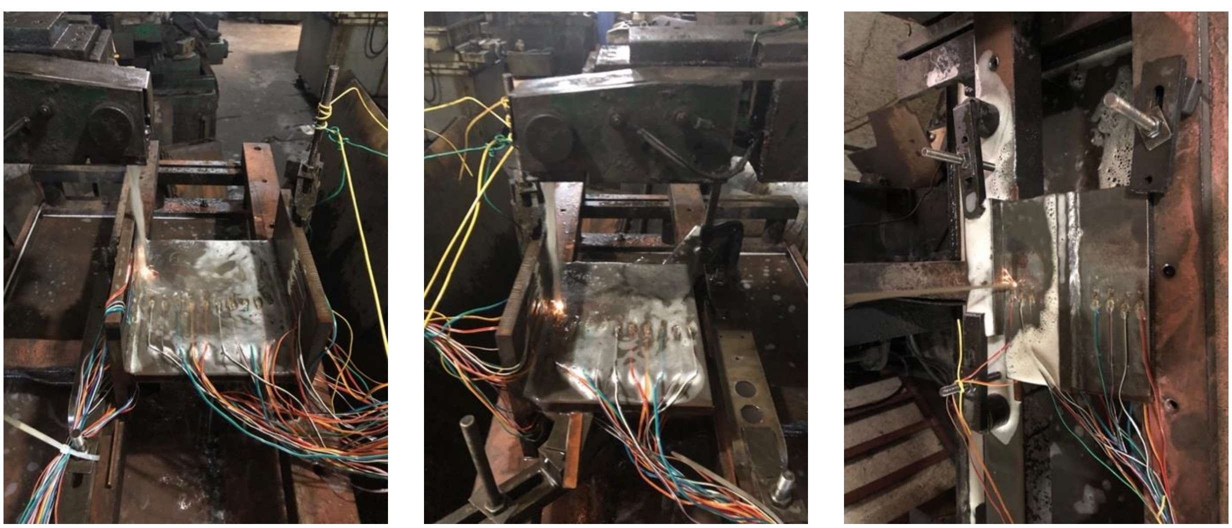

Figure 5-8 Wire-cut Electrical Discharge Machine

All strain gauges were connected to a data acquisition system shown in Figure 5-9. After setting all strain gauge readings to zero, data were recorded every minute during the cutting. After sectioning, the strips were let to sit for 24 hours to allow the induced stresses to release while data were continuously being recorded. Measurements were then made to calculate the residual stresses. Details of the calculations uesd to obtain residual stresswes from the measured strain data are given in the following section.

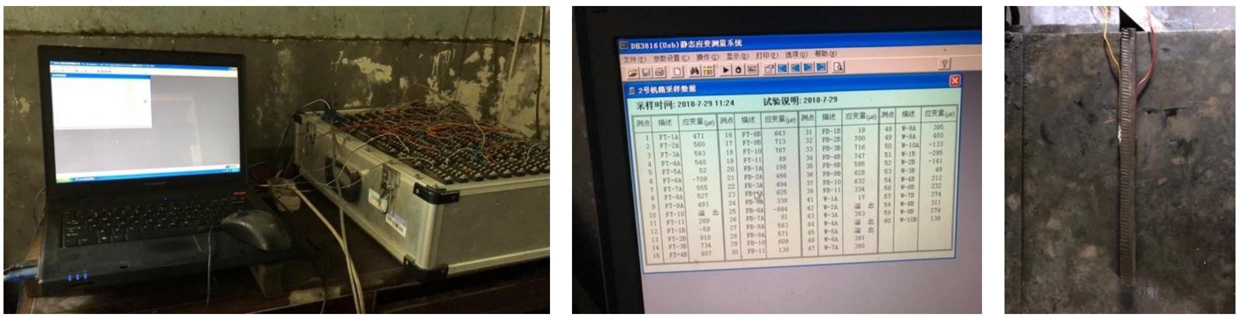

(a) (b) (c)

Figure 5-9 (a) Data Acquisition System, (b) Recorded Data, and (c) Cut Strip

Figure 5-10 shows the numbering system used for the strain gauges. It should be noted that in the event that the flange-to-web welds interfered with the placement of strain gauges such as gauges -5, -7, -25 and -27, they would not be mounted.

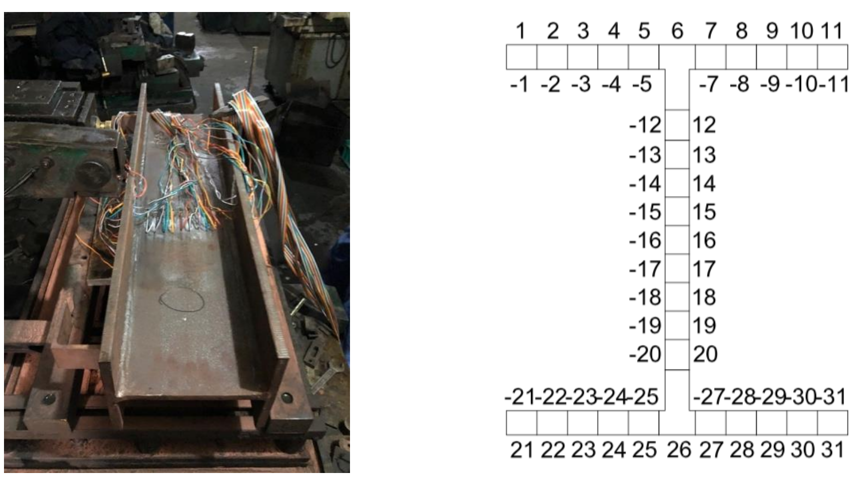

(a) (b)

Figure 5-10 (a) Specimen with Strain Gauges Attached, and (b) Strain Gauge Numbering System

To correct for measuring errors due to changes in room temperature, a set of temperature compensation reference strips were used. They were connected to the data acquisition system with the other strips. These reference strips were made from the same material as the test specimens [47].

5.5 Residual Stresses Calculation

In this section, the method used to calculate residual stresses from the measured strain data is discussed. When the sectioning or modified sectioning method is used to determine residual stresses, the strips cut at or near regions of high stress gradients will undergo noticeable curving. To obtain the true strain ε of the strip measured along its arc length L_o as shown in Figure 5-11, the following equation is used.

$$\varepsilon \approx \varepsilon_0 + \frac{(h/L)^2}{6(h/L)^4 + 1} \tag{5.1}$$

where ε_0 is the average strains = $(\varepsilon_T + \varepsilon_C)/2$, in which ε_T and ε_C are the strains measured by the strain gauges mounted on the convex and concave sides of the test strip, respectively. The sign convention used is tensile strain is considered positive and compressive strain is considered negative; L is the chord length of the strip; and h is the arc offset from the chord given by the equation

$$h = R\left(1 - \cos\frac{L_0}{2R}\right) \tag{5.2}$$

where R is the radius of curvature given by

$$R = \frac{t}{\varepsilon_T - \varepsilon_C} \tag{5.3}$$

in which t is the thickness of the strip.

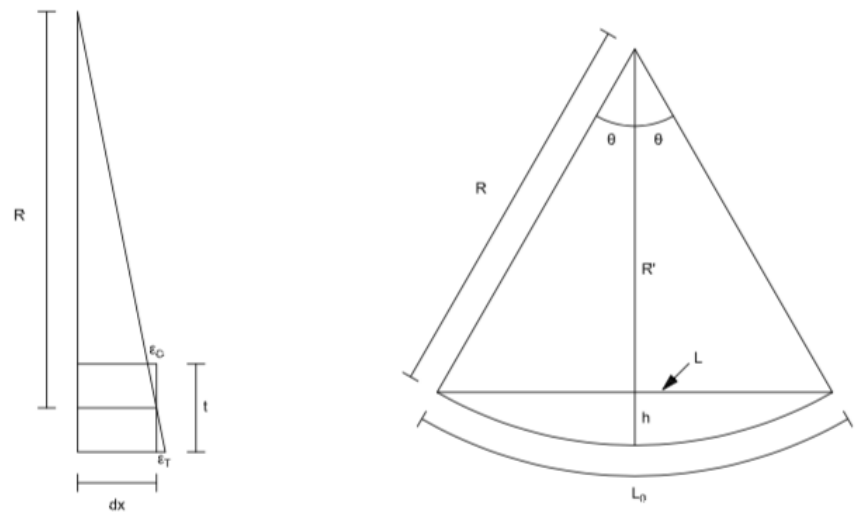

Figure 5-11 Arc Offset and Radius of Curvature

The first term of Eq. (5.1) represents the axial strain in the strip measured along its chord and the second term accounts for the additional axial strain due to the curvature effect.

Once the strain is calculated from Eq. (5.1), the residual stress can be obtained from the equation

$$\sigma = E\varepsilon \tag{5.4}$$

where *E* is the elastic modulus of steel after fire exposure.

5.6 Experimental Results

5.6.1 Effect of Temperature on Welded I-shaped Section Dimensions

In order to record the temperature of the Q690 welded I-shaped sections, four thermocouples placed at different locations and labelled A, B_1, B_2 and C as shown in Figure 5-12 were used. These labels also served as reference points for dimension measurements. The dimensions of the Q690 welded I-shaped sections before and after fire exposure are summarized in Table 5-3 and Table 5-4, respectively.

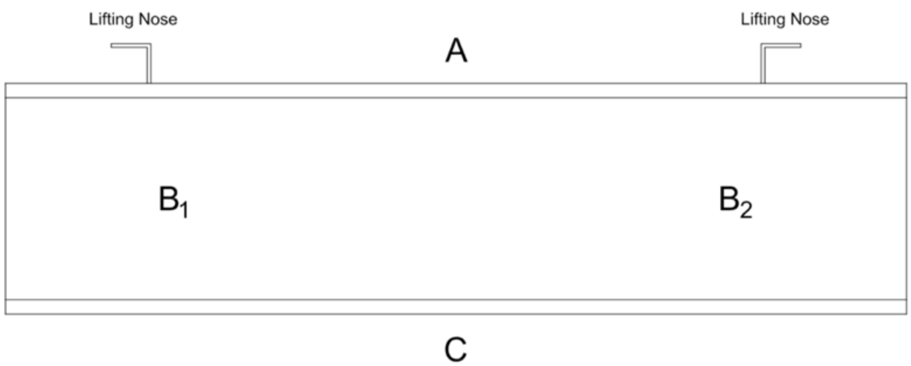

Figure 5-12 Placement of Thermocouples

(a) **(b)**

Figure 5-13 Specimens with Thermocouples: (a) Before, and (b) After Fire Exposure

Table 5-3 Dimensions of Q690 Welded I-shaped Sections before Fire Exposure

Heating Method	Temp. (°C)	Specimen	Flange B_1A (cm)	Flange B_1C (cm)	Web B_1 (cm)			Flange B_2A (cm)	Flange B_2C (cm)	Web B_2 (cm)			Length (cm)
ISO 834	900	8S9	19.1	19.2	19.1	19.4	19.5	19.2	19.2	19	19.5	19.6	79.9
		6S9	14.4	14.4	19.1	19.3	19.3	14.5	14.4	19.3	19.4	19	79.9
		7S9	16.8	17	19.3	19.1	18.9	16.9	17	19.3	19.2	18.8	800
		7S9W	16.6	16.6	19.2	19.3	19	16.6	16.8	19	19.3	19	79.9
	700	8S7	19.1	19.2	18.5	19.3	19.5	19.1	19.2	18.7	19.4	19.5	79.9
		6S7	14.2	14.1	19.5	19.5	19.2	14.3	14.2	19.5	19.6	19.1	80
		7S7	16.7	16.7	19	19.2	19.1	16.7	16.7	19	19.2	19	80
		7S7W	16.7	16.9	19.1	19.3	19.1	16.7	16.8	19.2	19.3	19	79.9
	500	8S5	19.2	19.2	19.1	19.5	19.3	19.2	19.3	19	19.4	19.3	80
		6S5	14.4	14.4	19.1	19.3	19.2	14.4	14.5	19.1	19.4	19.3	80
		7S5	16.9	16.9	19	19.4	19.6	16.9	16.9	18.8	19.4	19.6	79.9
		7S5W	16.9	16.9	19.1	19.5	19.5	16.9	16.9	18.9	19.4	19.6	79.8
	300	8S3	19.3	19.3	19	19.5	19.7	19.3	19.3	19	19.6	19.6	79.9
		6S3	14.4	14.4	19	19.4	19.6	14.3	14.3	19.2	19.5	19.6	79.9
		7S3	16.8	16.8	19.3	19.3	19.1	16.9	16.9	19	19.3	19.4	80.1
		7S3W	16.7	16.9	19.5	19.4	19	16.7	16.9	19.5	19.4	19	80.1
10°C/min	900	7S9L	16.7	16.7	19.4	19.3	19.1	16.7	16.7	19.2	19.4	19.1	79.9
	700	7S7L	16.7	16.7	19.1	19.2	19.1	16.7	16.7	19.2	19.2	19	80
	500	7S5L	16.7	16.9	19	19.3	19.2	16.7	16.9	19	19.3	19.3	79.9
	300	7S3L	16.7	16.7	18.9	19.2	19.2	16.7	16.7	18.9	19.2	19.2	79.9
None	N/A	8S0	19.3	19.2	18.8	19.3	19.5	19.2	19.3	18.7	19.2	19.4	80
		6S0	14.4	14.3	18.9	19.1	19	14.3	14.5	18.8	18.9	19	80
		7S0	16.8	16.9	19	19.4	19.5	16.9	16.9	19.1	19.4	19.5	79.8

Table 5-4 Dimensions of Q690 Welded I-shaped Sections after Fire Exposure

Heating Method	Temp. (°C)	Specimen	Flange B_1A (cm)	Flange B_1C (cm)	Web B_1 (cm)			Flange B_2A (cm)	Flange B_2C (cm)	Web B_2 (cm)			Length (cm)
ISO 834	900	8S9	19.1	19.3	18.9	19.4	19.6	19.3	19.2	18.8	19.4	19.7	79.9
		6S9	14.4	14.4	19.2	19.3	19.1	14.4	14.4	19.3	19.3	18.9	79.8
		7S9	16.9	16.9	19.2	19.2	18.9	16.9	16.9	19.2	19.2	18.8	80.05
		7S9W	16.6	16.5	19.1	19.3	19.1	16.6	16.7	19.2	19.3	19	79.7
	700	8S7	19.1	19.2	18.5	19.3	19.5	19.1	19.2	18.6	19.3	19.5	80
		6S7	14.1	14.1	19.6	19.5	19.2	14.4	14.2	19.6	19.6	19.2	80
		7S7	16.7	16.7	19	19.2	19.1	16.7	16.7	19.1	19.3	19.1	80
		7S7W	16.7	16.9	19.1	19.2	19.2	16.8	16.9	19.3	19.3	19	79.8
	500	8S5	19.2	19.2	19.2	19.5	19.4	19.3	19.3	19.1	19.4	19.3	80.1
		6S5	14.4	14.3	19.1	19.3	19.2	14.4	14.5	19	19.2	19.2	79.9
		7S5	16.8	16.9	19	19.5	19.6	16.9	16.9	18.8	19.4	19.6	80
		7S5W	16.9	16.9	19.1	19.4	19.5	16.9	16.9	19	19.4	19.6	79.9
	300	8S3	19.3	19.2	19.1	19.6	19.7	19.3	19.3	18.9	19.6	19.7	79.8
		6S3	14.3	14.4	19	19.5	19.6	14.4	14.45	19.1	19.5	19.5	80
		7S3	16.8	16.8	19.2	19.3	19	17	16.9	19	19.3	19.3	80.2
		7S3W	16.7	16.8	19.4	19.4	19	16.7	16.9	19.5	19.4	19	80.1
10°C/min	900	7S9L	16.7	16.7	19.3	19.3	18.9	16.7	16.7	19.2	19.3	19.1	79.9
	700	7S7L	16.7	16.7	19.1	19.3	19.1	16.8	16.7	19.2	19.2	19	80
	500	7S5L	16.7	16.9	19	19.3	19.1	16.7	16.9	18.9	19.3	19.3	80
	300	7S3L	16.7	16.7	18.9	19.3	19.2	16.7	16.7	19.1	19.3	19.1	79.9

Based on the data shown in the above tables, it can be concluded that deformations due to heating are not important and need not be considered in the analysis.

5.6.2 Time-temperature Curves

In the present study, two heating protocols (ISO 834 and 10°C/min) and two cooling methods (air cooling and water quenching) are used. Figures 5-14, 5-15 and 5-16 show typical time-temperature curves of three test specimens heated to 700°C and cooled. The five curves shown in each figure represent the temperature of the furnace and the temperature measured on the specimen by thermocouples A, C, B_1 and B_2.

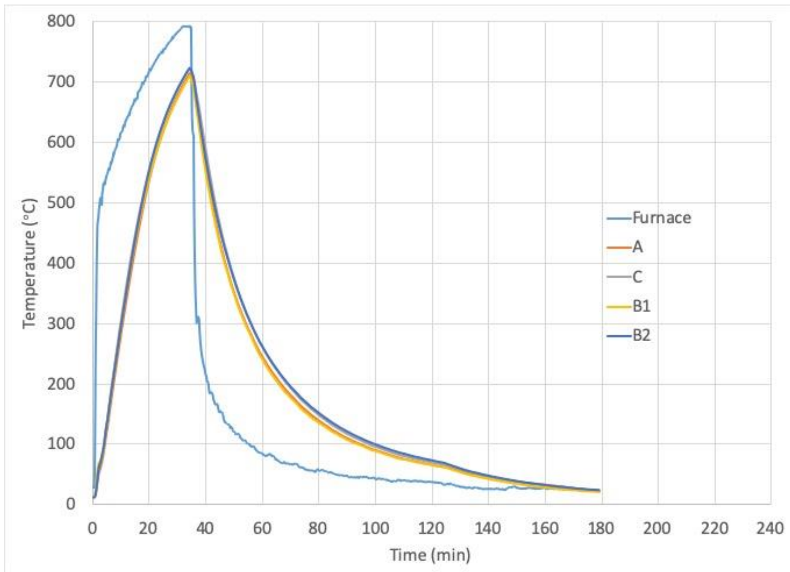

Figure 5-14 Time-temperature Curve (ISO 834 heating to 700°C, Air Cooling)

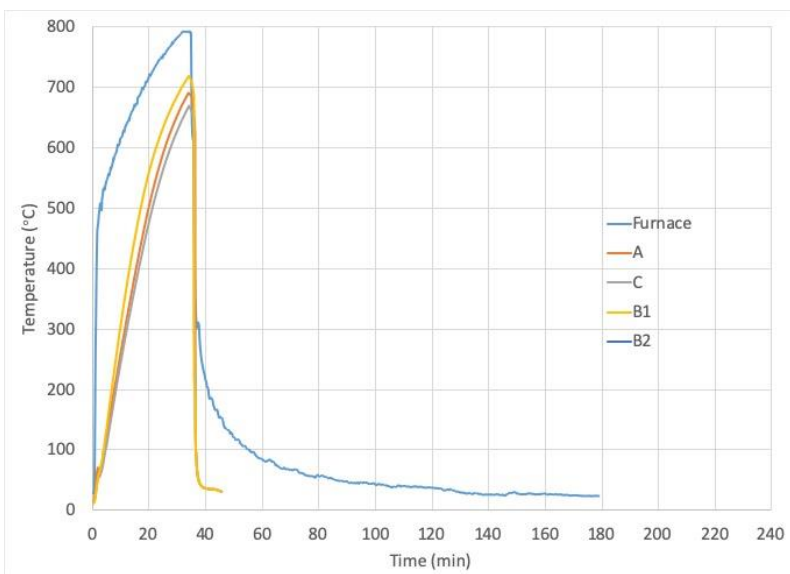

Figure 5-15 Time-temperature Curve (ISO 834 heating to 700°C, Water Cooling)

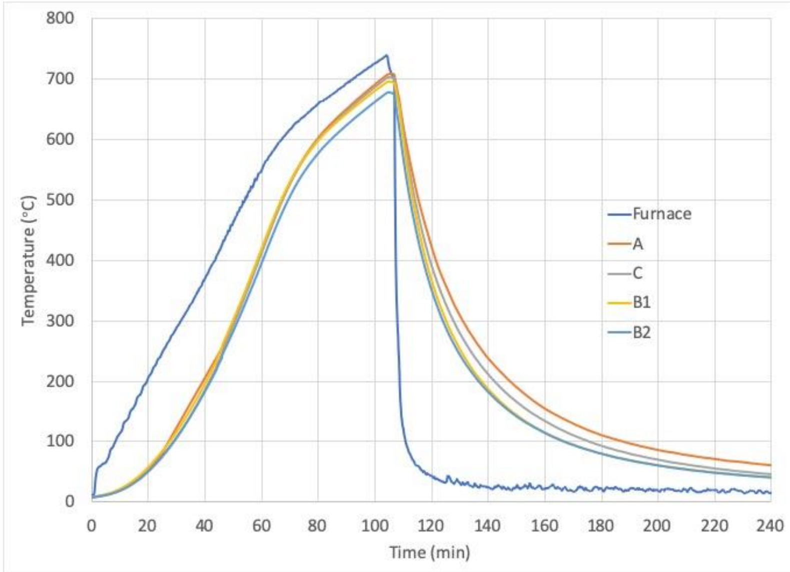

Figure 5-16 Time-temperature Curve (10°C/min heating to 700°C, Air Cooling)

As can be seen, the temperature measured at different locations on the specimen is rather uniform. This is because steel is a material with high thermal conductivity. However, the effects the different heating and cooling methods have on the time-temperature curves is quite apparent. The temperature of the specimen heated using the ISO 834 protocol is increasing much faster than the one heated using a slower heating rate of 10°C /min. The specimen cooled using water quenching experiences an instant temperature drop (as expected) when compared with air cooling. Therefore, the heating and cooling methods used will have an effect on the specimens and will be investigated in the present study.

5.6.3 Residual Stress Distributions of Welded I-shaped Sections

The magnitudes and distributions of residual stresses for Q690 welded I-shaped sections were measured experimentally using the modified sectioning method discussed in a previous section and calculated using the Equations (5.1) and (5.4). As mentioned earlier, strain measurements at the web-flange junction are sometimes difficult to perform. In the event that measurements were not made, the residual stresses at these locations would be obtained from equilibrium consideration since residual stresses are self-equilibrating over the entire cross-section.

* "Original" means no heating treatment; b/t is width-to-thickness ratio.

Figure 5-17 Specimens After Fire Exposure

Figure 5-18 shows the magnitudes and distributions of residual stresses (in MPa) for the unheated specimens with width/thickness (b/t_f) ratio of 6, 7 and 8. Similarly, Figures 5-19 to 5-22 show the corresponding magnitudes and distributions of residual stresses (in MPa) for specimens heated using the ISO 834 heating protocol to 300°C, 500°C, 700°C and 900°C, respectively, and cooled using natural air.

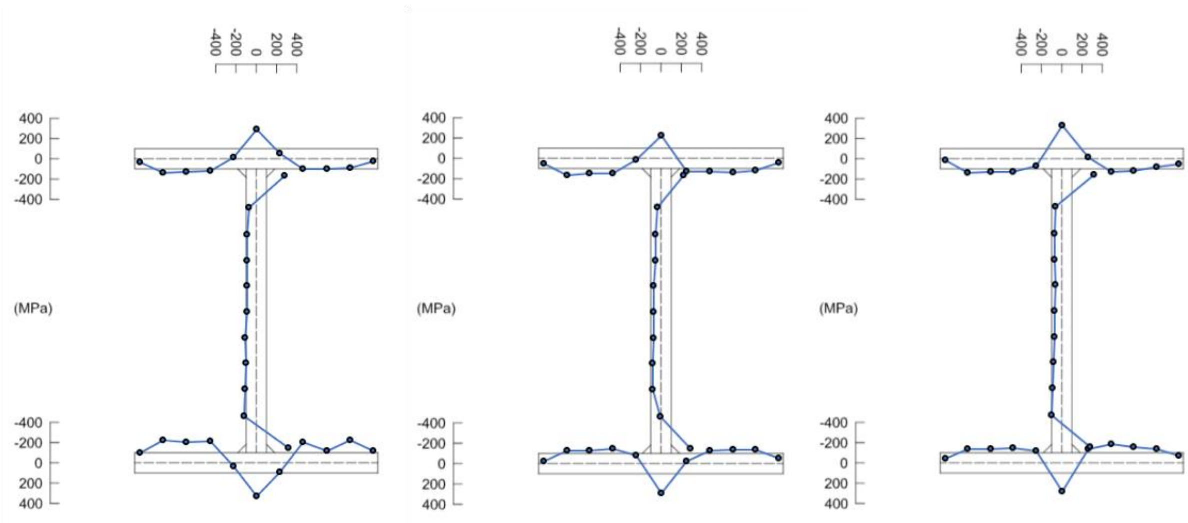

(a) (b) (c)

Figure 5-18 Residual Stress Distributions for Unheated Specimens: (a) b/t_f = 6, (b) b/t_f = 7 and (c) b/t_f = 8

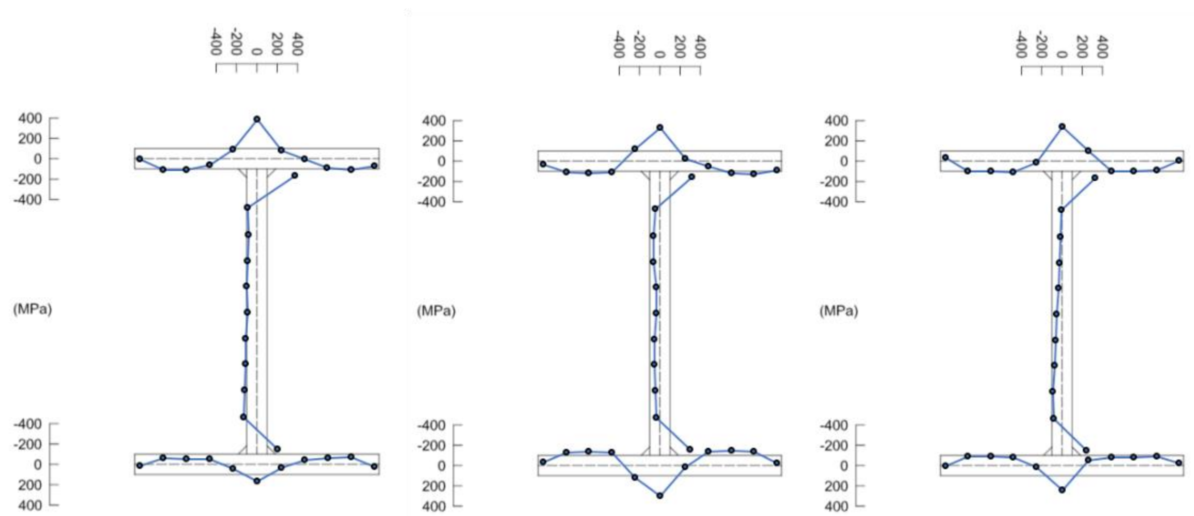

(a) (b) (c)

Figure 5-19 Residual Stress Distributions for Specimens Heated to 300°C: (a) b/t_f = 6, (b) b/t_f = 7 and (c) b/t_f = 8

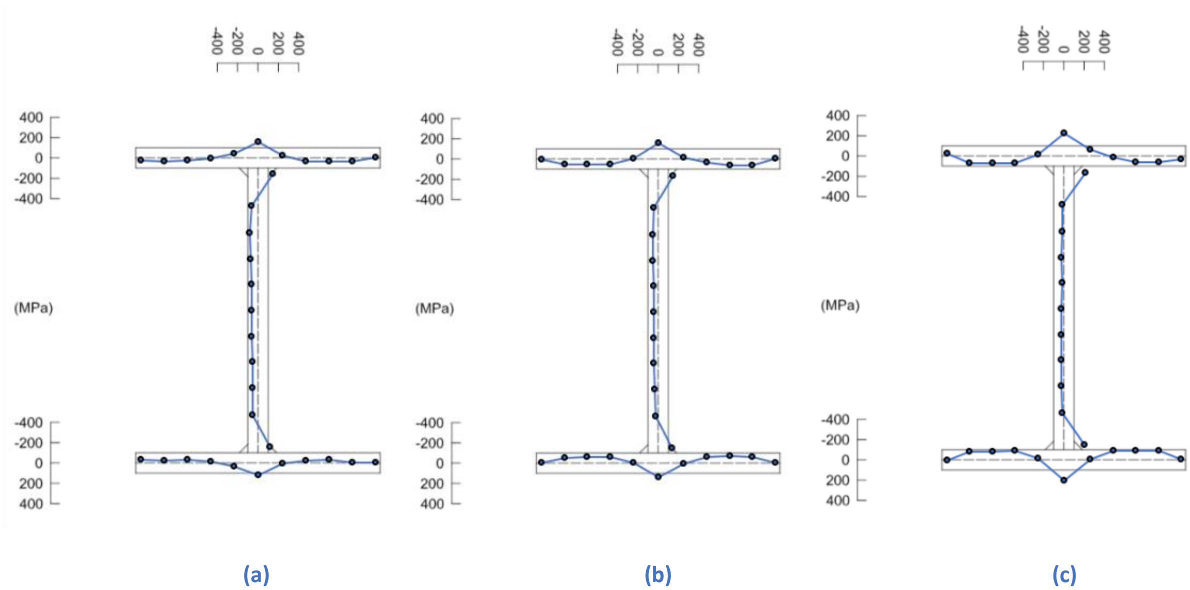

Figure 5-20 Residual Stress Distributions for Specimens Heated to 500°C: (a) b/t_f = 6, (b) b/t_f = 7 and (c) b/t_f = 8

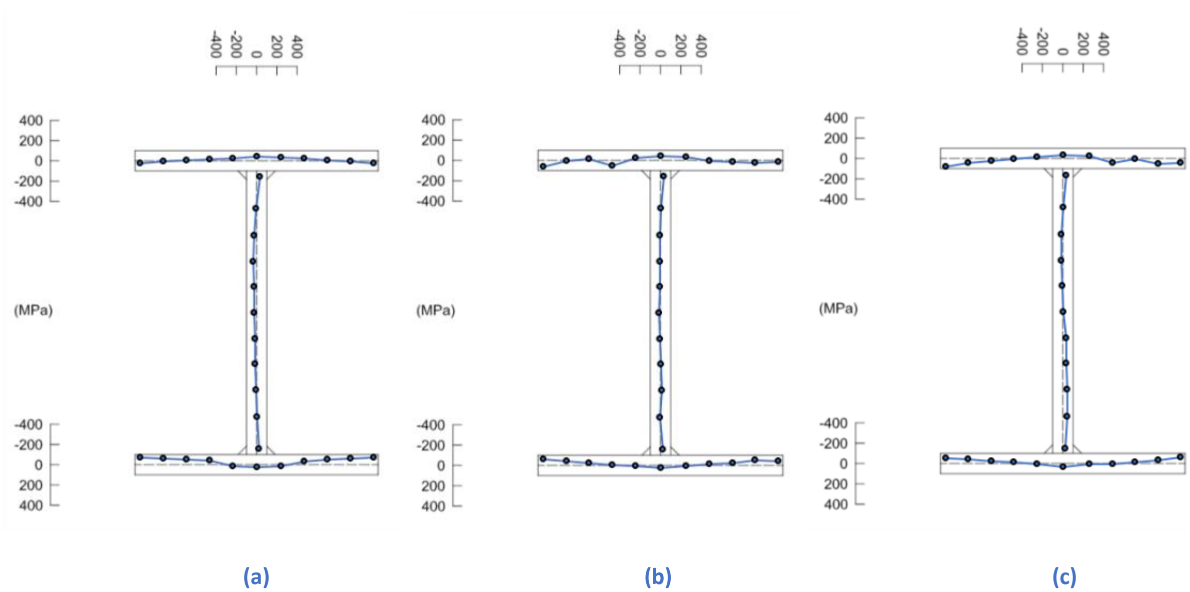

Figure 5-21 Residual Stress Distributions for Specimens Heated to 700°C: (a) b/t_f = 6, (b) b/t_f = 7 and (c) b/t_f = 8

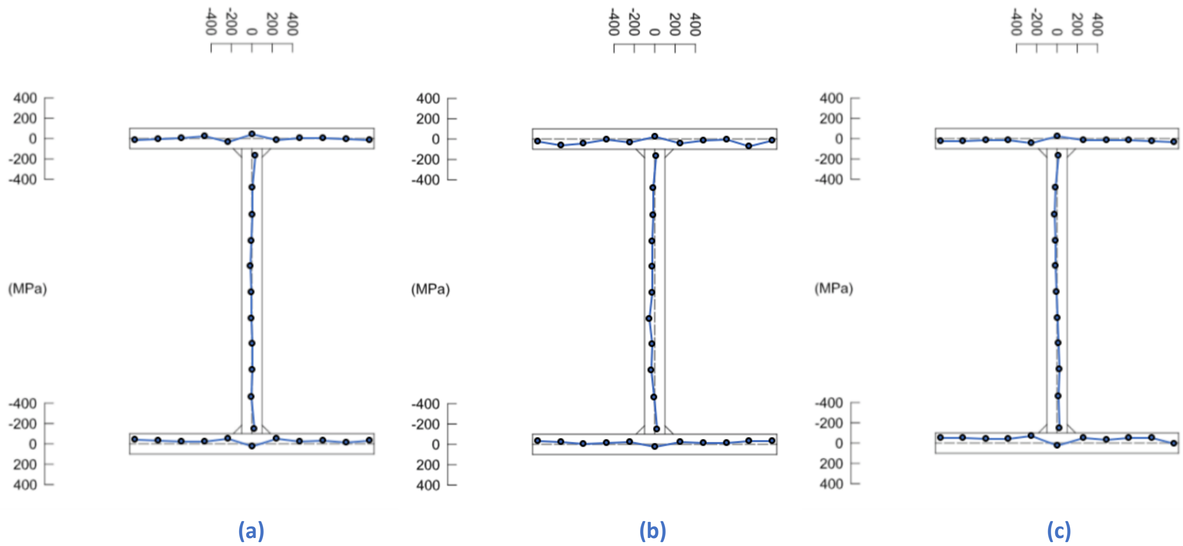

Figure 5-22 Residual Stress Distributions for Specimens Heated to 900°C: (a) b/t_f = 6, (b) b/t_f = 7 and (c) b/t_f = 8

From these figures, it can be seen that the maximum residual stress for welded Q690 I-shaped sections occurs at the web-flange junction regardless of the value of the width/thickness ratio, and that the magnitudes of residual stresses decrease as the exposed temperature increases. At or below 300°C, the magnitudes and distributions of residual stresses do not appear to change much. However, when the exposed temperature is over 300°C, the magnitudes show a noticeable decrease. When the exposed temperature reaches 900°C, the residual stresses are less than 5% of the nominal yield stress of Q690 steel. A decrease in the magnitudes of residual stresses under high temperature exposure can be explained by the fact that heat treatment is a commonly used method to reduce or remove residual stress in metals.

In Figure 5-23, the residual stresses obtained for three cross-sections with different width/thickness ratios are plotted. As can be seen, the effect of width/thickness ratios (which vary from 6 to 8) on residual stresses does not appear to be important.

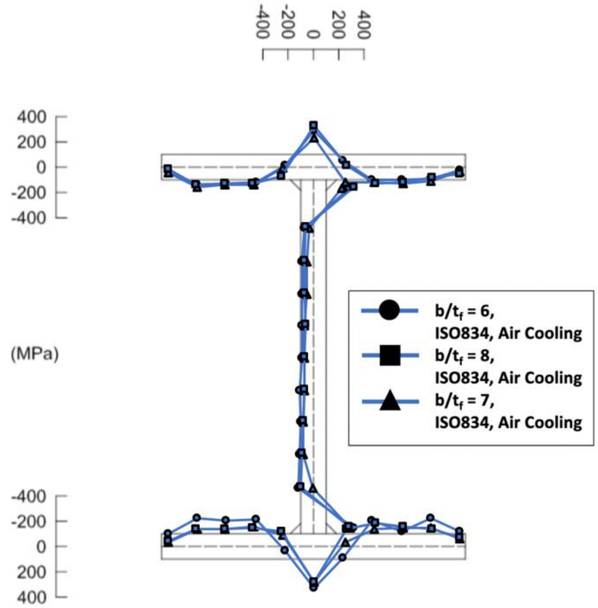

Figure 5-23 Comparison of Residual Stresses for Sections with Different Width-to-thickness Ratios

To investigate whether different heating and cooling methods would have an effect on the magnitudes and distributions of residual stresses, two additional sets of the tests were carried out. The first set uses a constant heating rate of 10°C/min while the second set uses water cooling. For these tests, the width/thickness (b/t_f) ratio used is 7.

The results of the tests are shown in Figures 5-24 to 5-27. For each figure, the cross-section on the left represents residual stresses (in MPa) obtained using the ISO 834 heating protocol followed by air cooling, the cross-section in the middle represents residual stresses (in MPa) obtained using 10°/min heating rate followed by air cooling, and the cross-section on the right represents residual stresses (in MPa) obtained using the ISO 834 heating protocol followed by water quenching. From these figures, it can be observed that the type of heating method used has only very minor effect on the residual stresses. However, the level of exposed temperature and the manner the specimens are cooled are important factors in affecting the residual stress magnitudes and distributions. Because of the fast cooling rate of water quenching (approximately 3400°C/min), the sudden temperature change does not allow stress relief to occur gradually and results in higher compressive residual stresses develop at the flange tips and higher tensile residual stresses develop in web-flange junctions especially when the exposed temperature is higher than 500°C.

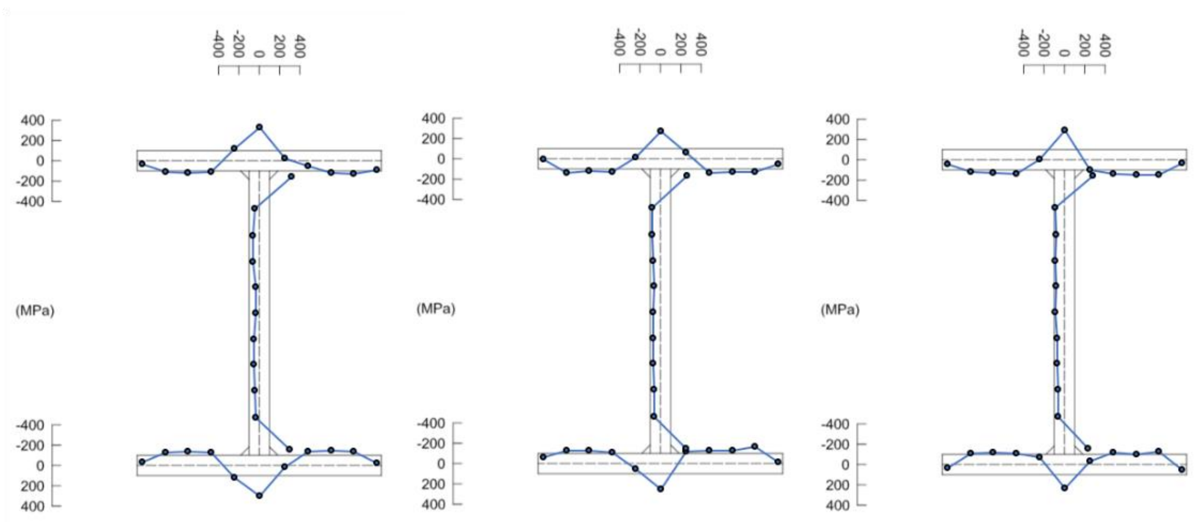

Figure 5-24 Residual Stress Distributions for Specimens Heated to 300°C

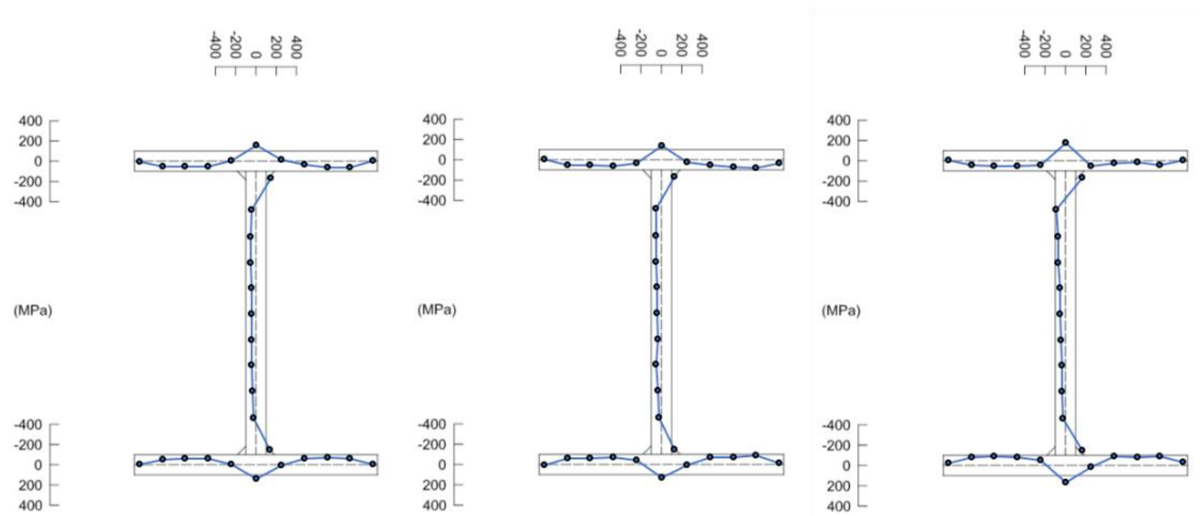

Figure 5-25 Residual Stress Distributions for Specimens Heated to 500°C

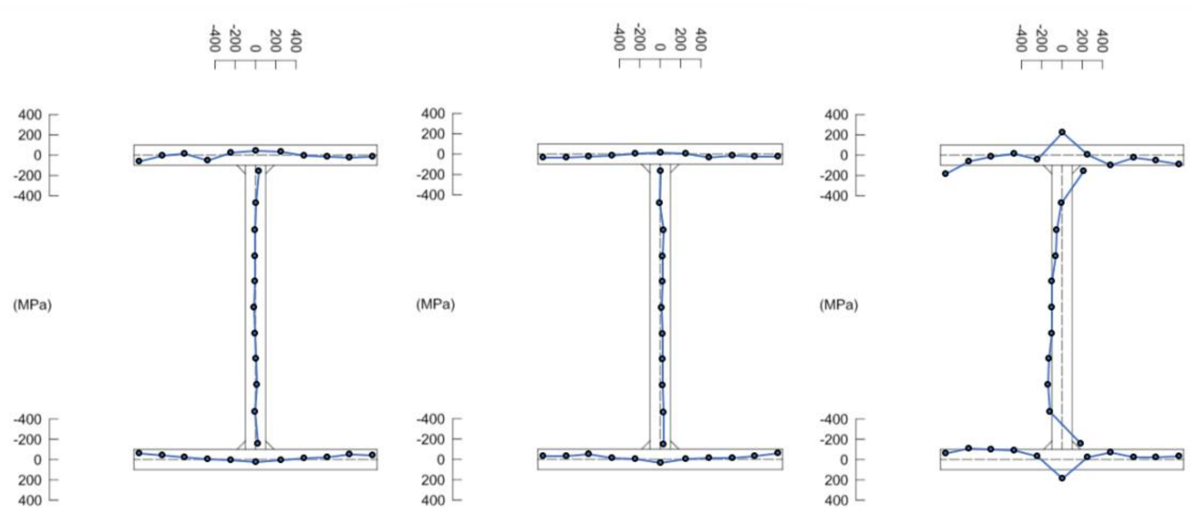

Figure 5-26 Residual Stress Distributions for Specimens Heated to 700°C

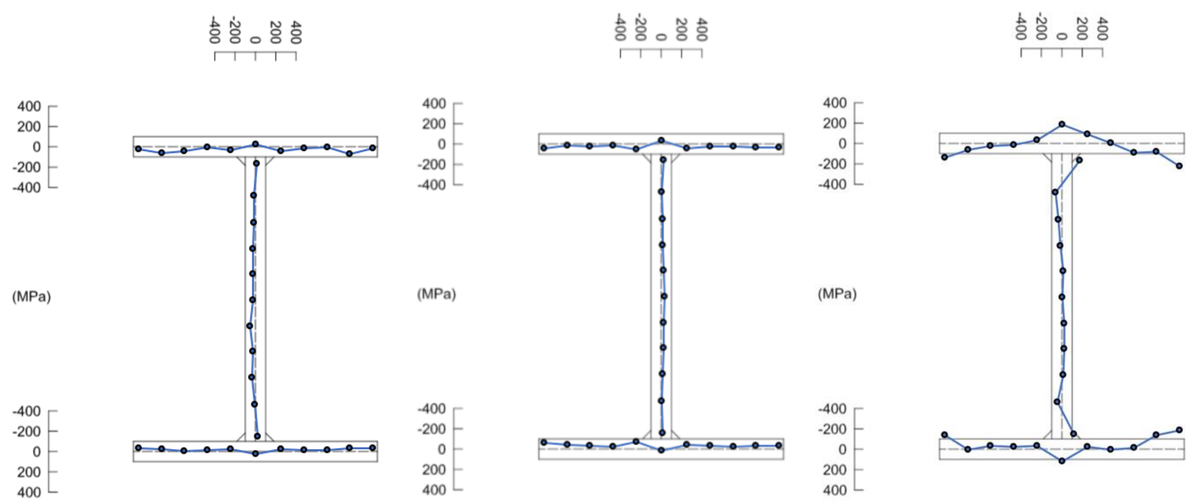

Figure 5-27 Residual Stress Distributions for Specimens Heated to 900°C

A comparison of the magnitudes and distributions of residual stresses (in MPa) under different heating and cooling conditions for specimens heated to four temperatures are shown in Figures 5-28 and 5-29. Generally speaking, welded Q690 I-shaped sections have a relatively low residual stress magnitudes when compared to the nominal steel yield strength. This is different from regular strength steels, where it is not unusual for residual stresses to have values at or near the nominal steel yield strength [69].

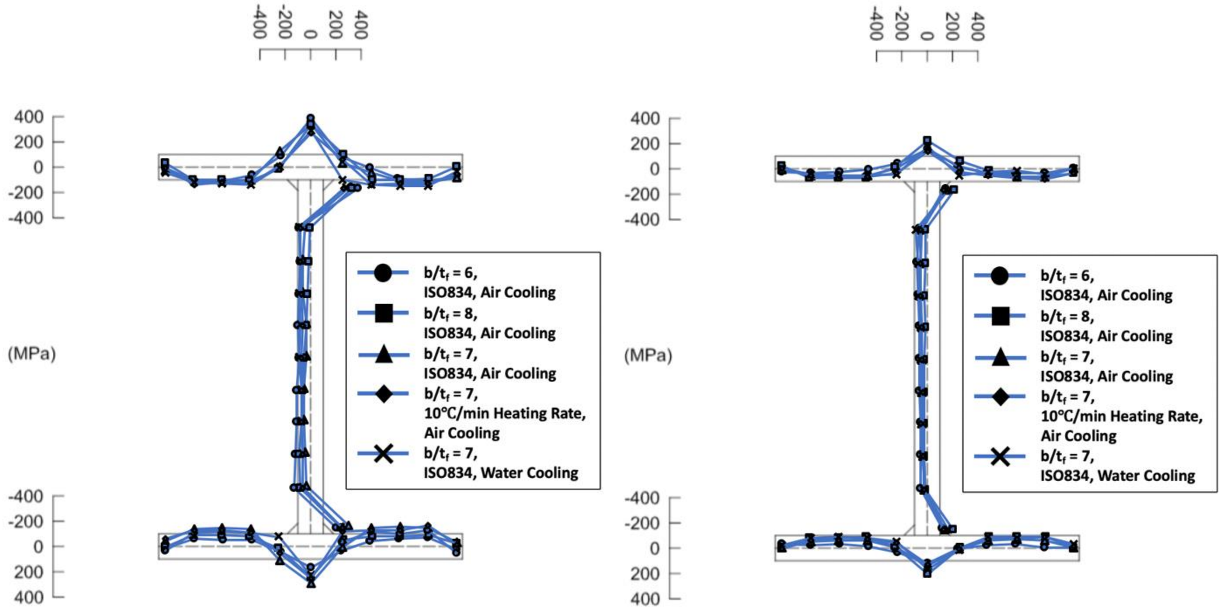

(a) (b)

Figure 5-28 Comparison of Residual Stresses for Specimens Heated to: (a) 300°C and (b) 500°C

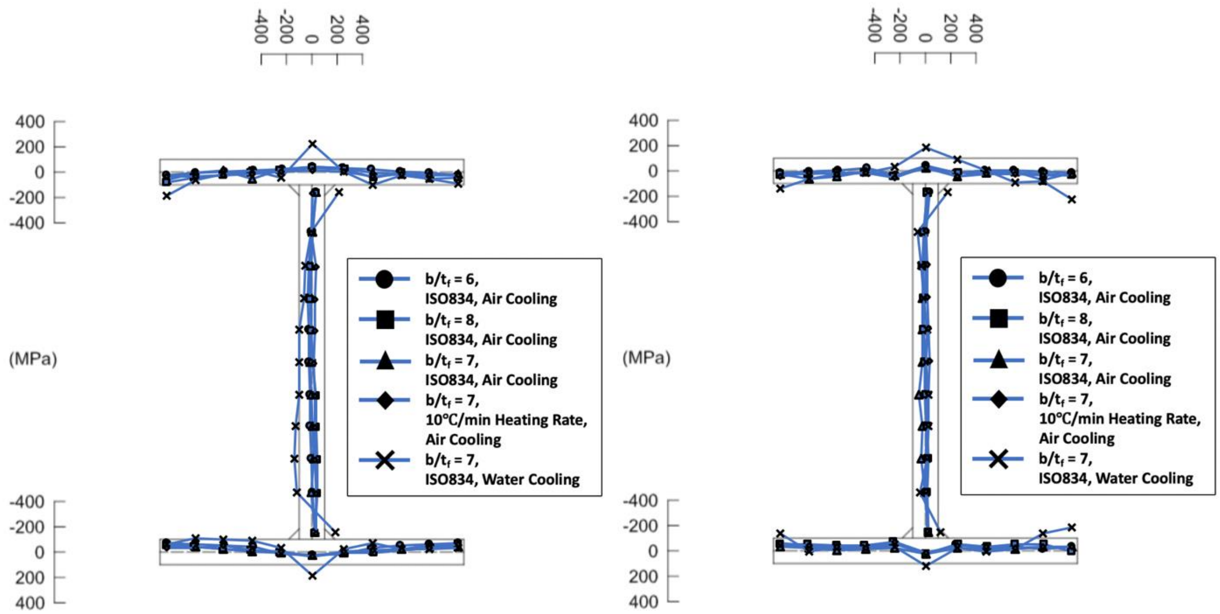

(a) (b)

Figure 5-29 Comparison of Residual Stresses for Specimens Heated to: (a) 700°C and (b) 900°C

5.7 Comparison with X-ray Diffraction Method

While hole-drilling and sectioning methods are considered destructive methods, a non-destructive method that can be used to measure residual stresses is the X-ray diffraction method [71]. This method is based on Bragg's Law. It uses the direction and magnitude of the diffraction peak of the crystal lattice to determine the magnitude of residual stresses as well as whether they are tensile or compressive. Some advantages of this method are its high measurement speed and high precision. However, a disadvantage is that the measured results are sensitive to test locations. Different detection depths can give significantly different results. Some test results obtained using the X-ray diffraction method are shown in Table 5-5. When compared with those obtained using the more generally accepted sectioning method, the results are considered unsatisfactory. Furthermore, since the distance between the sensor and testing surface exceeds 1 cm, the handheld X-ray stress meter (shown in Figure 5-30) cannot be used to measure residual stresses in the web unless it is cut, which could cause stress loss and thereby give fall readings. Because X-ray diffraction method can only measure residual stresses in the outer fibers (approximately 50 μm deep) of the cross-section, measuring errors can occur due to different measuring depths as a result of surface corrosion, even if the thickness of the surface corrosion is relatively small. Based on the results shown in Table 5-5, the X-ray diffraction method is considered unsuitable for measuring residual stress in welded I-shaped sections fabricated with thick plates.

Table 5-5 Residual Stresses Test Results Obtained using X-ray vs. Sectioning Method

Specimen Label*		Left	←------------------------------				Mid	------------------------------→				Right
6S0	Top Flange (MPa) X-ray/ Sectioning	-131	-144	-131	-100.5	-85.5	144.5	-229.5	-116	-216.5	-193	-254
		-34.8	-141.3	-131.7	-118.3	13.2	282.9	44.5	-106.1	-106.5	-93.4	-27.3
	Bottom Flange (MPa) X-ray/ Sectioning	-166	-219	-191	-211	-51	19.5	171.5	-220	-215.5	-212	-314.5
		-100.5	-224.0	-206.8	-212.0	28.6	315.4	88.2	-201.0	-125.1	-219.4	-119.0
7S0	Top Flange (MPa) X-ray/ Sectioning	-241.5	-262.5	-305	-254	-107.5	-235.5	-325.5	-224.5	-309	-294	-376.5
		-43.5	-154.5	-138.3	-141.5	-10.9	148.7	-116.6	-122.9	-126.7	-114.0	-37.6
	Bottom Flange (MPa) X-ray/ Sectioning	-132	-99.5	-262	-63	-26	127.5	-154.5	-155	-220.5	-120.5	-371
		-22.8	-122.5	-117.7	-144.1	-71.2	185.6	-17.0	-121.6	-125.9	-130.3	-48.8
8S0	Top Flange (MPa) X-ray/ Sectioning	-275	-183	-218.5	-241.5	-45	186	-151	-235.5	-167.5	-210	-118.5
		-14.0	-135.4	-129.3	-127.8	-76.0	319.6	7.6	-132.9	-121.4	-86.1	-55.2
	Bottom Flange (MPa) X-ray/ Sectioning	-141.5	-178	-188.5	-212.5	-120.5	60.5	-263.5	-267	-212.5	-168.5	-118
		-35.1	-126.7	-129.7	-142.7	-107.9	280.8	-128.9	-173.7	-148.3	-131.8	-64.7
6S5	Top Flange (MPa) X-ray/ Sectioning	-19	11.5	-41.5	-22	-74.5	-73	32.5	13	-8.5	-107.5	12.5
		-27.7	-33.8	-30.6	-13.9	36.9	114.0	14.8	-39.0	-35.4	-38.4	0.4
	Bottom Flange (MPa) X-ray/ Sectioning	9.5	4.5	-10.5	-63.5	198.5	37.5	17	-33	-20.5	-29.5	3.5
		-26.7	-20.5	-29.0	-12.6	40.2	85.9	5.9	-22.9	-31.8	2.9	-3.6

*see Table 5-2 for a description of these specimens

(a) (b)

Figure 5-30 (a) μ-360 Handheld X-ray Stress Meter, and (b) Measuring

5.8 Proposed Residual Stress Distribution Model

In this section, residual stress distribution model capable of accounting for the effect of the level of exposed temperature for welded Q690 I-shaped sections cooled under natural air is proposed. The proposed model followed the format used by Wang et al. [30] is shown in Figure 5-31.

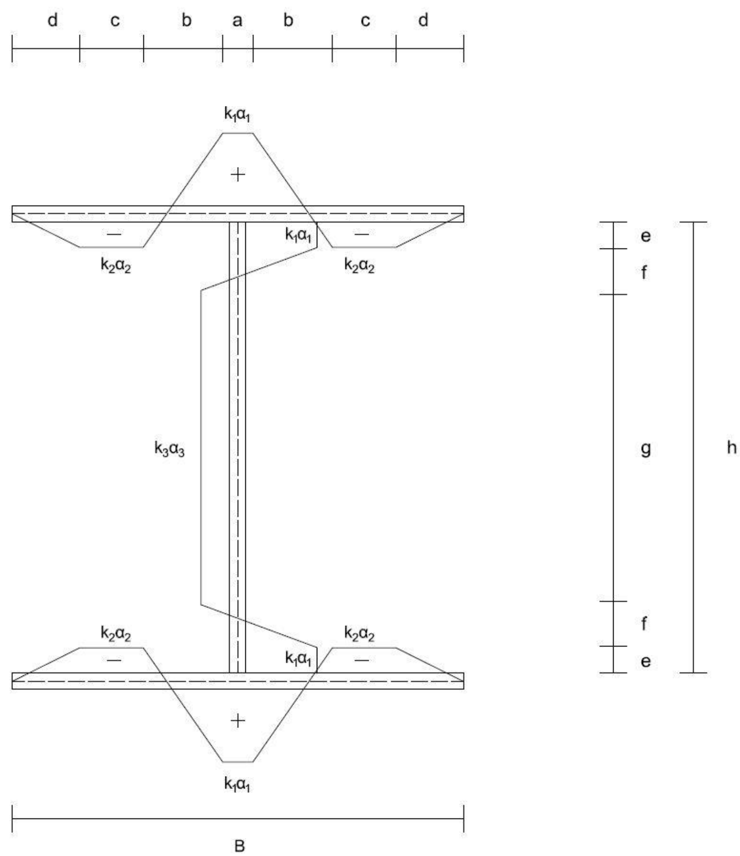

Figure 5-31 Proposed Residual Stress Distribution Model

The dimensions *a*, *b*, *c*, *d*, *e*, *f* and *g* represent the distribution range for the residual stresses. The constants α_1, α_2 and α_3 denote the ratios of residual stresses to the nominal yield stress of an unheated specimen made from Q690 steel (i.e. 690 MPa), and k_1, k_2, and k_3 are temperature modification factors. They are proposed as follows:

$a = t_w$, b is to be determined using cross-section stress equilibrium, $c = (B\text{-}a\text{-}2b\text{-}2d)/2$, $d = 0.13B$, $e = 0.21\alpha_1 h$, $f = 0.18h\text{-}e$, and $g = h\text{-}2e\text{-}2f$, where B is the flange width and h is the web height. $\alpha_1 = 0.45$, $\alpha_2 = -0.2$, and $\alpha_3 = -0.1$ (+/- represents tension or compression).

The temperature modification factors are proposed as:

$$k_1 = \begin{cases} 1 & T \leq 200°C \\ 1.365 - 0.00183T & 200°C < T < 700°C \\ 0.084 & T \geq 700°C \end{cases} \tag{5.5}$$

$$k_2 = \begin{cases} 1 & T \leq 200°C \\ 1.342 - 0.0017T & 200°C < T < 700°C \\ 0.152 & T \geq 700°C \end{cases} \tag{5.6}$$

$$k_3 = \begin{cases} 1 & T \leq 200°C \\ 1.43 - 0.00215T & 200°C < T < 700°C \\ -0.075 & T \geq 700°C \end{cases} \tag{5.7}$$

These modification factors were obtained by curve-fitting the measured magnitudes of residual stresses for different exposed temperatures at five points labelled *A, B, C, D* and *E* on the cross-section as shown in Figure 5-32(a). The determination of k_2 is illustrated in Figure 5-32(b).

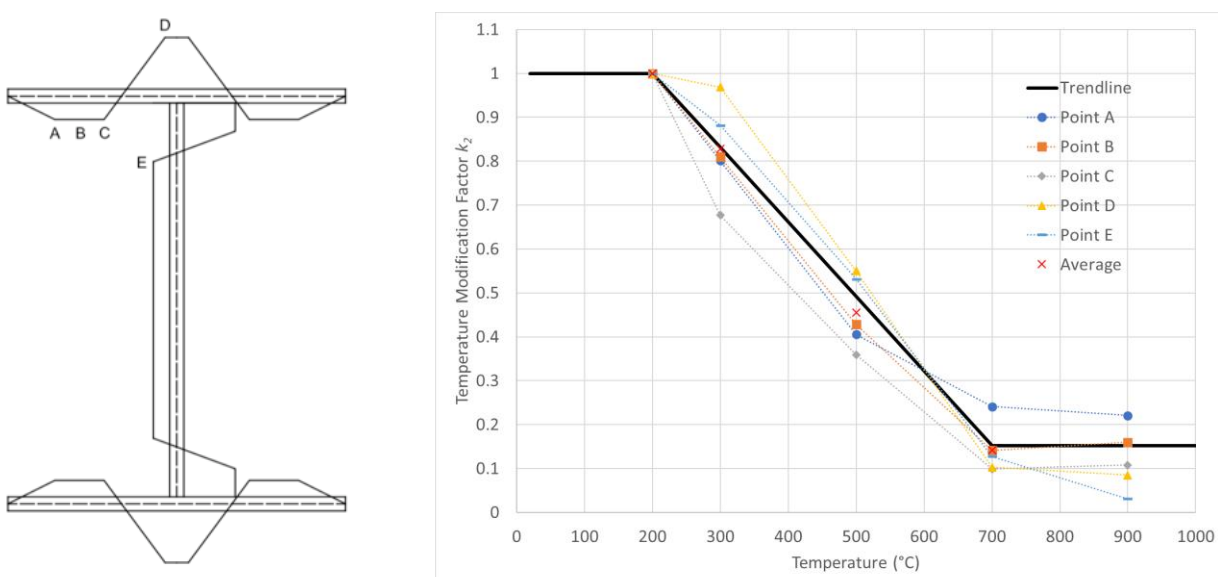

(a) (b)

Figure 5-32 Determination of Temperature Modification Factor k_2

The residual stresses calculated using the proposed residual stress distribution model are compared with the measured data in Figures 5-33 to 5-37 for the unheated, 300°C, 500°C, 700°C and 900°C temperature exposure, respectively. The black dash line represents the pattern of residual stresses calculated using the proposed model. Note that the measured residual stresses for 700°C and 900°C due to water cooling are not shown since they show noticeable changes when compared to their air-cooled counterparts at these levels of exposed temperature.

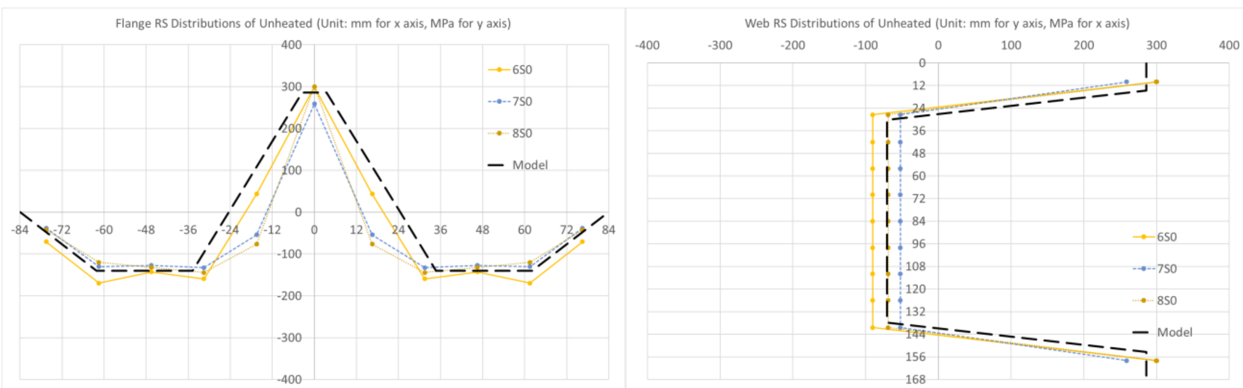

Figure 5-33 Comparison of the Proposed Model with Measured Data for Unheated Specimens

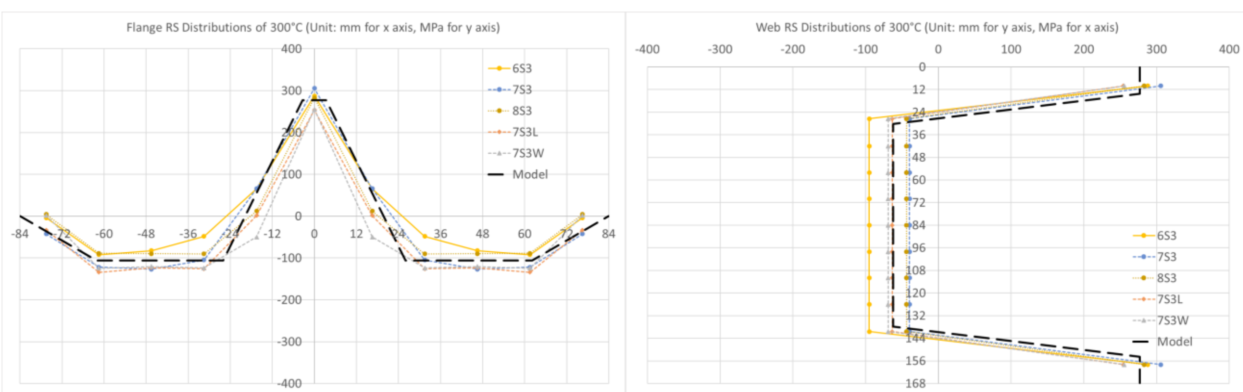

Figure 5-34 Comparison of the Proposed Model with Measured Data for Specimens Heated to 300°C

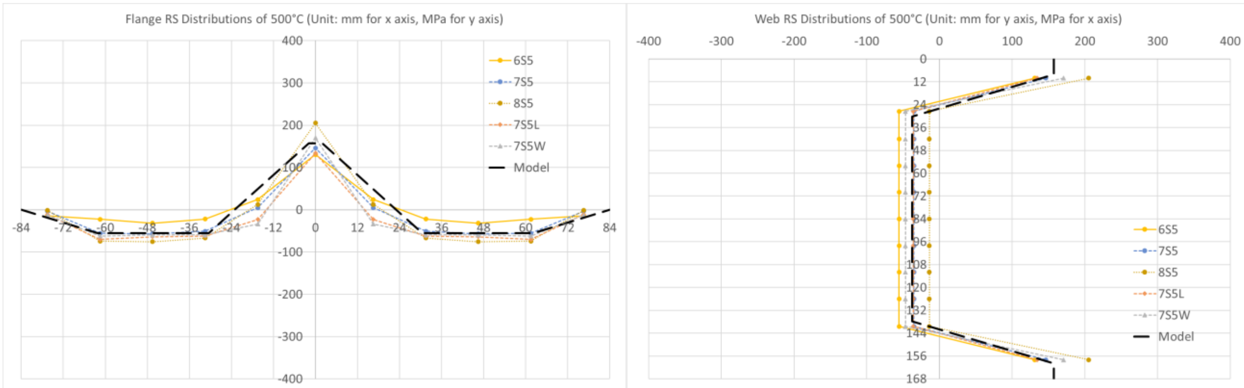

Figure 5-35 Comparison of the Proposed Model with Measured Data for Specimens Heated to 500°C

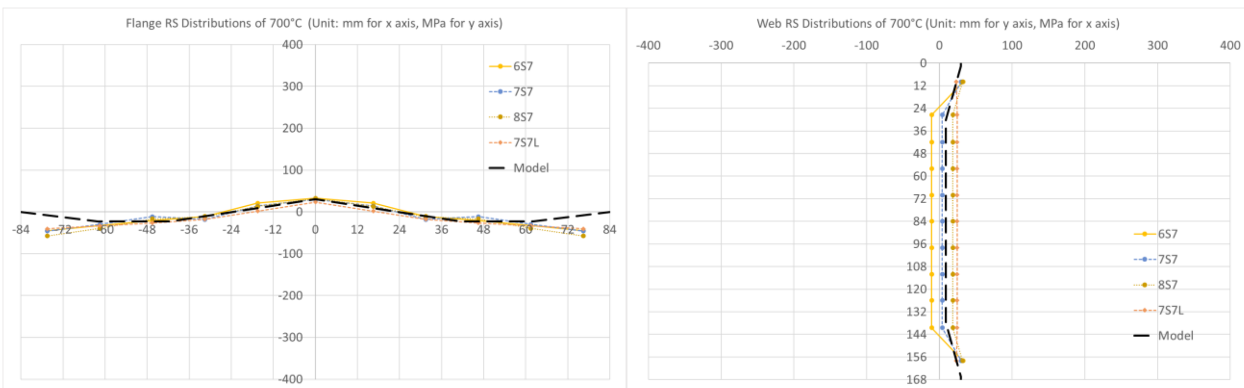

Figure 5-36 Comparison of the Proposed Model with Measured Data for Specimens Heated to 700°C

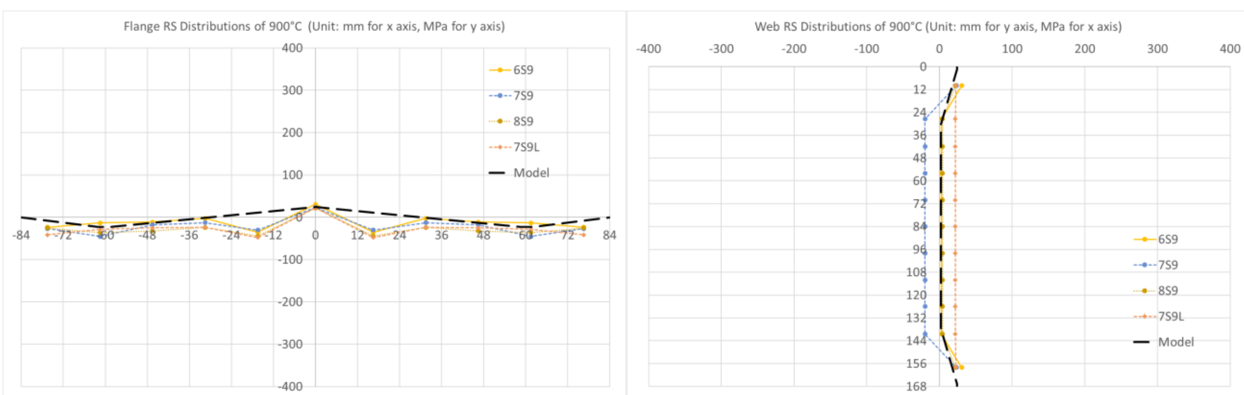

Figure 5-37 Comparison of the Proposed Model with Measured Data for Specimens Heated to 900°C

The proposed model can be used to estimate residual stresses for both air-cooled and water-cooled specimens when the exposed temperature is below 700°C, but it should only be used for air-cooled specimens when the exposed temperature is above 700°C. Since the measured residual stresses for water-cooled specimens heated above 700°C show noticeable differences when compared to their air-cooled counterparts, another residual stress distribution model as shown in Figure 5-38 is developed.

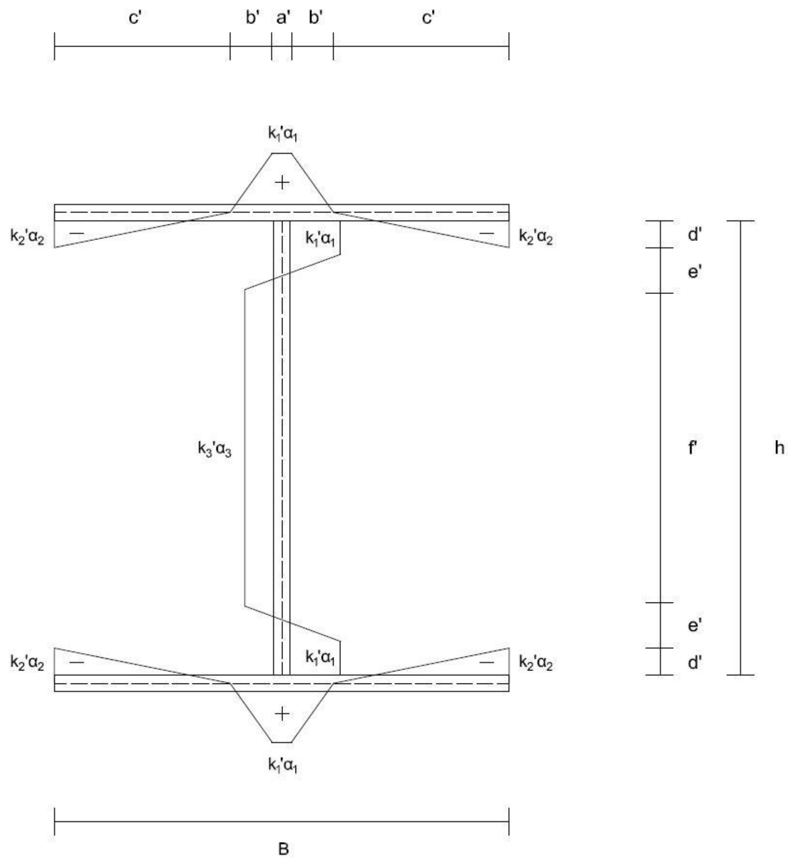

Figure 5-38 Proposed Residual Stress Distribution Model for Water-cooled Specimens heated to 700°C and 900°C

The dimensions *a'*, *b'*, *c'*, *d'*, *e'*, *f'* are calculated as follows: *a'*= t_w, *b'*= 0.06*B*, *c'*= (*B*-*a'*-*2b'*)/2, *d'*= 0.06*h*, *e'*= 0.12*h*, *f'*= *h*-*2d'*-*2e'*, where *B* is the flange width and *h* is the web height. α_1= 0.45, α_2= -0.2, and α_3= -0.1. The temperature modification factors are given as:

$$k_1' = 1.189 - 0.00078T \qquad 700°\text{C} \le T \le 900°\text{C} \qquad (5.8)$$

$$k_2' = 0.0014T - 0.138 \qquad 700°\text{C} \le T \le 900°\text{C} \qquad (5.9)$$

$$k_3' = 3.7 - 0.0038T \qquad 700°\text{C} \le T \le 900°\text{C} \qquad (5.10)$$

The comparisons of the residual stresses calculated using the proposed model with measured data for the water-cooled specimens heated to 700°C and 900°C are shown in Figure 5-39 and 5-40 respectively.

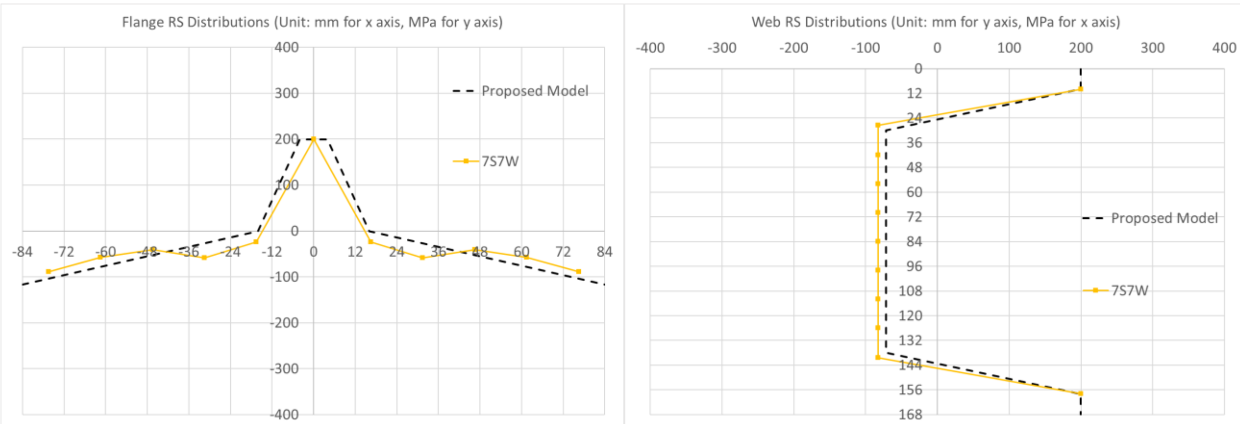

Figure 5-39 Comparison of the Proposed Model with Measured Data for Water-cooled Specimens Heated to 700°C

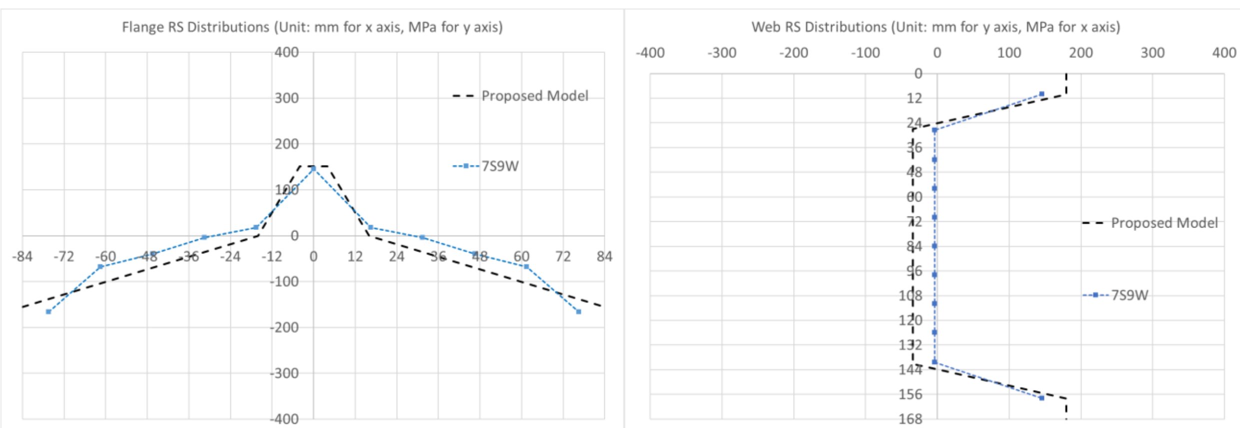

Figure 5-40 Comparison of the Proposed Model with Measured Data for Water-cooled Specimens Heated to 900°C

5.9 Conclusions

A total of 23 welded Q690 I-shaped section specimens were fabricated and tested to investigate the magnitudes and distributions of residual stresses before and after fire exposure. Two heating methods (ISO 834 and 10°C/min) and two cooling methods (air cooled and water quenched) were used. Based on the test results, the following conclusions can be made.

1. Regardless of the level of exposed temperature and cooling method used, the maximum residual stress to yield stress ratio in welded I-shaped sections made from Q690 High Strength Steel is lower than that for welded I-sections made from regular strength steel.
2. The level of exposed temperature has a noticeable influence on residual stresses. When the exposed temperature is below 300°C, the influence is not important. When the exposed temperature exceeds 300°C, the magnitudes of the maximum residual stresses start to decrease. Once the temperature reaches 700°C, the maximum residual stress magnitudes are less than 5% of the nominal steel yield strength.
3. The heating method and heating rate used do not seem to affect the residual stress results. However, for specimens heated to a temperature at or above 700°C and suddenly cooled by water quenching, noticeable residual stresses are generated on the edges of the flanges and at the web-flange junctions. The residual stress magnitudes on the flange edges are $-0.13F_y$ for 700°C and $-0.24F_y$ for 900°C, while the magnitudes at the web-flange junctions are $+0.29F_y$ for 700°C and $+0.21F_y$ for 900°C (where F_y is the nominal yield stress of Q690 steel and +/- represents tension or compression).
4. Two residual stress distribution models of welded Q690 I-shaped sections taking into consideration the level of exposed temperature are developed. One model is recommended for use for both air-cooled and water-cooled specimens heated below 700°C as well as for air-cooled specimens heated above 700°C, and another is recommended for use for water-cooled specimens heated above 700°C. These models have been shown to give reasonably good results when compared with the experimentally measured data.

6 CYCLIC BEHAVIOR OF POST-FIRE Q690 WELDED I-SHAPED COLUMNS

In this chapter, a Finite Element Model (FEM) developed and validated to simulate the cyclic behavior of a welded I-shaped column made from Q690 high strength steel will be presented. Based on the data presented in previous chapter, the post-fire cyclic behavior of this Q690 welded I-shaped column will be determined, and the relationship between material deterioration and cyclic performance will be investigated.

6.1 Introduction

Earthquake is one of the most harmful natural hazards in the world. According to the current AISC Seismic Provisions for Structural Steel Buildings [72], structural steel shall satisfy the following requirements: (1) has a pronounced yield plateau; (2) is able to undergo large inelastic deformation; (3) possesses good weldability; and (4) has a yield to tensile strength ratio of 0.85 or less. The AISC provisions also indicate that the specified minimum yield strength of structural steel used for ductile components should not exceed 50 ksi (345 MPa) unless tests are performed to justify its use. However, this provision is based on test results of normal strength steel. Since applications of high strength steel become more and more popular in construction and its mechanical properties often do not satisfy all the requirements specified in the standard, the performance of high strength steel when used in seismic applications needs to be investigated.

Compared with mild steel, high strength steel has a higher mechanical strength, but lower ductility, and its yield to tensile stress ratio is closer to 1, which means its seismic resistance needs to be investigated. Furthermore, the post-fire mechanical properties of high strength steel often decrease with an increased exposed temperature. Considering the potential deleterious effect of the bi-hazards of earthquake and fire, the post-fire cyclic response of an I-shaped column made from Q690 steel will be investigated in this chapter.

To this end, a FEM is developed and validated to study the cyclic performance of a welded I-shaped column fabricated from Q690 steel subject to different levels of fire exposure. The relationship between deteriorations of mechanical properties after fire exposure and their effect on the cyclic performance of the column is also studied.

6.2 Simplified Column Model

To simulate a typical frame column shown in Figure 6-1, a cantilever column having half the length of the original column and subject to a horizontal force and vertical load at the tip is proposed. Since the forces acting on this cantilever column should be the same as those acting at the mid-point of the original column, the magnitude of the horizontal force is assumed to be half that of the lateral force acting on the story. Thus, the horizontal force and vertical load acting on this cantilever column are equal to *P* and *N*, respectively. The column is assumed to orient in such a way that it will bend about its major axis under the applied forces.

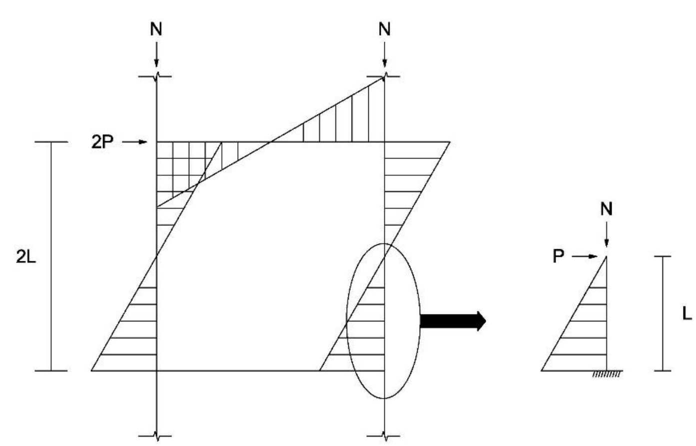

Figure 6-1 Simplified Frame Column

If we define the Axial Force Ratio (AFR) as the ratio of the axial compressive load and the cross-sectional yield resistance, then

$$AFR = N/f_y A \tag{6.1}$$

where A is the cross-section area and f_y is the nominal yield stress of steel.

In addition, if we denote the reference lateral load P_y as the load that will cause yielding at the outmost fiber of the column cross-section, we have

$$N/A + P_y L/S_x = f_y \tag{6.2}$$

where S_x is the elastic section modulus about the strong axis of the cross-section.

The reference displacement d_y that corresponds to this reference load can be written as

$$d_y = P_y L^3/3EI_x \tag{6.3}$$

where E is the elastic modulus and I_x is the moment of inertia about the strong axis.

d_y is referred to as the yield drift. It is to be used as the reference value to apply the lateral load on the simplified column model.

6.3 Experimental Tests (Chen et al., 2016)

Based on the simplified column model, Chen et al. [45] performed cyclic tests on two welded I-shaped column specimens (H-1 and H-2) made from Q690 steel. The dimensions of the test specimens are given in Table 6-1 and Figure 6-2. The mechanical properties of the Q690 steel used to fabricate the specimens are given in Table 6-2.

Table 6-1 Dimensions of the Test Specimens

Specimens	H (mm)	B (mm)	t_w (mm)	t_f (mm)	L (mm)
H-1 and H-2	250	250	16	16	2505

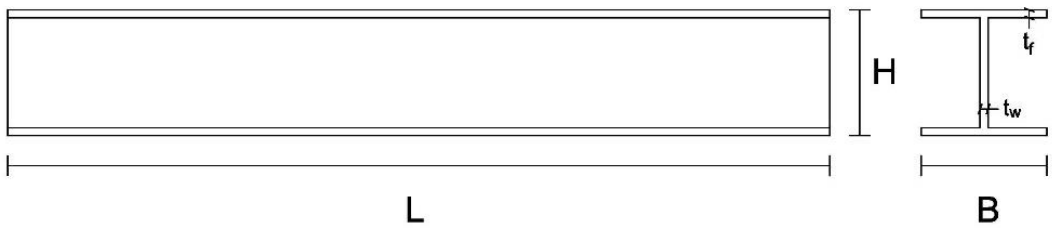

Figure 6-2 Dimensions of the Column Specimens

Table 6-2 Mechanical Properties of Q690 Steel

Elastic Modulus (GPa)	Yield Strength (MPa)	Tensile Strength (MPa)	Tensile Strain	Elongation (%)
206	779	834	0.059	19

Both specimens were tested as cantilever columns as shown in Figure 6-3. An L-link, which was able to rotate freely in the bending plane, was used to connect the vertical and horizontal actuators. The axial compressive force and yield drift calculated as per Equations (6.1) to (6.3) using the nominal yield strength (690 MPa) and the cross-section elastic moment resistance M_y and plastic moment resistance M_p calculated using the tested yield strength are presented in Table 6-3. Two cyclic lateral load protocols labelled Type 1 and Type 2 in Figure 6-4 were used. Type 1 was used for Specimen H-1 and Type 2 was used for Specimen H-2. For the Type 1 load protocol shown in Figure 6-4(a), the first displacement-based load step is applied until the displacement reaches $0.5d_y$ and is cycled only once. Then, three load cycles, each reaching a maximum displacement of d_y, will follow. After this, the load is increased so each successive tri-load cycle will increase the displacement by d_y. For the Type 2 load protocol shown in Figure 6-4(b), once the displacement reaches $3d_y$, all subsequent cycles will stay at this displacement level. For both load protocols, the tests would continue until failure occurred. Failure is said to have occurred when the load at the maximum displacement of one loop dropped below 85% of the peak load (i.e., the load that corresponds to the maximum displacement of each loop).

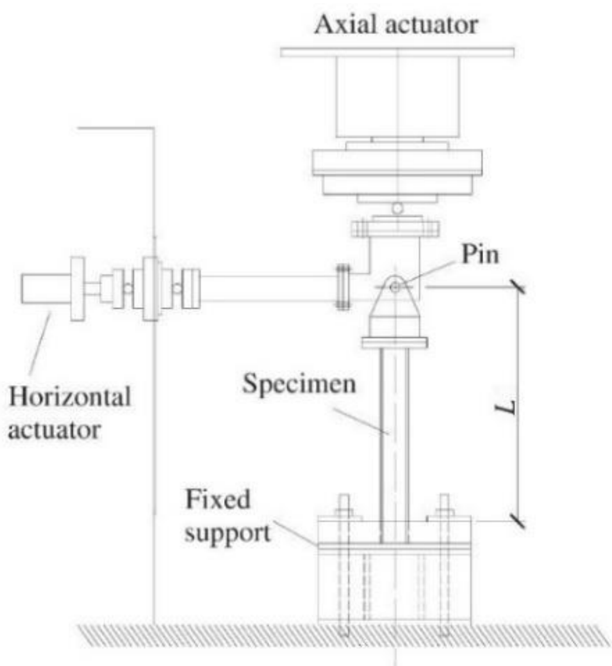

Figure 6-3 Test Setup [45]

Table 6-3 Loading Condition and Cross-section Moment Resistances of the Test Specimens

AFR	Axial Compressive Load *N* (kN)	Yield Drift d_y (mm)	Cross-section Elastic Moment Resistance M_y (kN-m)	Cross-section Plastic Moment Resistance M_p (kN-m)
0.35	2774.5	36.4	769.6	877.2

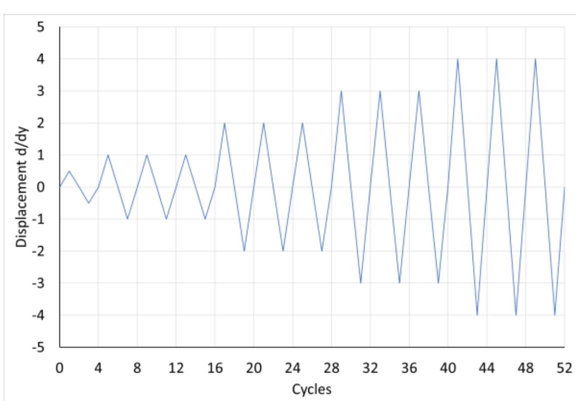

(a)

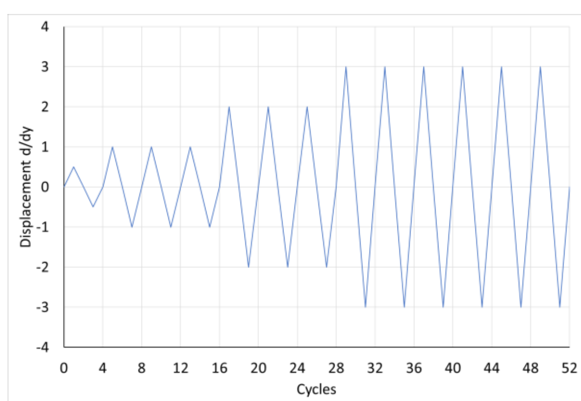

(b)

Figure 6-4 Lateral Loading Protocols: (a) Type 1 and (b) Type 2

The cyclic behavior of these two specimens was expressed in terms of their hysteretic curves. Both specimens were observed to exhibit good energy dissipation capacity and no pinching occurred. In addition, the failure mode of both specimens was local buckling of the flanges as shown in Figure 6-5. The drift ratio, i.e. the ratio of the maximum lateral displacement of the specimen to its height, was 1/17 for Specimen H-1 and 1/23 for Specimen H-2. They are both much higher than the 1/50 limit for the story drift ratio as per ASCE 7-10 [73], indicating that these column specimens have sufficient ductility under the applied loads.


(a) Specimen H-1 (b) Specimen H-2

Figure 6-5 Failure Mode of Test Specimens [45]

6.4 Verification

Using the test data presented by Chen et al. [45], a FEM is developed and proposed to simulate the hysteretic behavior of these columns.

6.4.1 Proposed Finite Element Model

The general finite element software ABAQUS 6.14 is used to perform the numerical simulation. The dimensions of the column, shown in Figure 6-6, are the same as those of the test specimens, except that two rigid plates are added to the column for load application and to apply the boundary conditions. The 3-D element C3D8R, which is a general purpose linear brick element with reduced integration as shown in Figure 6-7(b), is used to model the column and the rigid plates.

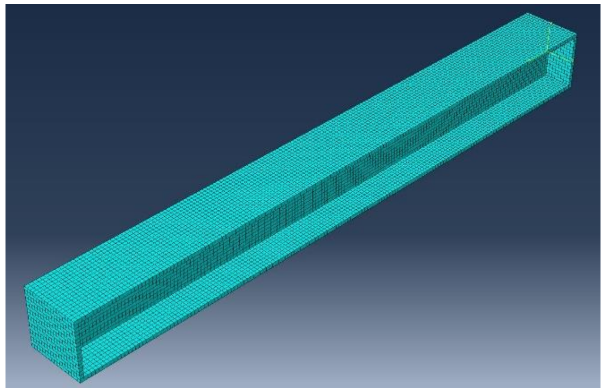

Figure 6-6 Finite Element Model of a Column

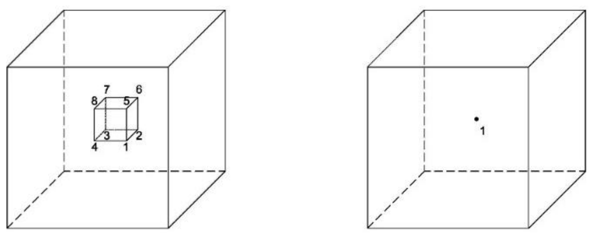

(a) (b)

Figure 6-7 Integration Point Scheme of a: (a) C3D8 vs. (b) C3D8R Element

The bottom plate is constrained rotationally and translationally in all directions to simulate the fixed boundary condition, while the top plate is only translationally constrained in the direction normal to the bending plane to simulate a free boundary condition without out-of-plane movement. The axial compressive load, which is applied to the column prior to the horizontal cyclic load, is applied at the center of the top rigid plate. The horizontal displacements are then applied as a boundary condition at the top rigid plate in accordance with the loading protocol. The stress-strain curve used is shown in Figure 6-8. It is generated from measured data given in Table 6-2 and fitted with a multiple linear kinematic hardening model [45]. Since ABAQUS requires users to input mechanical properties in the form of a true stress-strain curve, engineering stress-strain is converted to true stress-strain using the following equations.

$$\sigma_{true} = \sigma_{engineering} \times \left(1 + \varepsilon_{engineering}\right) \tag{6.4}$$

$$\varepsilon_{true} = ln\left(1 + \varepsilon_{engineering}\right) \tag{6.5}$$

Note that, the stress-strain curve is divided into an elastic region and a plastic region. In the elastic region, the elastic modulus defines the linear relationship between stress and strain. The plastic region starts when the true yield stress σ_{true} is reached. Stresses above the true yield stress generate a total true strain composed of an elastic true strain and a plastic true strain. The plastic true strain can be calculated using the equation

$$\varepsilon_{plastic} = \varepsilon_{total} - \varepsilon_{elastic} = ln\left(1 + \varepsilon_{engineering}\right) - \frac{\sigma_{true}}{Elastic\ Modulus} \tag{6.6}$$

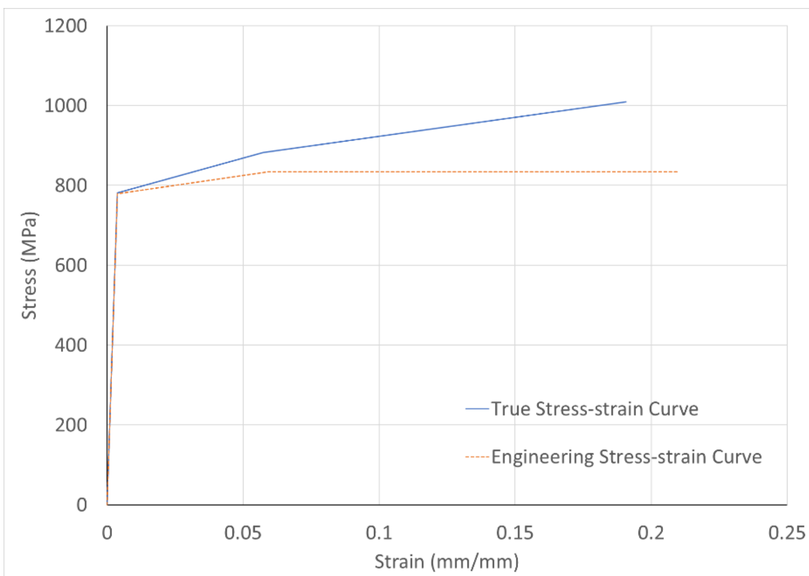

Figure 6-8 Engineering Stress-strain Curve vs. True Stress-strain Curve

6.4.2 Comparison with Experimental Tests

The test data reported by Chen et al. [45] will be used to evaluate the proposed FEM. Three finite element models with mesh size approximately equal to 10 mm, 15 mm and 20 mm were developed. The hysteresis loops generated using these three meshes (labelled Mesh-10, Mesh-15 and Mesh-20) together with the test data (shown as black solid lines) are shown in Figure 6-9. As can be seen, the results for Mesh-10 and Mesh-15 are very close to each other. As a result, Mesh-15 will be used for all subsequent finite element simulations.

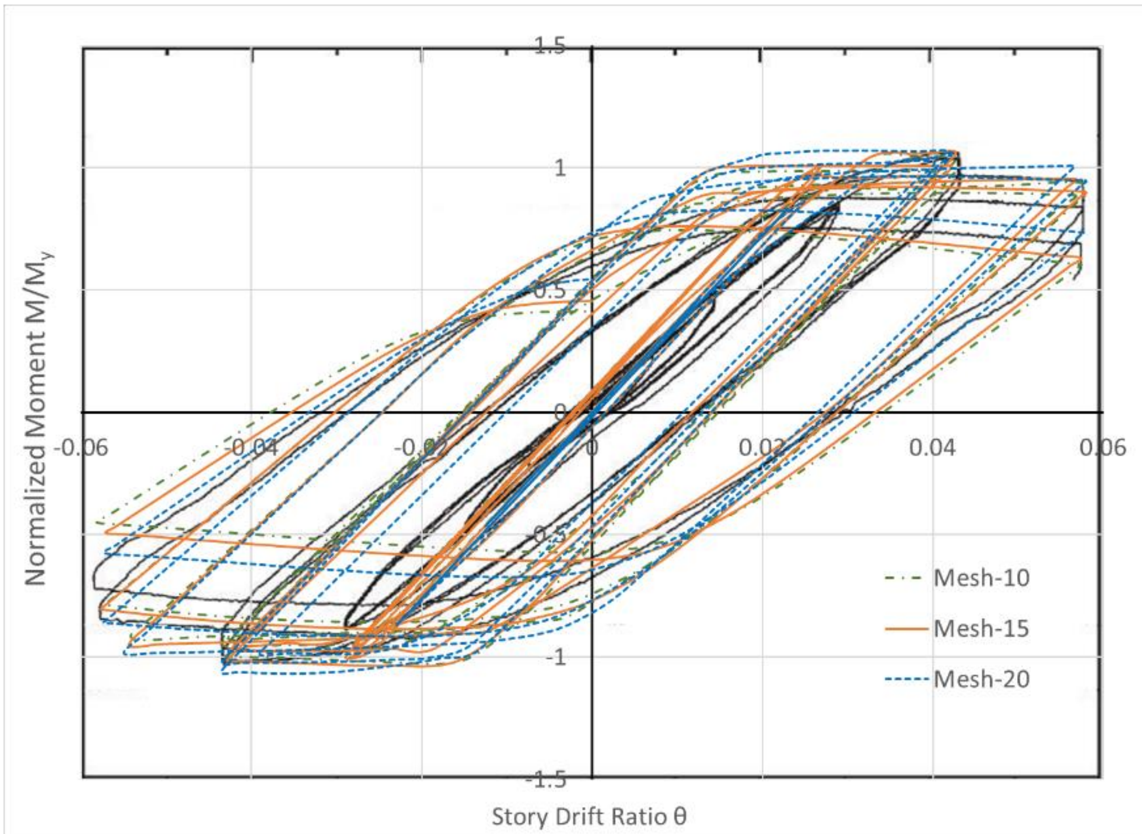

Figure 6-9 Mesh Sensitivity Analysis

In Figure 6-9, the x-axis is the story drift ratio, and the y-axis is the normalized moment M/M_y. For a given axial force ratio (AFR) defined in Eq. (6.1), the axial force of a column made from high strength steel is much higher than that of the same column made from mild steel. As a result, secondary moment should be considered in computing *M* at the fixed support. should be the sum of the first- and second-order moments. The equations used to compute the story drift ratio and normalized moment are therefore

$$\theta = d/L \quad (6.7)$$

$$M_1 = PL \quad (6.8)$$

$$M_2 = Nd \quad (6.9)$$

$$M/M_y = (M_1 + M_2)/M_y \quad (6.10)$$

where d is the horizontal displacement at the tip of the column, M_1 is the first-order moment, M_2 is the second-order moment and P is the horizontal applied force that produces d.

Using Mesh-15, the FE generated hysteresis loops are compared in Figures 6-10 and 6-11 with the hysteretic loops obtained experimentally (shown as solid black lines) for Specimens H-1 and H-2, respectively. A comparison of the skeleton curves is given in Figure 6-10. The skeleton curves are obtained by connecting the peak value of M/M_y for each story drift ratio.

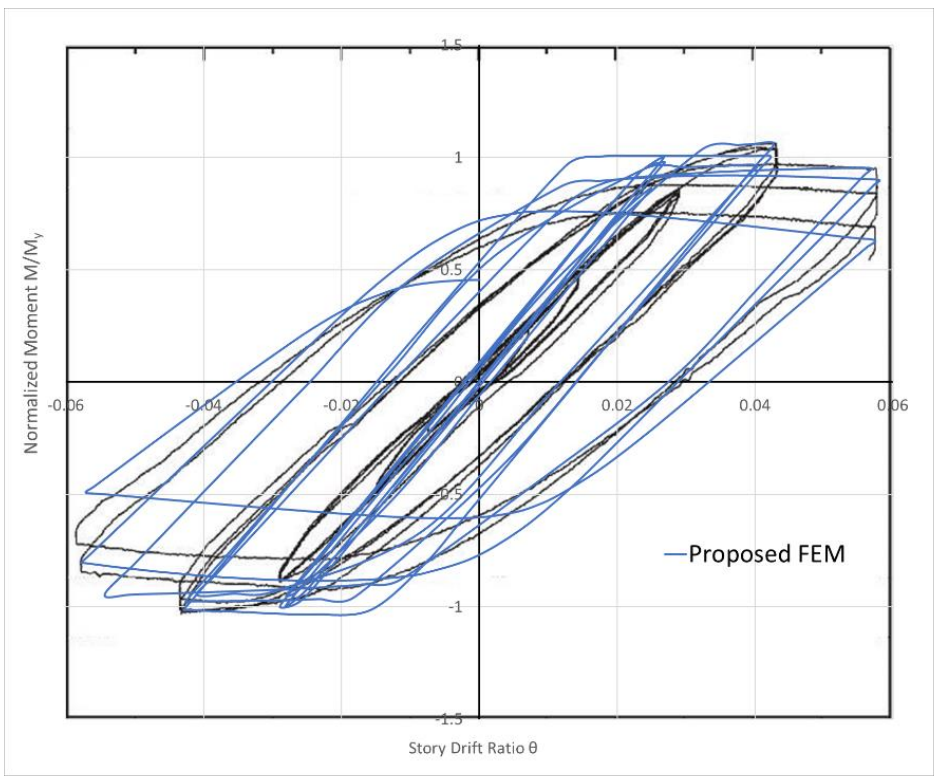

Figure 6-10 Comparison of Hysteresis Loops for Specimen H-1

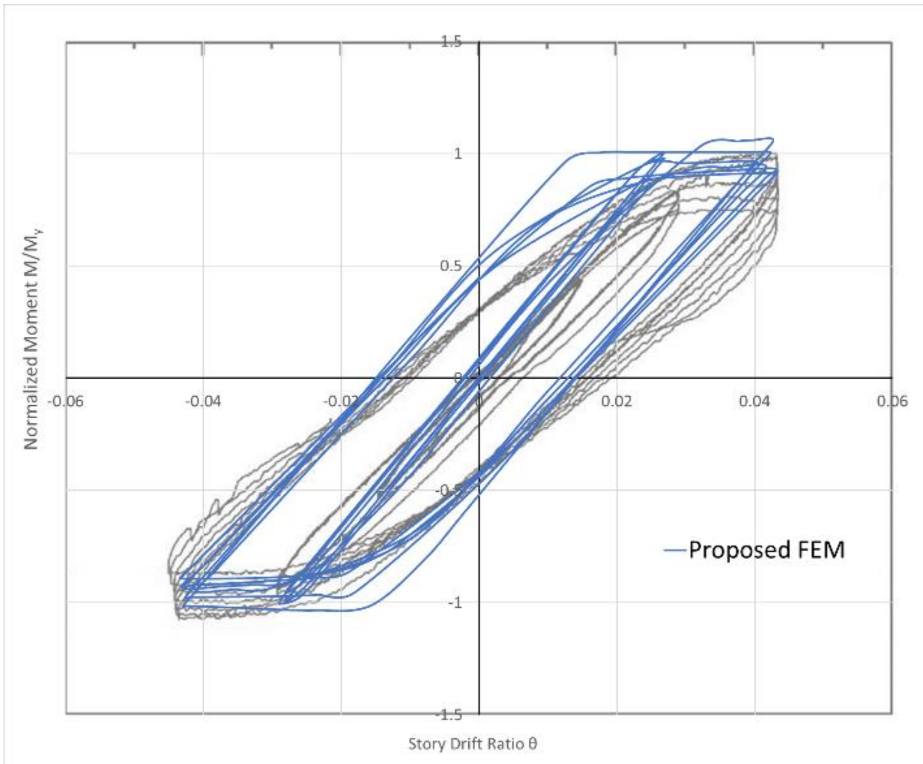

Figure 6-11 Comparison of Hysteresis Loops for Specimen H-2

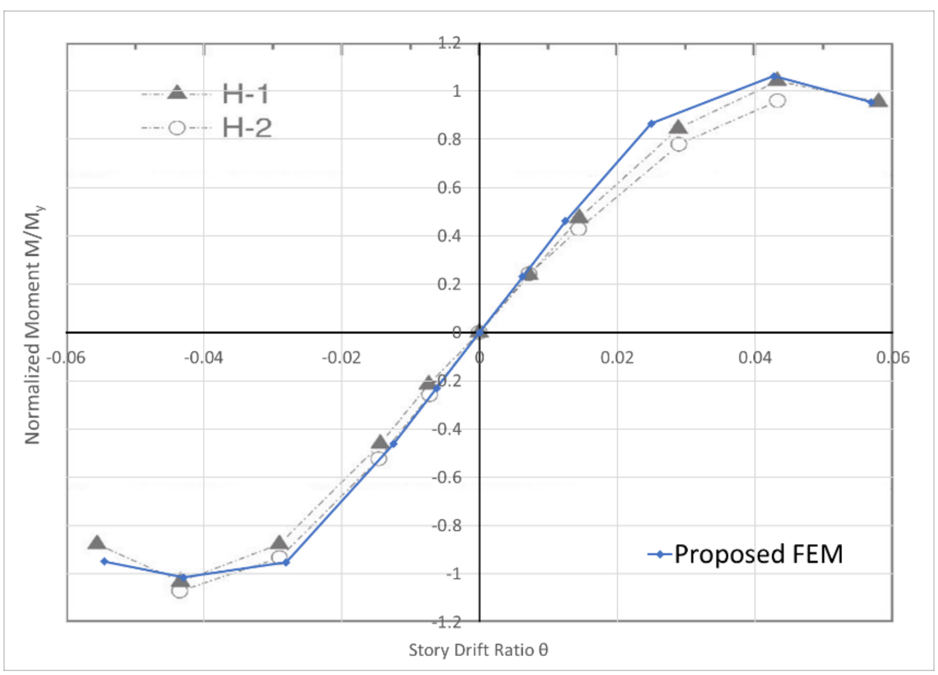

Figure 6-12 Skeleton Curve Comparison

From these figures, it can be seen that the finite element generated hysteresis loops and skeleton curves compare fairly well with the experimental data, except that the areas enclosed by the hysteresis loops obtained from the finite element analysis are somewhat smaller than those of the experimental tests and that the proposed FEM gives results that show higher stiffness for the columns when compared with the test data. This can be explained by the fact that while an ideally fixed support condition was used in the FEM, the actual support can undergo small rotation and slippage between the test specimens and support of the test frame could occur during the experimental tests.

Recall that both test specimens experienced flange local buckling (see Figure 6-5) when failure occurred. In Figure 6-13, the failure mode obtained using finite element for Specimen H-1 is compared with that observed in the test, good correlation is observed.

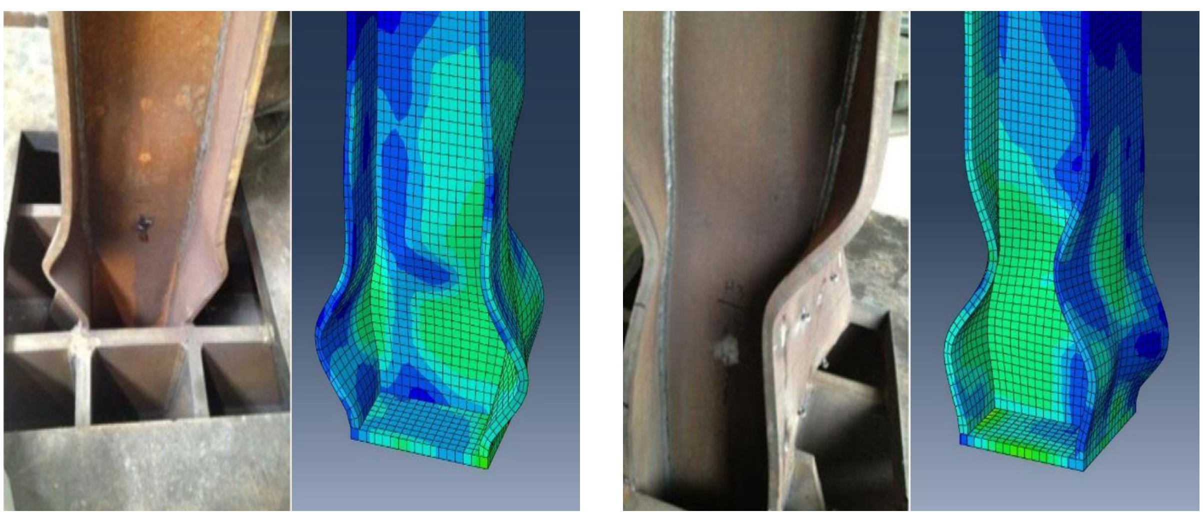

(a) (b)

Figure 6-13 Comparison of Failure Mode obtained from Tests and FEM for Test Column H-1: (a) Front View, and (b) Back View

From these comparisons, it can be said the proposed FEM can properly simulate the cyclic behavior of these welded Q690 I-section columns subject to combined axial force and lateral load.

6.5 Finite Element Analysis

The cyclic performance of a welded Q690 I-shaped column after fire exposure is studied using the proposed FEM and experimentally obtained mechanical properties of Q690 steel described in Chapter 4. In addition, the influences of residual stresses and simplifications made to the stress-strain curve are investigated.

6.5.1 Column and Material Properties

The column dimensions, load condition, yield drift, mesh size and load protocol used in the finite element analysis are given in Table 6-4.

Table 6-4 Column Properties and Load Protocol

H (mm)	B (mm)	t_w (mm)	t_f (mm)	L (mm)
250	250	16	16	2505
AFR	**Axial Compressive Load *N* (kN)**	**Yield Drift d_y (mm)**	**Mesh Size (Brick Size)**	**Lateral Load Protocol**
0.35	2774.5	36.4	15	Type 1

In addition, the post-fire mechanical properties of Q690 steel and corresponding yield moment, yield drift ratio and plastic moment are given in Table 6-5 and Table 6-6, respectively.

Table 6-5 Post-fire Mechanical Properties of Q690 Steel

Exposed Temperature (°C)	Cooling Method	Elastic Modulus (GPa)	Yield Strength (MPa)	Tensile Strength (MPa)	Elongation (%)
Unheated	-	210.5	866	1037	21.86
300	Air Cooling	217.4	915	1094.4	20.33
400	Air Cooling	203.9	910	1049	20.44
500	Air Cooling	199.6	815	968	20.68
600	Air Cooling	199.5	685	980.4	20.64
700	Air Cooling	205.4	635	943	20.63
800	Air Cooling	196.8	505	997.6	24.55
900	Air Cooling	193.7	461	999.2	26.64
300	Water Cooling	205.0	880	1034.2	20.63
400	Water Cooling	201.9	852	964.7	22.45
500	Water Cooling	196.7	865	1017.1	21.53
600	Water Cooling	206.0	738	1007.5	21.5
700	Water Cooling	201.9	562	971.4	24.6
800	Water Cooling	196.4	540	1337.9	9.84
900	Water Cooling	201.4	705	1694.8	16.77

Table 6-6 Post-fire Yield Moment, Yield Drift Ratio and Plastic Moment of the Welded I-shaped Columns

Exposed Temperature (°C)	Cooling Method	Yield Moment M_y (kN-m)	Yield Drift Ratio θ_y	Plastic Moment M_p (kN-m)
Unheated	-	855.6	0.01786	975.2
300	Air Cooling	904	0.01827	1030.4
400	Air Cooling	899	0.01938	1024.7
500	Air Cooling	805.2	0.01773	917.8
600	Air Cooling	676.8	0.01491	771.4
700	Air Cooling	627.4	0.01342	715
800	Air Cooling	498.9	0.01114	568.7
900	Air Cooling	455.5	0.01034	519.1
300	Water Cooling	869.4	0.01864	991
400	Water Cooling	841.8	0.01832	959.4
500	Water Cooling	854.6	0.01909	974.1
600	Water Cooling	729.1	0.01556	831.1
700	Water Cooling	533.5	0.01161	608.1
800	Water Cooling	555.2	0.01242	632.9
900	Water Cooling	696.5	0.0152	793.9

The yield moment, yield drift ratio, and plastic moment are calculated as follows.

$$M_y = S_x f_{ym} \quad (6.11)$$

$$\theta_y = \frac{(1 - AFR) f_{ym} S_x L}{3 E_m I_x} \quad (6.12)$$

$$M_p = Z_x f_{ym} \quad (6.13)$$

where S_x is the elastic section modulus about the strong axis, I_x is the moment of inertia about the strong axis, Z_x is the plastic section modulus about the strong axis, f_{ym} is the measured yield strength and E_m is the measured elastic modulus.

Usually, the range of AFR for frame columns under the combined action of a compressive force and bending moment is 0.2 to 0.5. According to FEMA-356 [74], this range falls under deformation-controlled for flexural behavior but force-controlled for compressive behavior. The AFR selected in the present analysis is 0.35, which represents an average value of 0.2 and 0.5.

6.5.2 Effect of Residual Stresses

Residual stresses generated during the fabricating process of welded columns may affect their cyclic performance. However, according to the results presented in Chapter 5, the magnitude of residual stresses decreases when the exposed temperature increases. To investigate how residual stresses may affect the cyclic performance of welded columns, finite element analysis results obtained for columns with and without considering residual stresses are compared to that of an unheated column. The residual stress pattern used is shown in Figure 6-14, which is a simplified version of the residual stress model described in Chapter 5.

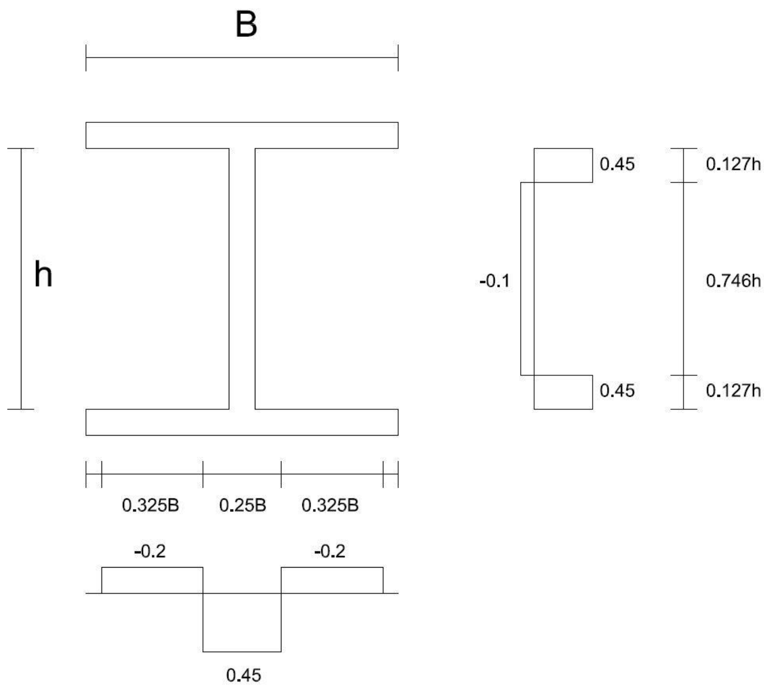

Figure 6-14 Simplified Residual Stress Pattern (expressed in terms of the nominal material yield strength 690MPa)

A comparison of the FE analysis results obtained with and without considering residual stresses is shown in Figure 6-15. The difference in hysteresis behavior of the two columns is negligible and the skeleton curves show good consistency. The effect of residual stresses does not seem to be important. This observation is in agreement with that of Chen et al. [45].

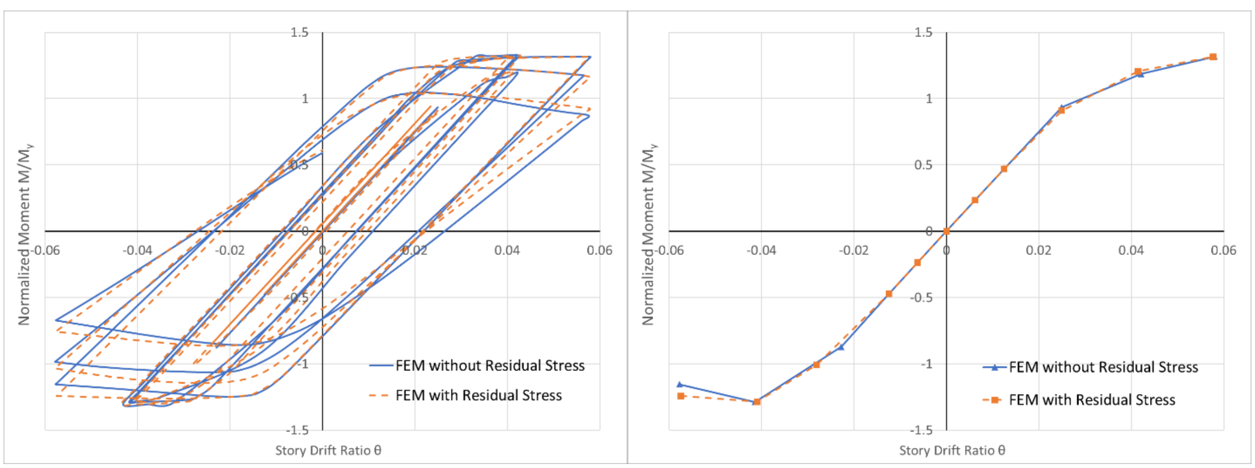

(a) (b)

Figure 6-15 Comparison of Column Behavior with and without Residual Stresses: (a) Hysteresis Loop, and (b) Skeleton Curve

6.5.3 Effect of using a Simplified Stress-strain Curve

In the proposed FEM, the stress-strain curve is modeled using a multiple linear kinematic hardening model. In order to investigate how the result may change if a simplified stress-strain model is used, a comparison of results obtained using the measured stress-strain curve and a simplified stress-strain curve shown in Figure 6-16 is made. The experimentally obtained stress-strain curve is that of an unheated Q690 specimen as described in Chapter 4.

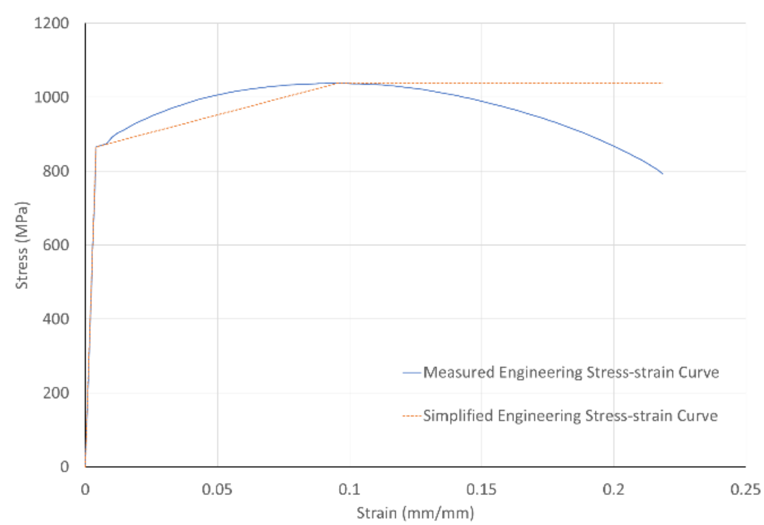

Figure 6-16 Measured vs. Simplified Stress-strain Curves of an Unheated Specimen

The comparison is made in terms of the hysteresis loops and skeleton curves shown in Figure 6-17. Since the simplified stress-strain curve gives a lower stress in the hardening region of the curve, the maximum moment attained and the amount of energy dissipated are smaller. Furthermore, when the exposed temperature is higher than 600°C, the stress-strain curve of post-fire Q690 steel has a much higher ultimate to yield stress ratio (if the yield stress is obtained using the 0.2% offset method) as shown in Figure 6-18, and so larger errors are expected. To avoid incurring these errors, the measured engineering stress-strain curves will be used in the finite element analysis.

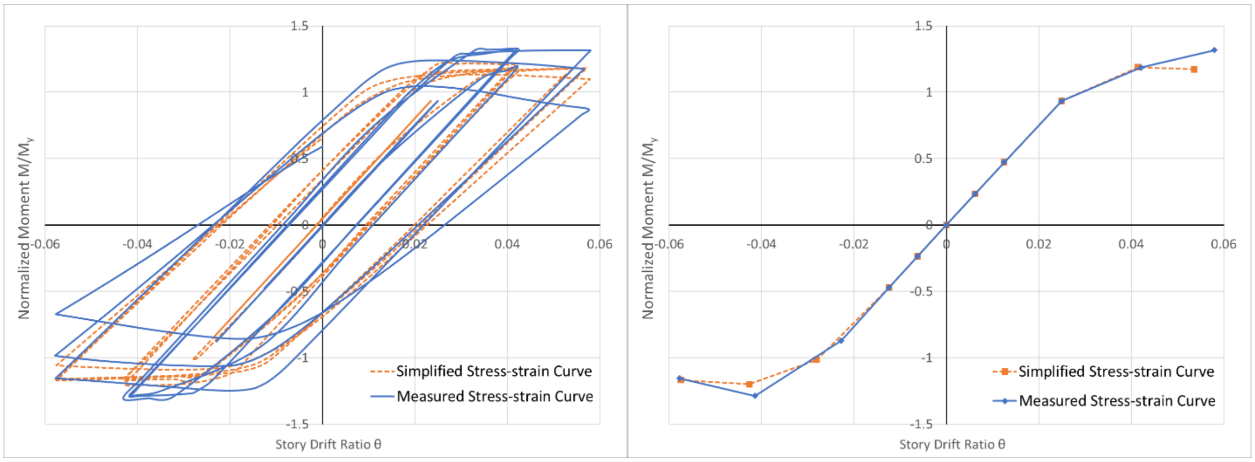

(a) **(b)**

Figure 6-17 Comparison of Column Behavior modeled using Measured vs. Simplified Stress-strain Curves: (a) Hysteresis Loops, and (b) Skeleton Curves

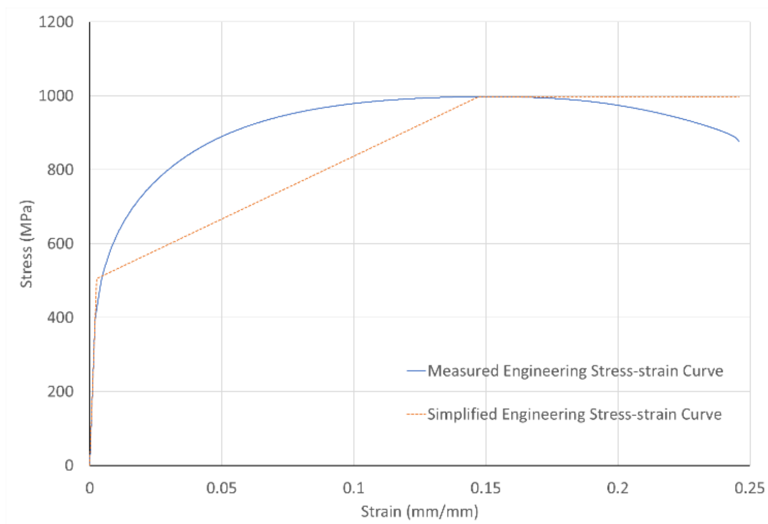

Figure 6-18 Measured vs. Simplified Stress-strain Curves for a Specimen Heated to 800°C followed by Air Cooling

6.5.4 Analysis of an Unheated Column

The finite element model (FEM) described and verified earlier will now be used to perform cyclic analysis of columns made from Q690 steel. In this section, the analysis results of an unheated column will be presented; and in the next section, the analysis results of columns exposed to elevated temperatures and cooled using air or water will be presented. The column dimensions and material properties used for these analyses are given in Tables 6-4 to 6-6. Type 1 load protocol as shown in Figure 6-4(a) will be used.

In the tests reported by Chen et al. [45], failure was assumed to have occurred when the load that corresponded to the maximum displacement of one loop dropped below 85% of the peak load attained during the test. However, given that the yield strength of Q690 steel is higher than mild steel, and if AFR is kept the same the corresponding axial compressive force and yield drift will be greater. A higher axial force and yield drift means the secondary (P-delta) effect will be more pronounced. Therefore, in the present analysis failure is assumed to have occurred when the column end moment that corresponds to the maximum displacement of one loop drops below 85% of the peak moment attained during the analysis.

The hysteresis loops obtained from the finite element analysis are shown Figure 6-19. The column shows good energy dissipation and no pinching is observed. The normalized column end moment that occurs at the maximum displacement point for each loop is plotted against the loop number in Figure 6-20. In the figure, the red dotted lines mark the condition when the moment drops to 85% of the peak moment, and the black dotted lines represent the plastic moment resistance of the cross-section. For this column, failure occurs at the third loop when d/d_y = 4, and full yielding occurs at the fixed end of the column at the second loop when d/d_y = 3.

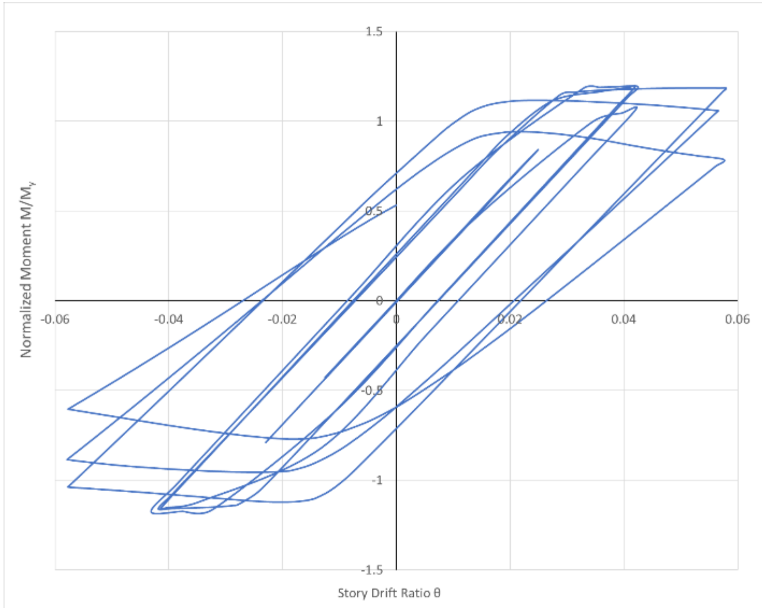

Figure 6-19 Hysteresis Loop of an Unheated Column

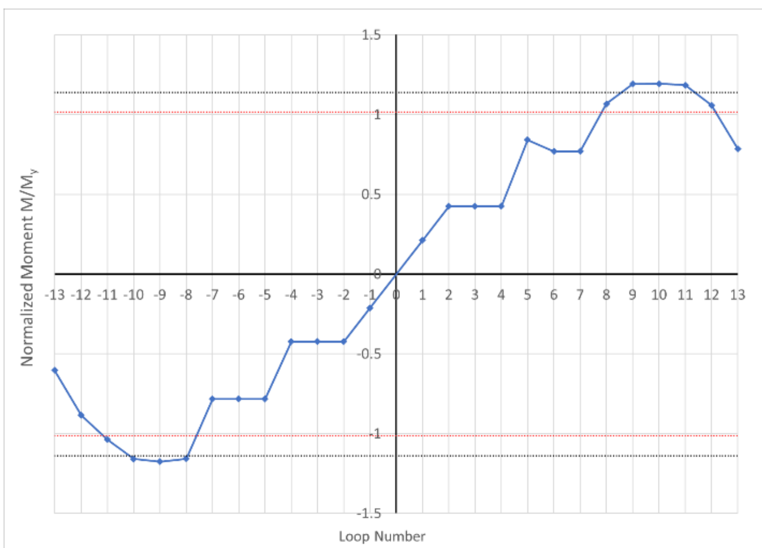

Figure 6-20 Normalized Moment vs. Loop Number

To quantify the hysteretic performance of this column, a normalized hysteretic energy dissipation index *h* for the i^{th} loop is proposed as follows.

$$h = \frac{S_i}{E_y} \tag{6.14}$$

where S_i is the area enclosed by the i^{th} loop, and E_y is the elastic strain energy given by

$$E_y = M_y\theta_y \tag{6.15}$$

In which M_y is the cross-section yield moment and θ_y is the corresponding yield drift ratio.

The cyclic performance H of the column is defined as the sum of all the normalized hysteretic energy dissipation indices before the failure occurs. That is

$$H = \frac{\sum_{i=1}^{k-1} S_i}{E_y} \tag{6.16}$$

where k is the loop when failure occurs, and the numerator represents the total energy dissipated by the column when it is subjected to these load cycles, i.e.,

$$S_t = \sum_{i=1}^{k-1} S_i = E_y H \tag{6.17}$$

Since no inelastic behavior was observed until the imposed displacement reached $3d_y$ and because failure occurred at the 13^{th} cycle, the cyclic performance and total energy dissipation for this column are evaluated for loops 8 to 12 as shown in Figure 6-21. The cyclic performance index H is obtained as 16.02 and the total energy dissipation is computed to be 244.79 kJ.

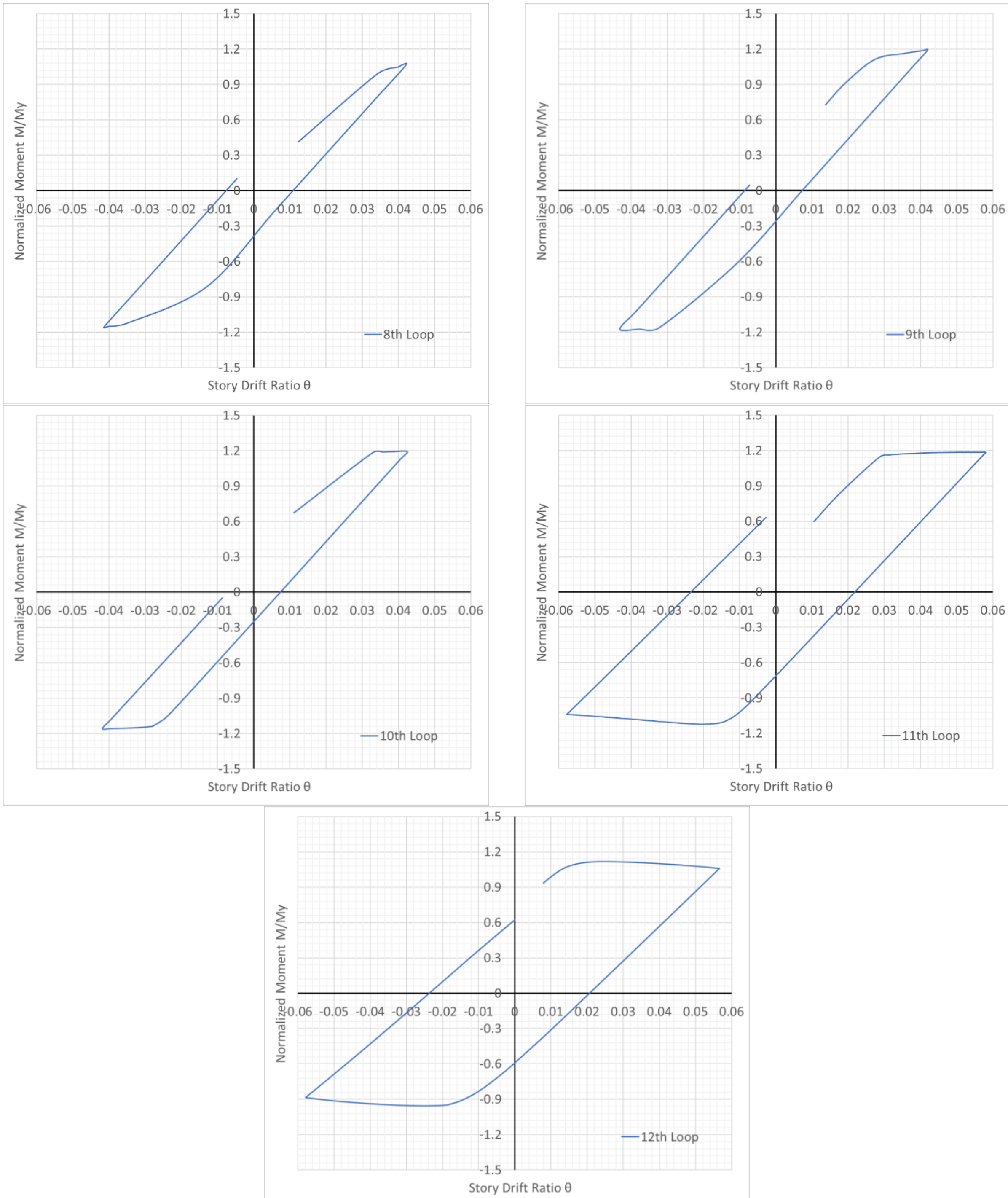

Figure 6-21 Hysteresis Loops 8 to 12

6.5.5 Analyses of Post-fire Columns

In this section, the post-fire cyclic performance of welded Q690 I-shaped columns subject to Type 1 load protocol as shown in Figure 6-4(a) is investigated. According to Qiang's research on

S690 steel (with F_y= 690 MPa) subjected to elevated temperatures [17,22], the steel loses about 63% of its mechanical properties when the exposed temperature is around 600°C, but regain some of its properties upon cooling. Therefore, the present analyses only consider an exposed temperature range from 300°C to 600°C. Another assumption made in this study is that all the columns are capable of withstanding the fire without obvious deformations or damage.

The analyses are carried out using the FEM described earlier, with column dimensions and material properties given in Tables 6-4 to 6-6. Both air and water cooling will be considered. The hysteresis loops and the normalized moment vs. loop number curves so obtained are shown in Figure 6-22 to Figure 6-29 for different temperature exposures and cooling methods. For all scenarios, the hysteresis loops show good energy dissipation capacity and no pinching is observed. Further, plasticity is fully developed at the fixed end of the columns since the maximum moment exceeds M_p, the plastic moment. Since the ratio of tensile to yield strength reaches 1.4 when the exposed temperature is 600°C with either air cooling or water cooling, this column experiences full yielding earlier than the others. All columns are capable of sustaining large plastic deformation before the failure occurs.

From the normalized moment vs. loop number plots, it can be seen that as the load cycle reaches 9 (i.e., the second of the three cycles that corresponds to d/d_y = 3), a noticeable reduction in maximum moment is observed thereafter. This decrease is the result of local buckling occurring in the column flanges.

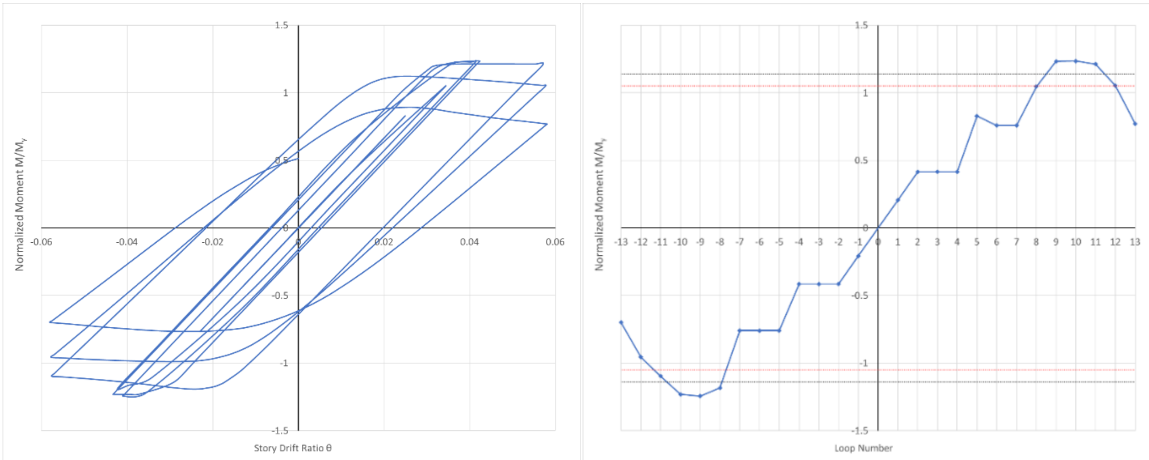

Figure 6-22 Hysteresis Loops and Normalized Moment vs. Loop Number Curve (300°C with Air Cooling)

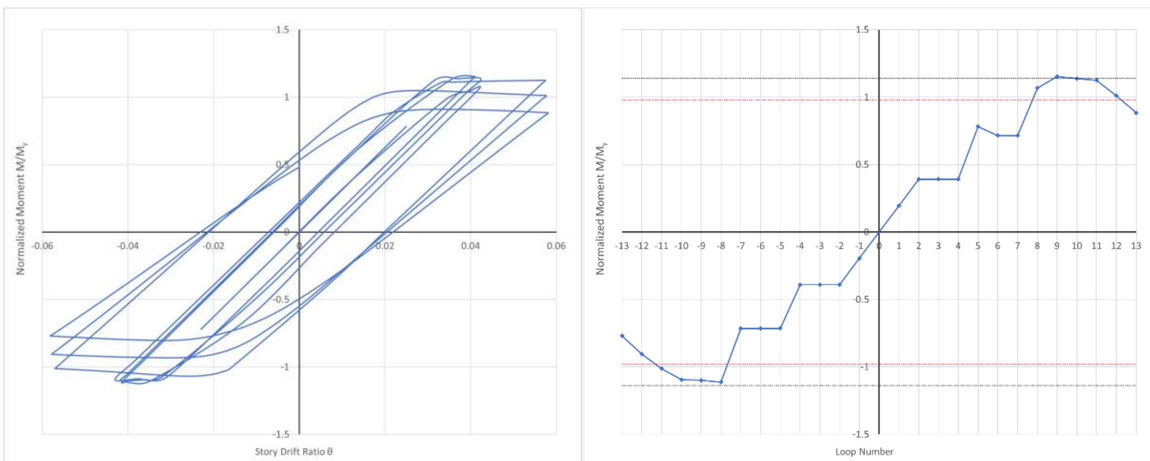

Figure 6-23 Hysteresis Loops and Normalized Moment vs. Loop Number Curve (400°C with Air Cooling)

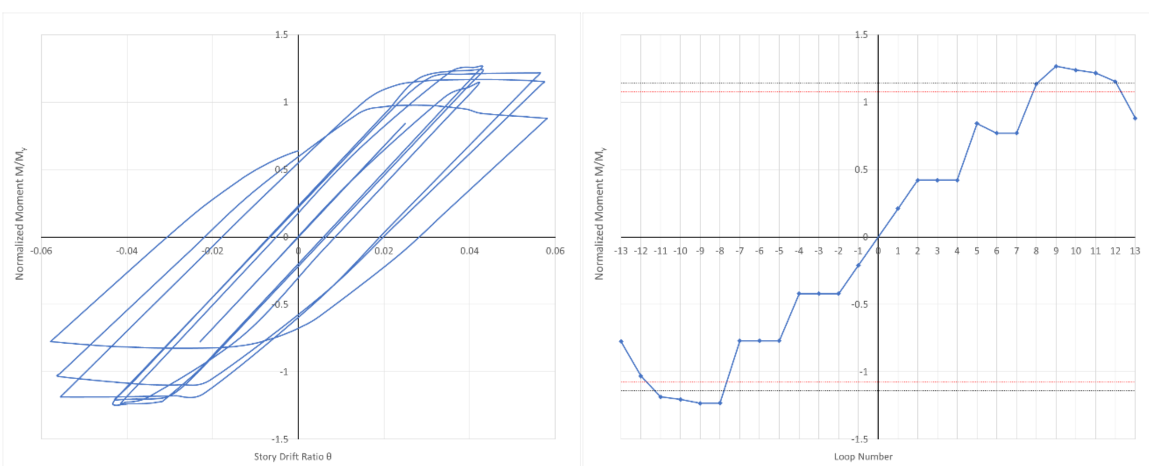

Figure 6-24 Hysteresis Loops and Normalized Moment vs. Loop Number Curve (500°C with Air Cooling)

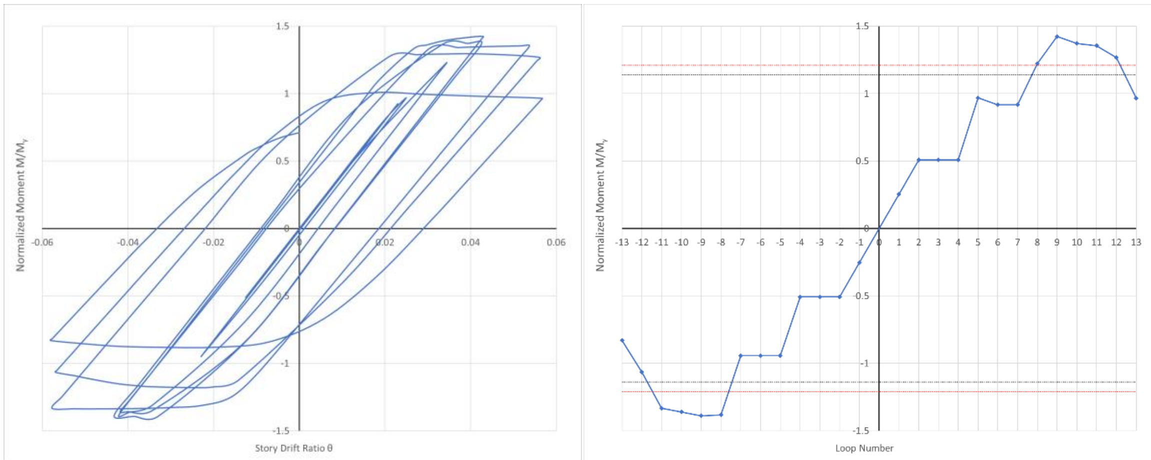

Figure 6-25 Hysteresis Loops and Normalized Moment vs. Loop Number Curve (600°C with Air Cooling)

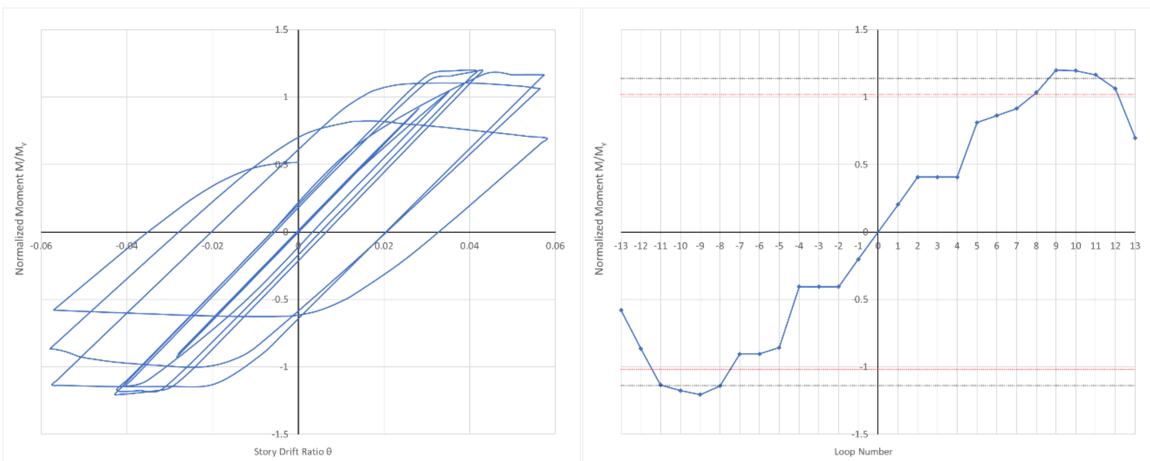

Figure 6-26 Hysteresis Loops and Normalized Moment vs. Loop Number Curve (300°C with Water Cooling)

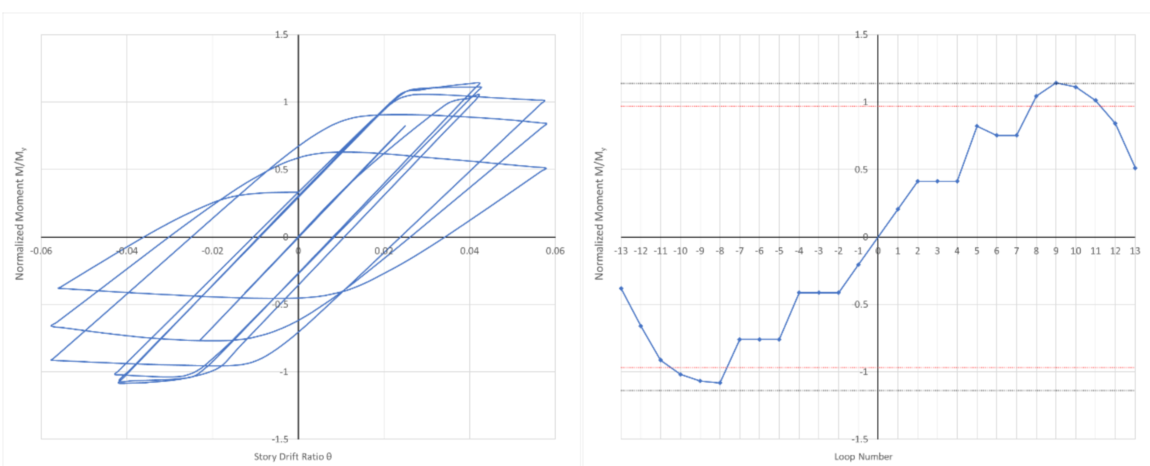

Figure 6-27 Hysteresis Loops and Normalized Moment vs. Loop Number Curve (400°C with Water Cooling)

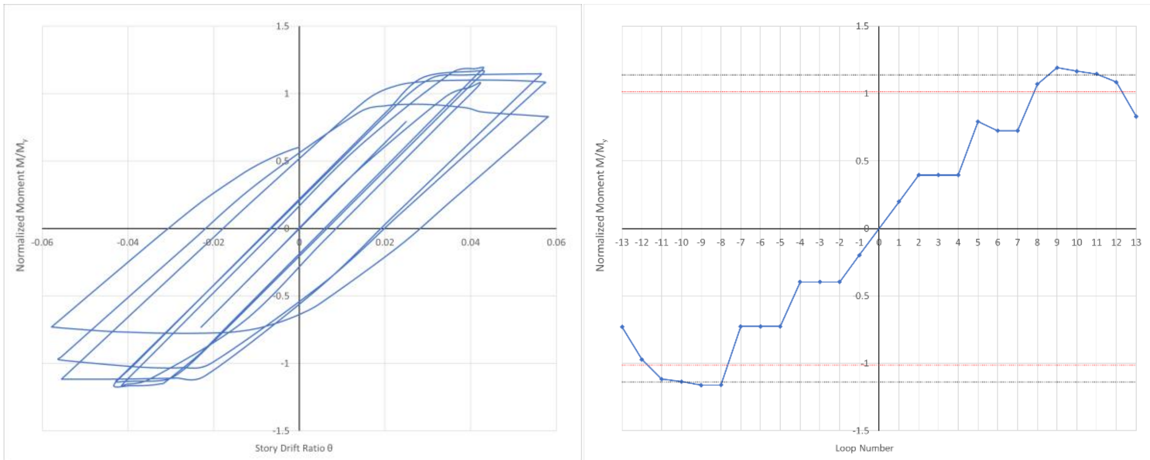

Figure 6-28 Hysteresis Loops and Normalized Moment vs. Loop Number Curve (500°C with Water Cooling)

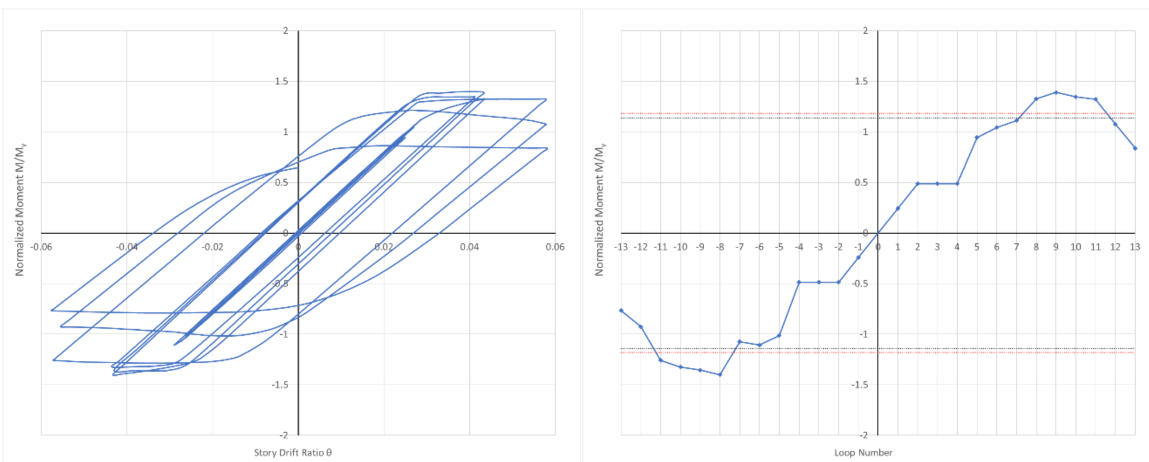

Figure 6-29 Hysteresis Loops and Normalized Moment vs. Loop Number Curve (600°C with Water Cooling)

The cyclic performance of these columns is summarized in Table 6-7. In general, when the exposed temperature increases, the total energy dissipation decreases regardless of the type of cooling methods used. The maximum column end moment occurs at the 9th cycle, which is the second load cycle when $d = 3d_y$. Further, for columns exposed to 400°C and 600°C with water cooling, failure occurs at the 12th load cycle, while other columns fail at the 13th load cycle. For this reason, the total energy dissipation for these two columns is noticeably lower. However, the difference in magnitude of the maximum column end moment that can be attained is not large.

As for the cyclic performance index *H,* it increases when the exposed temperature increases. This is because *H* is normalized by the elastic strain energy E_y, which according to Eq. (6.15) is the product of M_y and θ_y. When the yield strength decreases, the corresponding values for M_y and θ_y decrease, and so E_y decreases as well.

Table 6-7 Summary of Cyclic Performance

Exposed Temperature (°C)	Cooling Method	Failure Occurred	Max. Moment Occurred	Max. Moment (kN-m)	Total Energy Dissipation S_t (kJ)	Cyclic Performance Index H
Unheated	-	13th Cycle ($4d_y$)	9th Cycle ($3d_y$)	1020.8	244.8	16.02
300	Air Cooling	13th Cycle ($4d_y$)	9th Cycle ($3d_y$)	1117.1	229.6	13.9
400	Air Cooling	13th Cycle ($4d_y$)	9th Cycle ($3d_y$)	1036.6	224.2	12.87
500	Air Cooling	13th Cycle ($4d_y$)	9th Cycle ($3d_y$)	974.3	217.2	15.21
600	Air Cooling	13th Cycle ($4d_y$)	9th Cycle ($3d_y$)	963.2	202.1	20.03
300	Water Cooling	13th Cycle ($4d_y$)	9th Cycle ($3d_y$)	1042.5	229.8	14.18
400	Water Cooling	12th Cycle ($4d_y$)	9th Cycle ($3d_y$)	961.1	164.1	10.64
500	Water Cooling	13th Cycle ($4d_y$)	9th Cycle ($3d_y$)	1019.5	220.6	13.52
600	Water Cooling	12th Cycle ($4d_y$)	9th Cycle ($3d_y$)	1013.9	153.3	13.51

6.5.6 Correlation between Material Deterioration and Total Energy Dissipation

To establish a relationship between material deterioration due to temperature exposure and total energy dissipation, the total energy dissipation at various exposed temperatures normalized by the total energy dissipation of the column at room temperature (20°C) are given in Table 6-8. For the water-cooled analysis, the results for 400°C and 600°C are not shown because failure occurred at the 12^{th} (as opposed to the 13^{th}) cycle of loading.

Table 6-8 Normalized Total Energy Dissipation

Exposed Temperature (°C)	Cooling Method	Normalized Total Energy Dissipation $S_t/S_{t,20°C}$
Unheated	-	1
300	Air Cooling	0.94
400	Air Cooling	0.916
500	Air Cooling	0.89
600	Air Cooling	0.83
300	Water Cooling	0.94
400	Water Cooling	-
500	Water Cooling	0.9
600	Water Cooling	-

Using the data presented in Table 6-8, an empirical equation relating the normalized total energy dissipation $S_t/S_{t,20°C}$ with exposed temperature T can be obtained using regression analysis. The resulting equation is given as Eq. (6.18) with an R^2 value of 0.948, and the comparison is shown in Figure 6-30. The equation is applicable to both air and water cooling.

$$S_t/S_{t,20°C} = -2.7 \times 10^{-4} T + 1.015 \qquad 20°C \leq T \leq 600°C \qquad (6.18)$$

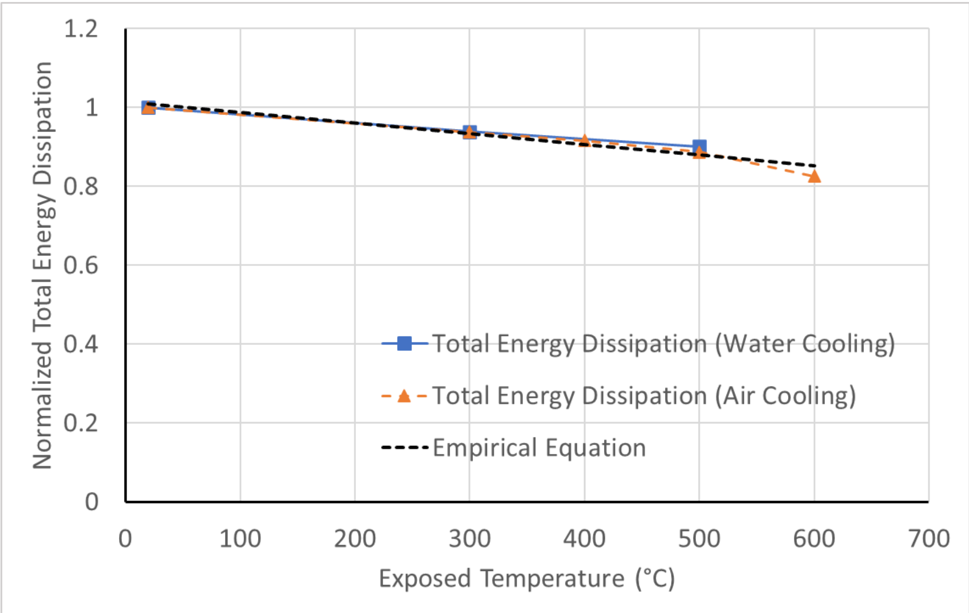

Figure 6-30 Post-fire Total Energy Dissipation

6.6 Conclusions

In this chapter, a FEM was developed and validated to study the cyclic performance of the welded I-shaped columns fabricated from Q690 steel after fire exposure. In addition, the analysis of the relationship between material deterioration and cyclic performance was conducted for the columns exposed up to 600°C with both air cooling and water quenching methods. The following conclusions were drawn:

1. Without exposure to high temperature, welded Q690 I-shaped columns are shown to exhibit good hysteretic behavior when subject to a constant axial compressive load and a cyclic lateral load. The story drift ratio satisfies the ASCE 7-16 requirement. This means the member is capable of providing good seismic resistance. In addition, since the yield strength of Q690 steel is much larger than that of mild steel, for a given axial force ratio, the secondary (P-delta) effect becomes more important.
2. After exposed to a temperature of up to 600°C and with either air or water cooling, welded Q690 I-shaped columns are able to provide good hysteretic performance. Because the post-fire tensile strength does not decrease, the members continue to be able to carry large moments before failure. However, the use of water cooling after the members are exposed to a temperature above the austenitic temperature (about 723°C) could result in their premature failure due to the formation of martensite in steel.
3. The relationship between material deterioration and cyclic performance for both cooling methods is investigated for the columns exposed up to 600°C. The post-fire maximum column end moment is more related to the post-fire tensile strength of Q690

steel, while the change of post-fire total energy dissipation is more related to the post-fire yield strength of Q690 steel.

4. The total energy dissipation tends to decrease with an increasing level of fire exposure. This is because of the reduction of yield strength when the exposed temperature is between 400°C to 700°C. An empirical equation has been developed to estimate this loss.
5. In practice, the evaluation of cyclic performance of welded Q690 I-shaped columns after fire exposure could be simplified by comparing the mechanical properties of steel.

7 SUMMARY

The research presented herein is a study of the mechanical properties and cyclic behavior of high strength steel after exposure to fire. At the material level, the post-fire mechanical properties of Q690 steel subjected to different cooling methods, namely natural air cooling and water quenching, were determined experimentally. Based on the experimental data, empirical equations expressed as functions of the level of exposed temperature and the manner of cooling were developed to estimate these post-fire mechanical properties. Furthermore, the distribution of residual stresses in post-fire welded I-shaped sections were examined, and residual stress distribution models developed for welded Q690 I-shaped sections before and after fire exposure were proposed. Finally, considering the potential effect of bi-hazards of earthquake and fire, numerical analysis on the post-fire cyclic response of Q690 welded I-shaped columns was performed.

7.1 Conclusions

Based on the results of this study, the following conclusions can be drawn:

(a) Post-fire Mechanical Properties of Q690 steel

1. For post-fire elastic modulus, it is observed that the type of cooling method used and the level of exposed temperature will not have a significant effect and can therefore be ignored.
2. For post-fire yield strength, it is observed that when the exposed temperature is 300°C and 400°C, a light increase in yield strength occurs as a result of the blue brittleness effect. However, when the temperature is between 400°C to 700°C, the yield strength

decreases with increasing exposed temperature for both cooling methods. Once the exposed temperature is above 700°C, while the post-fire yield strength continues to decrease when air cooling is used, it increases slightly when water cooling is used.

3. For post-fire tensile strength, it is observed that the change is not very significant when air cooling is used. However, when the exposed temperature is above 700°C, the post-fire tensile strength increases drastically when water cooling is used. This is because when steel is heated above its austenitic temperature (about 723°C) and rapidly cooled, martensite will form which makes steel stronger and harder but less ductile.
4. For post-fire fracture strain, it is observed that when the temperature is below 600°C, the change is not significant regardless of the type of cooling methods used. However, when the exposed temperature is higher than 600°C, the post-fire Q690 steel becomes more ductile when the air cooling method is used but less ductile when the water cooling method is used. In addition, when the temperature is above 800°C, non-ductile fracture without necking may occur for specimens that are water-cooled.
5. Both the heating rate and repeated heating/cooling can affect the post-fire mechanical properties of Q690 steel. On average, the post-fire elastic modulus and yield strength drop about 10%, but their effect on tensile strength and fracture strain is not significant and can be neglected.
6. When an axial load is applied to the specimens during the heating and cooling process, their post-fire mechanical properties are reduced by 10% to 20%. However, when the exposed temperature is 300°C, the magnitude of the axial load does not seem to have a significant effect on the mechanical properties.

7. By comparing steels with different steel grades and several Q690 steels with different chemical compositions, it is observed that their post-fire mechanical properties do not show large variation when the exposed temperature is below 500°C, but noticeable differences are observed for temperature higher than 500°C. The current standards, which were primarily developed based on the behavior of normal strength steels, need to be updated for the design of high strength steels.
8. Empirical equations that can be used to estimate the post-fire mechanical properties of Q690 steel have been developed for both air- and water-cooling methods. Moreover, reduction coefficients have been proposed to account for the influence of the heating method used, repeated heating/cooling and the presence of an axial load in calculating the post-fire mechanical properties of Q690 steel.

(b) Post-fire residual stresses of Q690 welded I-shaped sections

1. Regardless of the level of exposed temperature and cooling method used, the maximum residual stress to yield stress ratio in welded I-shaped sections made from Q690 High Strength Steel is lower than that for welded I-sections made from regular strength steel.
2. The level of exposed temperature has a noticeable influence on residual stresses. When the exposed temperature is below 300°C, the influence is not important. When the exposed temperature exceeds 300°C, the magnitudes of the maximum residual stresses start to decrease. Once the temperature reaches 700°C, the maximum residual stress magnitudes are less than 5% of the nominal steel yield strength.
3. The heating method and heating rate used do not seem to affect the residual stress results. However, for specimens heated to a temperature at or above 700°C and

suddenly cooled by water quenching, noticeable residual stresses are generated on the edges of the flanges and at the web-flange junctions. The residual stress magnitudes on the flange edges are -0.13F_y for 700°C and -0.24F_y for 900°C, while the magnitudes at the web-flange junctions are +0.29F_y for 700°C and +0.21F_y for 900°C (where F_y is the nominal yield stress of Q690 steel and +/- represents tension or compression).

4. Residual stress distribution models for welded Q690 I-shaped sections taking into consideration the level of exposed temperature have been developed. These models have been shown to give reasonably good results when compared with the experimentally measured data.

(c) Cyclic behavior of post-fire Q690 welded I-shaped columns

1. Without exposure to high temperature, welded Q690 I-shaped columns are shown to exhibit good hysteretic behavior when subject to a constant axial compressive load and a cyclic lateral load. The story drift ratio satisfies the ASCE 7-16 requirement. This means the member is capable of providing good seismic resistance. In addition, since the yield strength of Q690 steel is much larger than that of mild steel, for a given axial force ratio, the secondary (P-delta) effect becomes more importance.
2. After exposed to a temperature of up to 600°C and with either air or water cooling, welded Q690 I-shaped columns are able to provide good hysteretic performance. Because the post-fire tensile strength does not decrease, the members continue to be able to carry large moments before failure. However, the use of water cooling after the members are exposed to a temperature above the austenitic temperature (about 723°C) could result in their premature failure due to the formation of martensite in steel.

3. The total energy dissipation tends to decrease with an increasing level of fire exposure. This is because of the reduction of yield strength when the exposed temperature is between 400°C to 700°C. An empirical equation has been developed to estimate this loss.

7.2 Further Studies

Some further research on the mechanical properties and cyclic behavior of high strength steel after fire exposure includes:

1. Use of spraying water for cooling, which leads to a non-uniform distribution of temperature on the test specimens or members, should be considered. In particular, research into how water pressure, locations and area of the spraying surface, and the amount of water used could affect the results is recommended.
2. For the experimental tests of the post-fire mechanical properties, the use of more than one specimen for each set of test parameters should be attempted. In addition, more tests should be conducted to verify the empirical equations, and the effect of specimen's thickness should be investigated.
3. Generally, the width-to-thickness ratio of welded sections will affect both the magnitude and distribution of residual stresses generated from the fabrication process. Therefore, the use of a larger range of width-to-thickness ratios is recommended.
4. Since high strength steel shows good cyclic performance, more experimental tests using different axial to lateral load combinations should be conducted to study the cyclic behavior of welded Q690 I-shaped columns after fire exposure. Furthermore, a

parametric study of different axial force ratios, slenderness ratios and width-to-thickness ratios should be undertaken.

5. Tests on the post-fire mechanical properties and cyclic performance of other high strength steels can be performed to expand the experimental database.

REFERENCES

1. Gustafson K. Steelwise: evaluation of existing structures. Modern Steel Construction, 2007, February
2. NIST TN 1842. Structural design for fire: a survey of building codes and standards. 2014
3. ISO 834: Fire Resistance Tests – Elements of Building Construction (1999).
4. Qu L, Li H. Study on strength of Q420 steel section at elevated temperature. Fire Science and Technology, 2004, 5(3): 223-225 (in Chinese)
5. Wang W Y, Liu B, Kodur V. Effect of temperature on strength and elastic modulus of high strength steel. Journal of Materials in Civil Engineering, 2012, 25(2): 174-182
6. Wang W Y, Liu B, Li G Q. Experimental study on mechanical properties of Q460 high strength steel at elevated temperature. Journal of Disaster Prevent and Mitigation Engineering, 2012, 35(Suppl): 30-35 (in Chinese)
7. Mäkeläinen P, Outinen J, Kesti J. Fire design model for structural steel S420M based upon transient-state tensile test results. Journal of Constructional Steel Research, 1998, 48(1): 47-57
8. Outinen J, Mäkeläinen P. Mechanical properties of structural steel at elevated temperatures and after cooling down. Fire and Materials, 2004, 28(2/3/4): 237-251
9. Schneider R, Lange J. Constitutive equations of structural steel S460 at high temperatures. Nordic Steel Construction Conference. Malmö, Sweden, 2009: 204-211
10. Schneider R, Lange J. Analysis of the time-dependent mechanical behavior of S460 in case of fire. Stahlbau, 2012, 81(5); 379-390 (in German)

11. Schneider R, Lange J. Constitutive equations and empirical creep law of steel S460 under high temperatures. Journal of Structural Fire Engineering, 2011, 2(3): 217-230
12. Lange J, Wohlfeil N. Examination of the mechanical properties of steel S460 for fire. Journal of Structural Fire Engineering, 2010, 1(3): 189-204
13. Qiang X, Bijlaard F S K, Kolstein H. Deterioration of mechanical properties of high strength steel S460N under steady state fire condition. Materials & Design, 2012, 36: 438-442
14. Qiang X, Bijlaard F S K, Kolstein H. Deterioration of mechanical properties of high strength steel S460N under transient state fire condition. Materials & Design, 2012, 40: 521-527
15. Qiang X, Bijlaard F S K, Kolstein H. Elevated-temperature mechanical properties of high strength structural steel S460N: Experimental study and recommendations for fire-resistance design. Fire Safety Journal, 2013, 55: 15-21
16. Chen J, Young B, Uy B. Behavior of high strength structural steel at elevated temperatures. Journal of Structural Engineering, 2006, 132(12): 1948-1954
17. Qiang X, Bijlaard F S K, Kolstein H. Dependence of mechanical properties of high strength steel S690 on elevated temperatures. Construction and Building Materials, 2012, 30: 73-79
18. Chiew S P, Zhao M S, Lee C K. Mechanical properties of heat-treated high strength steel under fire/post-fire conditions. Journal of Constructional Steel Research, 2014, 98: 12-19
19. Li G Q, Jiang S C, Yin Y Z, et al. Experimental studies on the properties of constructional steel at elevated temperatures. Journal of Structural Engineering, 2003, 129(12): 1717-1721
20. ASTM E21-09. Standard test methods for elevated temperature tension tests of metallic materials. 2009

21. Wang W Y, Liu T, Liu J. Experimental study on post-fire mechanical properties of high strength Q460 steel. Journal of Constructional Steel Research, 2015,114: 100-109

22. Qiang X, Bijlaard F S K, Kolstein H. Post-fire mechanical properties of high strength structural steels S460 and S690. Engineering Structures, 2012, 35: 1-10

23. Qiang X, Bijlaard F S K, Kolstein H. Post-fire performance of very high strength steel S960. Engineering Structures, 2013, 80: 235-242

24. Wang Y B, Li G Q, Chen S W. Residual stresses in welded flame-cut high strength steel H-sections. Journal of Constructional Steel Research, 2012, 79: 159-165

25. Ban H, Shi G, Bai Y. Residual stress of 460MPa high strength steel welded I section: experimental investigation and modeling. International Journal of Steel Structures, 2013, 13(4): 691-705

26. Yang B, Nie S, Xiong G. Residual stresses in welded I-shaped sections fabricated from Q460GJ structural steel plates. Journal of Constructional Steel Research, 2016, 122: 261-273

27. Kim D K, Lee C H, Han K H. Strength and residual stress evaluation of stub columns fabricated from 800MPa high-strength steel. Journal of Constructional Steel Research, 2014, 102: 111-120

28. Li T J, Li G Q, Wang Y B. Residual stress tests of welded Q690 high-strength steel box- and H-sections. Journal of Constructional Steel Research, 2015, 115: 283-289

29. Wang W Y, Li G Q, Ge Y. Residual stress study on welded section of high strength Q460 steel after fire exposure. Advanced Steel Construction, 2015, 11(2): 150-164

30. Wang W Y, Qin S Q. Experimental investigation of residual stresses in thin-walled welded H-sections after fire exposure. Thin-Walled Structures, 2016, 101: 109-119

31. Valente J C, Neves I C. Fire resistance of steel columns with elastically restrained axial elongation and bending. Journal of Constructional Steel Research, 1999, 52(3): 319-331

32. Rodrigues J P C, Neves I C, Valente J C. Experimental research on the critical temperature of compressed steel elements with restrained thermal elongation. Fire Journal, 2000, 35(2): 77-98

33. Tan K H, Toh W S, Huang Z F, et al. Structural responses of restrained steel columns at elevated temperatures. Part 1- Experiments. Engineering Structures, 2007, 29(8): 1641-1652

34. Wang W Y, Ge Y. Experimental study on fire resistance of axially restrained high strength Q460 steel columns. Journal of Building Structures, 2012, 36(8): 116-122 (in Chinese)

35. Ge Y, Wang W Y. Fire resistance analysis of restrained high strength steel Q460 columns. Journal of Disaster Prevent and Mitigation Engineering, 2012, 32(1): 99-104 (in Chinese)

36. Wang W Y, Yang X, Wang B, et al. Experimental study on local stability of welded H-shaped steel stub columns under axial compression at elevated temperature. Journal of Building Structures, 2014, 35(11): 134-142 (in Chinese)

37. Chen J, Young B. Design of high strength steel columns at elevated temperatures. Journal of Constructional Steel Research, 2008, 64(6): 689-703

38. Wang Y B, Li G Q, Cui W et al. Experimental investigation and modeling of cyclic behavior of high strength steel. Journal of Constructional Steel Research, 2015, 104: 37-48

39. Shi G, Wang M, Bai Y. Experimental and modeling study of high-strength structural steel under cyclic loading. Engineering Structures, 2012, 37: 1-13

40. Lamarche C-P, Tremblay R. Seismically induced cyclic buckling of steel columns including residual-stress and strain-rate effects. Journal of Constructional Steel Research, 2011, 67(9): 1401-1410

41. Newell J, Uang C. Cyclic behavior of steel wide-flange columns subjected to large drift. Journal of Structural Engineering, 2008, 134:1334-1342

42. Nakashima M, Liu D. Instability and complete failure of steel columns subjected to cyclic loading. Journal of Engineering Mechanics. 2005, 131: 559-567

43. Kurata M, Nakashima M, Suita K. Effect of column base behaviour on the seismic response of steel moment frames. Journal of Earthquake Engineering. 2005, 9: 415-438

44. Wang J J, Shi G, Shi Y J. Experimental research on behavior of 460 MPa high strength steel I-section columns under cyclic loading. Earthquake Engineering and Engineering Vibration, 2014, 13(4): 611-622

45. Chen S W, Chen X, Wang Y B. Experimental and numerical investigations of Q690D H-section columns under lateral cyclic loading. Journal of Constructional Steel Research, 2016, 121: 268-281

46. ASTM E8/E8M. Standard test methods for tensile testing of metallic materials. 2016

47. Tebedge N, Alpsten G A, Tall L. Residual stress measurement by the sectioning method, presented at SESA Spring Meeting, May 1972 (73-5). Fritz Laboratory Reports, 1972: Paper 342

48. Li G Q, Lyu H, Zhang C. Post-fire mechanical properties of high strength Q690 structural steel. Journal of Constructional Steel Research, 2017, 132: 108-116

49. Zhou H T, Wang W Y, Wang K, Xu L. Mechanical properties deterioration of high strength steels after high temperature exposure. Construction and Building Materials, 2019, 199: 664-675

50. Kang L, Suzuki M, Ge H B, Wu B. Experiment of ductile fracture performances of HSSS Q690 after a fire. Journal of Constructional Steel Research, 2018, 146: 109-121

51. Lu J, Liu H B, Chen Z H, Liao X W. Experimental investigation into the post-fire mechanical properties of hot-rolled and cold-formed steels. Journal of Constructional Steel Research, 2016, 121: 291-310

52. Chen J F, Cao P Z. Experimental investigation into mechanical properties of steel post high temperatures. Journal of PLA University of Science and Technology. 2010, 11(3): 328–333 (in Chinese)

53. Zhang Y J, Zhu Y, Zhao S, Hu K X. Experimental research on mechanical properties of steel cooled in different modes after high temperature treatment. Structural Engineers. 2009, 25(5): 104–109

54. Sajid H U, Kiran R. Influence of stress concentration and cooling methods on post-fire mechanical behavior of ASTM A36 steels. Construction and Building Materials, 2018, 186: 920-945

55. Aziz M E, Kodur K V. Effect of temperature and cooling regime on mechanical properties of high-strength low-alloy steel. Fire and Materials, 2016, 40(7): 926-939

56. Lee J, Engelhardt D M, Taleff M E. Mechanical Properties of ASTM A992 Steel After Fire. Engineering Journal, 2012, 49(1): 33-44

57. Nassirnia M, Heidarpour A, Zhao X L and Minkkinen J. Innovative hollow corrugated columns comprising corrugated plates and ultra-high-strength steel tubes. Thin-Walled Structures, 2016, 101: 14-25

58. Farahi M, Heidarpour A, Zhao X L and Al-Mahaidi R. Effect of ultra-high strength steel on mitigation of non-ductile yielding of concrete-filled double-skin columns. Construction & Building Materials, 2017, 147: 736-749

59. Javidan F, Heidarpour A, Zhao X L and Minkkinen J. Application of high strength and ultrahigh strength steel tubes in long hybrid compressive members: Experimental and numerical investigation. Thin-Walled Structures, 2016, 102: 273-285

60. Azhari F, Heidarpour A, Zhao X L, Hutchinson C. Effect of creep strain on mechanical behaviour of ultra-high strength (Grade 1200) steel subject to cooling phase of a fire. Construction and Building Materials, 2017, 136: 18-30

61. Horn R M, Ritchie R.O. Mechanisms of tempered martensite embrittlement in low alloy steels. Metallurgical Transactions A, 1978, 9: 1039-1053

62. Yen H-W, Chiang M-H, Lin Y-C, Chen D, Huang C.Y., Lin H-C. High temperature tempered martensite embrittlement in quenched-and-tempered offshore steels. Metals, 2017, 7, 253, DOI:10.3390/met7070253

63. van den Beukel A. Theory of the effect of dynamic strain aging on mechanical properties. Phys. Stat. Sol. (a), 1975, 30: 197-206.

64. Mesarovic S D. Dynamic strain aging and plastic instabilities. Journal of the Mechanics and Physics of Solids, 1995, 43: 671-700

65. Kishkin S T, Klypin A A. Effect of repeated heating and cooling on the properties of steels and alloys. Metallovedenie i Termicheskaya Obrabotka Metallov, 1959, 5: 15-19

66. Agbadua S A, Mgbemena C O, Mgbemena C E, Chima L O. Thermal cycling effects on the fatigue behavior of low carbon steel. Journal of Minerals & Materials Characterization & Engineering, 2011, 10(14): 1345-1357

67. Xu H F, Cao W Q, Dong H, Li J. Effects of aluminum on the microstructure and mechanical properties in 0.2C-5Mn steels under different heat treatment conditions. ISIJ International, 2015, 55(3): 662-669

68. Mochizuki M. Control of welding residual stress for ensuring integrity against fatigue and stress-corrosion cracking. Nuclear Engineering and Design, 2007, 237(2): 107-123

69. NagarajaRao N, Estuar F, and Tall L. Residual stresses in welded shapes. The Welding Journal, 1964, 43: 295s [Publication No. 241 (64-4). Fritz Laboratory Reports. Paper 64]

70. Rossini N S, Dassisti M, Benyounis, K Y, Olabi A G. Methods of measuring residual stresses in components. Materials and Design, 2012, 35: 572-588

71. Lin J, Ma N S, Lei Y P, Murakawa H. Measurement of residual stress in arc welded lap joints by cosα X-ray diffraction method. Journal of Materials Processing Technology, 2017, 243: 387-394

72. AISC, AISC 341 Seismic Provisions for Structural Steel Buildings. 2016

73. ASCE, ASCE 7-10 Minimum Design Loads for Buildings and Other Structures. 2010

74. FEMA, FEMA 356 Prestandard and Commentary for the Seismic Rehabilitation of Buildings. 2000

VITA

NAME OF AUTHOR	Fang Wang
PLACE OF BIRTH	Wuhan, China
DATE OF BIRTH	March 13, 1989
EDUCATION	
June 2020	Ph.D. in Civil Engineering, Department of Civil and Environmental Engineering, Syracuse University, Syracuse, NY, USA
MAY 2013	M.S. in Civil Engineering, Department of Civil and Environmental Engineering, Syracuse University, Syracuse, NY, USA
MAY 2011	B.S. in Civil Engineering, Department of Civil and Architectural Engineering, Hubei University of Technology, Wuhan, Hubei, China
EXPERIENCES	
JAN. 2020 to PRESENT	Research Engineer, Genex Systems, FHWA Turner-Fairbank Highway Research Center, McLean, VA, USA

JAN. 2019 to JAN. 2020 Teaching Assistant,

Syracuse University,

Syracuse, NY, USA

MAY 2013 to MAY 2014 Entry Level Engineer,

Times Buildings P.C. Engineering Services,

New York, NY, USA

PUBLICATIONS

Wang F, Lui E M, Experimental study of the post-fire mechanical properties of Q690 high strength steel, Journal of Constructional Steel Research, 2020, 167, 105966, https://doi.org/10.1016/j.jcsr.2020.105966

Wang F, Lui E M, Behavior of high strength steels under and after high temperature exposure, Journal of Steel Structures & Construction, 2016, 2:2, DOI: 10.4172/2472-0437.1000123